ANNUAL REPORT

Center for Experimental Nuclear Physics and Astrophysics
University of Washington
May, 2006

Sponsored in part by the United States Department of Energy
under Grant #DE-FG02-97ER41020.

Cover photos, from top to bottom: Stephan Schlamminger and Todd Wagner, adjusting the apparatus for the Eöt-Wash equivalence principle test. Jessica Mitchell, assembling the e-gun for testing the KATRIN detector. The prototype PIN diode pixilated array, built by the Washington Technology Center, for the KATRIN detector.

INTRODUCTION

CENPA pursues a broad program of research in nuclear physics, astrophysics and related fields. Research activities are conducted locally and at remote sites. CENPA is a major participant in the Sudbury Neutrino Observatory (SNO), the KATRIN tritium experiment and the Majorana double-beta decay experiment. The current program includes "in-house" research on nuclear collisions and fundamental interactions using the local tandem Van de Graaff, as well as local and remote non-accelerator research on fundamental interactions and user-mode research on relativistic heavy ions at large accelerator facilities in the U.S. and Europe.

We thank our external advisory committee, Baha Balantekin, Russell Betts, and Stuart Freedman, for their continuing valuable recommendations and advice. The committee reviewed our program in May, 2005.

A comprehensive analysis of the complete data taken in the Sudbury Neutrino Observatory when salt was present in the heavy water was completed and published. The SNO data provides a precise measure, $33.9^{+2.4}_{-2.2}$ degrees, of the "solar" mixing angle. In combination with other experiments (KamLAND in particular), the mass splitting Δm^2_{12} is found to be $(8.0^{+0.6}_{-0.4}) \times 10^{-5}$ eV^2.

The Neutral-Current Detection array has been operating in production mode in SNO since November 2004. The solar-neutrino-live fraction has been good, > 60 %, and most of the remaining time is calibration data. The array produces a clear neutron signal at the level anticipated. The UW-designed data acquisition systems, ORCA for NCDs and SHaRC for the photomultiplier system, have been integrated and are operating successfully.

We finished a determination of the mass of the lowest T=2 state in ^{32}S with a precision/accuracy of approx 0.3 keV. This allowed for a stringent test of the Isobaric Mass Multiplet Equation, where we found a significant discrepancy. Our result provides the best test of the limits of the approximations inherent in the IMME and of its utility for predicting masses away from the valley of stability.

Construction of the KATRIN experiment is proceeding apace with contracts placed for the major components and construction started on the experimental hall. Commissioning has started on the prespectrometer using the ORCA based data acquisition system. The prespectrometer's internal electrode, that was supplied by CENPA, has successfully passed the extreme high vacuum test. In the US, the detector design document and a project execution plan have been completed, allowing detailed design and cost estimating to begin. Using the CENPA electron gun, we have been working closely with manufacturers to optimize the properties of PIN diode arrays we are considering for the focal plane detector. The experiment remains on track to begin data taking in Fall '09.

The Majorana Scientific Collaboration proposes to search for neutrinoless double-beta decay by building an array of 86% enriched ^{76}Ge segmented radiation detectors that serve as both source and detector. In September, the collaboration received a favorable review by the Joint NSAC-HEPAP Neutrino Scientific Assessment Group (NuSAG)[1] sub-committee.

---

[1]Neutrino Scientific Assessment Group, *Recommendations to the Department of Energy and the National*

Efforts at CENPA this past year have concentrated on developing a conceptual design report, carrying out a variety of simulation studies within the Majorana- GERDA (MaGE) simulation framework, and R&D studies of the potential for future use of an active liquid Ar shield.

The Object Oriented Realtime Control and Acquisition (ORCA) system, which was developed at CENPA, has been expanded to support many additional CAMAC modules, several stepper motor controllers, and general process control capabilities. ORCA has been successfully taking production data for the SNO NCD experiment and, in addition, is being used in development systems at UW, LANL, PNNL, FZK, and MIT associated with the SNO, KATRIN, and Majorana projects.

In nuclear astrophysics, we have begun our precision ^{4}He + ^{3}He fusion cross section measurements, and we have produced several test ^{23}Na and ^{22}Na targets for our planned ^{22}Na(p,γ)^{23}Mg study.

We have observed that much of the correlation structure in RHIC heavy ion collisions is dominated by low-Q^2 parton scattering and fragmentation, observed for the first time with our analysis techniques. Because low-Q^2 parton scattering is possibly the dominant formation mechanism and the best probe of the colored medium produced at RHIC we have pursued this phenomenon in elementary collisions, first in p-p collisions and more recently with an extensive analysis of e^+-e^- fragmentation functions. A coherent picture of nonperturbative QCD processes at small energy scales is emerging.

The HBT interferometry analysis activity in the STAR experiment at RHIC continues to provide provocative results that challenge theoretical ideas. Our recent work in developing the distorted wave emission function (DWEF) model has proved very successful in simultaneously reproducing HBT radii and the magnitude and shape of the pion momentum spectrum. New results show that to explain STAR data the DWEF model prefers an emission temperature of 193 MeV, the same temperature that lattice gauge calculations predict for the transition from a quark-gluon plasma to a hadronic phase in the medium. We have also shown that the space-time part of the emission function can be scaled with participant number to the one-third power to fairly accurately predict the observables of non-central Au+Au collisions and central and non-central Cu+Cu collisions.

We have developed a "spin pendulum" for a novel torsion-balance test of CP and Lorentz symmetries. Our upper limit on the energy required to reverse the direction of an electron spin about an arbitrary direction fixed in inertial space is roughly 10^{-21} eV, which is comparable to the electrostatic energy of two electrons separated by 10 astronomical units. Our value is well below the benchmark expectation, based on the electron and Planck masses, $m_e^2/M_P = 2 \times 10^{-17}$ eV.

Our tests of the gravitational inverse-square law have shown that the law holds down to the "dark energy length scale" of 85 micrometers. We are developing a next-generation instrument that should increase our sensitivity at the 50 micron length scale by about a factor of 50.

Science Foundation on a United States Program in Neutrinoless Double Beta Decay: Report to the Nuclear Science Advisory Committee and the High Energy Physics Advisory Panel, 2005.

Five CENPA graduate students obtained their PhD degree during the period of this report.

As always, we encourage outside applications for the use of our facilities. As a convenient reference for potential users, the table on the following page lists the capabilities of our accelerators. For further information, please contact Prof. Derek W. Storm, Executive Director, CENPA, Box 354290, University of Washington, Seattle, WA 98195; (206) 543-4080, or storm@npl.washington.edu. Further information is also available on our web page: http://www.npl.washington.edu.

We close this introduction with a reminder that the articles in this report describe work in progress and are not to be regarded as publications or to be quoted without permission of the authors. In each article the names of the investigators are listed alphabetically, with the primary author underlined, to whom inquiries should be addressed.

Derek Storm, Editor Barbara Fulton, Assistant Editor

TANDEM VAN DE GRAAFF ACCELERATOR

A High Voltage Engineering Corporation Model FN purchased in 1966 with NSF funds, operation funded primarily by the U.S. Department of Energy. See W. G. Weitkamp and F. H. Schmidt, "The University of Washington Three Stage Van de Graaff Accelerator," Nucl. Instrum. Meth. **122**, 65 (1974). Recently adapted to an (optional) terminal ion source and a non-inclined tube #3, which enables the accelerator to produce high intensity beams of helium and hydrogen isotopes at energies from 100 keV to 7.5 MeV.

Some Available Energy Analyzed Beams

Ion	Max. Current (particle μA)	Max. Energy (MeV)	Ion Source
^{1}H or ^{2}H	50	18	DEIS or 860
^{3}He or ^{4}He	2	27	Double Charge-Exchange Source
^{3}He or ^{4}He	30	7.5	Tandem Terminal Source
^{6}Li or ^{7}Li	1	36	860
^{11}B	5	54	860
^{12}C or ^{13}C	10	63	860
*^{14}N	1	63	DEIS or 860
^{16}O or ^{18}O	10	72	DEIS or 860
F	10	72	DEIS or 860
* Ca	0.5	99	860
Ni	0.2	99	860
I	0.001	108	860

*Negative ion is the hydride, dihydride, or trihydride.

Additional ion species available including the following: Mg, Al, Si, P, S, Cl, Fe, Cu, Ge, Se, Br and Ag. Less common isotopes are generated from enriched material.
In addition, we are now producing a separated beam of 15-MeV ^{8}B at 6 particles/second.

BOOSTER ACCELERATOR

See "Status of and Operating Experience with the University of Washington Superconducting Booster Linac," D. W. Storm *et al.*, Nucl. Instrum. Meth. A **287**, 247 (1990). The Booster is presently in a "mothballed" state.

Contents

1 Neutrino Research

SNO

1.1 Status of the SNO Project

J. F. Amsbaugh, G. A. Cox, J. A. Detwiler, P. J. Doe, C. A. Duba, G. C. Harper, M. A. Howe, S. R. McGee, A. Myers, N. S. Oblath, K. Rielage,* R. G. H. Robertson, L. C. Stonehill,* T. D. Van Wechel, B. VanDevender and J. F. Wilkerson

The Sudbury Neutrino Observatory detector is now in its third configuration for solar neutrino detection, in which ^{3}He-filled proportional counters have been deployed in the heavy water. There are 36 'strings' of individual counters filled with ^{3}He and another 4 filled with ^{4}He for investigation of backgrounds. The total deployed length of counter is 398 m. Production running in this mode began in November, 2004, and will continue until December 31, 2006, at which time the collaboration will begin decommissioning SNO in order to return the heavy water to its owners.

The array has been running successfully and produces a clear neutron signal that is approximately of the magnitude expected from neutral-current disintegration of deuterium by solar neutrinos. Data are being recorded under blindness protocols designed by the UW group. Two strings (one ^{3}He and one ^{4}He) are presently out of commission with breakdown or high-rate noise problems. Another eight have various minor problems that can be dealt with in data processing. Data are recorded in two parallel streams, one a high-speed integrating shaper-ADC path to handle bursts such as a supernova, and the other a low-rate path in which the ionization current signals are fully digitized at 1 Gs/s for 15 μs. The information contained in the two data streams provides powerful means for sorting valid neutron events from other types.

Analysis of the radioactivity in the "NCDs" by studying the time-correlated alpha decays characteristic of the U and Th chains indicates that U is about a factor of 10 below the specified 25 pg/g level, and Th is about a factor of 3 above the specified 2 pg/g level. The additional photodisintegration background implied is about 5% of the solar neutrino signal, which compromises slightly but not seriously the obtainable accuracy.

During this phase of SNO operation UW is responsible for the maintenance of the NCD array, and we have on occasion sent technical personnel to site on short notice to deal with problems. We maintain complete functional systems at UW and in the underground control room at SNO to aid in tests, code development, and diagnostics. Many subsidiary measurements in support of analysis have been carried out with the UW system. We continue to provide our yearly average of 150 SNO operator shifts on site, the largest number (together with Oxford) in the collaboration. Both data-acquisition (DAQ) and NCD experts are available on call round the clock.

---

*Presently at Los Alamos National Laboratory, Los Alamos, NM 87545.

SNO Neutral Current Detectors (NCDs)

1.2 NCD-array pulse-shape fitting

N. S. Oblath and R. G. H. Robertson

We are developing a method for fitting the pulses from the Neutral-Current-Detection (NCD) Array at SNO. The NCD Array is a set of 40 strings of ^{3}He and ^{4}He proportional counters installed in the heavy-water volume of SNO. The purpose of the array is to capture neutrons from the Neutral-Current (NC) neutrino interaction that occurs in the heavy water ($\nu_x + d \rightarrow n + p + \nu_x$). The pulses primarily come from neutron-capture events, ^{3}He(n,p)^{3}H, or the alpha-decays of radioactive contaminants in the NCDs themselves. The back-to-back proton and triton in the neutron-capture events and the alpha particles ionize the gas in the counters, and the ionization electrons are collected on the central-wire anode creating a current pulse. To accurately count the number of neutrons detected we need to be able to separate neutron pulses from backgrounds such as alphas.

The pulse-shape analysis group within SNO is working on several methods of identifying pulses. Our method uses deconvolution to simplify the pulses prior to fitting them with simulated pulses. The entire algorithm is a three-stage process. First, after the pulse is extracted from the data, two pre-fitting routines are used. One determines the z-position of the pulse, or where along the length of the NCD the event occurred. This routine takes advantage of the fact that certain frequencies in the frequency-space representation of a pulse will cancel upon reflection from the bottom of the NCD. By looking for those minima in each pulse the z position can be determined. Determining the z position is necessary so the reflection can be deconvolved in the second stage. The z-position-determination algorithm has had the best results so far of any previous z-position efforts.

The other prefitting routine makes initial guesses for three remaining event parameters that describe the track orientation and radial location. This will be done with a multilayer-perceptron neural-network by the ROOT class TMultiLayerPerceptron. Two networks will be trained, using sets of simulated neutrons and alphas respectively. The two networks will be used to guess the parameters under the assumptions that the event was due to an alpha particle and that it was due to a neutron capture.

The second stage, deconvolution, removes various effects that modify the pulse shapes, such as the reflection of the pulse from the bottom of the NCD string, and the various electronics components. The deconvolution is done in Fourier space. A point-spread function is simulated for each effect, which describes how a delta function is transformed. Once all of the deconvolutions are complete the pulse is transformed back into the time representation.

The final stage is the actual pulse fitting using simulated neutron and alpha pulses. Minuit (as implemented in the ROOT class TMinuit) will be used to minimize the χ^2 between the data and simulation, once assuming the event is from an alpha particle, and once assuming the event is from neutron capture. Fits of simulated pulses have shown that the fitting routine works well, and work is under way to identify the best way to separate neutron-capture and alpha events. Care is needed because the parameter space is highly correlated. All stages of the process have been shown to work and efforts to optimize each of them are underway.

1.3 NCD electronics calibrations

G. A. Cox, M. A. Howe, S. R. McGee, A. W. Myers, K. Rielage, R. G. H. Robertson, T. D. Van Wechel and J. F. Wilkerson

The NCD Electronics Calibration Program consists of a weekly probing of the system's shaper/ADC cards, multiplexers, and digital oscilloscopes. The tests include threshold measurements, linearity checks, and characterization of the multiplexers' logarithmic amplifiers. A known test signal is injected at the front end of the electronics and its output is measured, thereby showing the effects of the various electronic settings. These automated tests, which have been performed since the beginning of data acquisition, have shown that our electronics system is stable.[1]

Work on these electronics calibrations over the last year has been more of the same. Due to a more advanced analysis approach of the NCD data, our software model of the NCD electronics system has become increasingly more sophisticated. The transformation of the physics and calibration pulses through each component in the system is now included. Methods are also being developed to create a single "transfer function" that can be used to convolve the effects of the electronics with simulated NCD events.

In April 2005, a special data set was produced to facilitate characterization of our electronics model. The data acquisition system is robust enough to allow us to acquire data with the hardware in various configurations. Using various setups, the pulse transformation effects caused by individual electronics components were isolated and measured.

One problem that had been plaguing the electronics calibration analysis was the determination of the uncertainties of the parameters which characterize the logarithmic amplifiers in the system. The uncertainties estimated by the MINUIT package from a χ^2 minimization routine for an single event were smaller than expected, based upon a very large sample of measurements. The uncertainties returned by the fitting routine were approximately a factor of 10 too small. The problem was due to small error bars on each bin of the digitized waveform. The reason that our bin errors were too small was because they were estimated from the RMS of the baseline. However, the bandwidth in our system filters out some of the high frequency noise and effectively smoothes our baseline (the digitizers have a 1GHz sampling rate). The bandwidth filtering produces a correlation between each of the 1ns wide bins of the waveform to its nearby bins, a smaller measured RMS along the baseline, and subsequently results in a smaller bin error estimate. Monte Carlo and simulation software was written to produce simulated waveforms. By producing a very large number of simulated waveforms and then performing a χ^2 minimization analysis and histogramming the resulting best-fit logamp parameters, the uncertainty of the logamp parameters can be accurately estimated from their distributions. Automation of this work is currently ongoing.

[1]CENPA Annual Report, University of Washington (2005) p. 35.

1.4 Livetime studies in the SNO NCD phase

J. A. Detwiler

Two important changes to the SNO detector in the NCD phase impact the estimate of the experiment's livetime, essential for converting event counts into measured fluxes. The first is the addition of the NCDs themselves, which are operated as a distinct detector system from the PMTs used in the experiment's previous data taking phases and hence require their own livetime estimate. The second change is the incorporation of the "NHIT monitor" diagnostic, whose operation imposes a negligible deadtime but significantly impacts the livetime calculation.

The NCD and PMT signals are digitized and read out with independent electronics and data acquisition systems. The livetime for the PMT data stream is obtained from a 10 MHz clock on the master trigger card (MTC), which is referenced to the GPS time standard at periodic intervals. The NCD system has its own 10 MHz clock to determine its livetime. However, since this clock is not directly referenced to the GPS time standard, we have measured the relative frequency shift and jitter between it and the 10 MHz clock on the MTC. The measured frequency shift and jitter were small enough that estimating the NCD livetime from the 10 MHz clock on the MTC would contribute negligible uncertainty. The same comparison was performed with a second 50 MHz clock on the MTC. The two comparisons were consistent with each other.

The NHIT monitor is a diagnostic that regularly measures the thresholds of the NHIT triggers in order to identify drifts in those thresholds quickly so that action can be taken when necessary to maintain trigger efficiency while keeping data taking rates at acceptable levels. The diagnostic works by pulsing a particular set of PMT channels while measuring the response of the trigger. The process imposes a negligible deadtime on the detector; however, a fraction of the NHIT monitor events "steal" PULSE_GT triggers, a periodic trigger signal whose count forms the basis of a run's livetime estimate. As a result, the NHIT monitor triggers must be identified and incorporated into the the PULSE_GT count in order to correctly calculate livetime. A worry was expressed that NHIT monitor events were not being tagged correctly by the trigger, and therefore would be miscounted. In response, an independent method to efficiently tag the NHIT monitor events was developed based on their hit pattern in the PMT channels. From this, it was demonstrated that the NHIT monitor events were indeed being properly tagged by the trigger, and hence the livetime calculation could be performed without additional complications.

1.5 Determination of the efficiency function of the NCD MUX system through raised threshold source runs

S. R. McGee and L. P. Mannisto

The Neutral Current Detector (NCD) data acquisition system at the Sudbury Neutrino Observatory (SNO) has two independent triggering paths; fast and slow. The fast (or shaper) path triggers on the integrated energy of an event. Intended to collect as much data as possible during a supernova-neutrino shower, this path also allows for a determination of the neutron acceptance efficiency of the NCDs during high-rate neutron source runs. The slow (or MUX) path triggers on the instantaneous current of the NCD event and allows for particle identification through various pulse-shape analysis algorithms. Any event acceptable for analysis in the NCD phase must have triggered both the MUX and the shaper systems to allow for identification of the pulse and an accurate measure of its energy, respectively.

Calibrations are done periodically at SNO with neutron-emitting sources to calibrate the nominal MUX threshold efficiencies. However, due to changes in the NCD hardware or increased noise pick-up in the NCD system from ambient sources, it occasionally is necessary to temporarily raise the MUX thresholds on some or all of the NCDs to keep the MUX trigger rate low. The level to which the threshold is raised is chosen to minimize the effect of deadtime in that particular instance, so it is necessary to know accurately the MUX threshold efficiency over a wide range of threshold values.

To determine these efficiencies when the MUX threshold is raised, a collection of source runs were taken in various locations (to optimize the neutron flux through a particular set of NCDs) and with various values of raised MUX thresholds. Since this is a test of the correlation efficiency between two triggering systems, it is necessary to optimize the neutron efficiency while minimizing the amount of noise that may effect the efficiency calculation (i.e., events that may naturally trigger only the shaper or the MUX independently). For this reason, runs where the 67-Hz AmBe source is less than 1 m from the NCD are being considered for the determination of the raised MUX threshold efficiency. Runs where the source is further than 1 m may be used as a check of consistency.

To determine the efficiency function, a fit is made to the efficiency (i.e., the fraction of events in which both a shaper and a MUX trigger are present) versus raised MUX-threshold value as shown in Fig. 1.5-1. This fit is made at least three times for different increasing shaper lower limits. As can be seen in the plot, as the lower limit of the shaper increases the efficiency remains higher for increased range of MUX-threshold values.

Currently, a two-dimensional polynomial function has been shown to fit well to most strings for most shaper ranges. Refinement of the fitting technique may include adding a second function in the range of lower MUX threshold values for better fits to the higher shaper ranges. Also, a method is being investigated to better determine the error bars on the MUX threshold values.

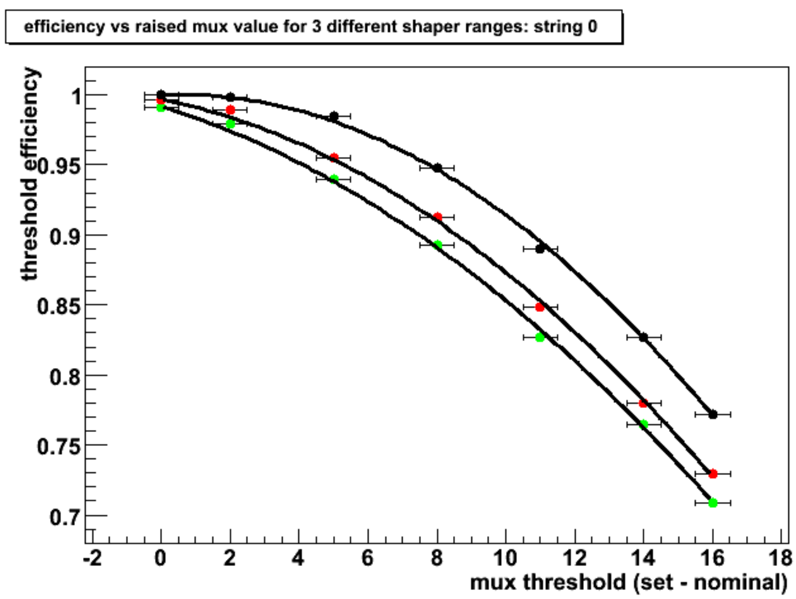

Figure 1.5-1. Plot of the efficiency of neutron acceptance on string 0 versus the MUX threshold value setting above the nominal value (in bits). Each curve is a fit to data taken with a fixed value of the shaper lower limit. The left most curve corresponds to the lowest setting of the lower limit. The curves to the right correspond to increasing shaper lower limits, illustrating a trend of increasing efficiency as the lower limit of the shaper is increased. Data shown here were taken during a central source run (source is at the midplane of SNO and is placed less than 1 m from string 0).

1.6 SNO muon chamber data acquisition verification

M. A. Howe and B. L. Wall

An external measurement of through-going muons at the Sudbury Neutrino Observatory is underway. The purpose is to verify the accuracy of muon-track reconstruction algorithms used in SNO. The University of Washington contribution to the project is the development and verification of the data acquisition system for the project. MIT is handling the detector assembly.

The full detector system includes eight gas drift chambers, measuring 101”x47”x3”, in a 4x2 stack running in a Geiger-counter mode. Each chamber has 16 channels connected to a LeCroy 3377 TDC. Two scintillator paddles are used to trigger the TDC for read out. Data readout and control is done via a G4 Macintosh by the ORCA program developed by Mark Howe.

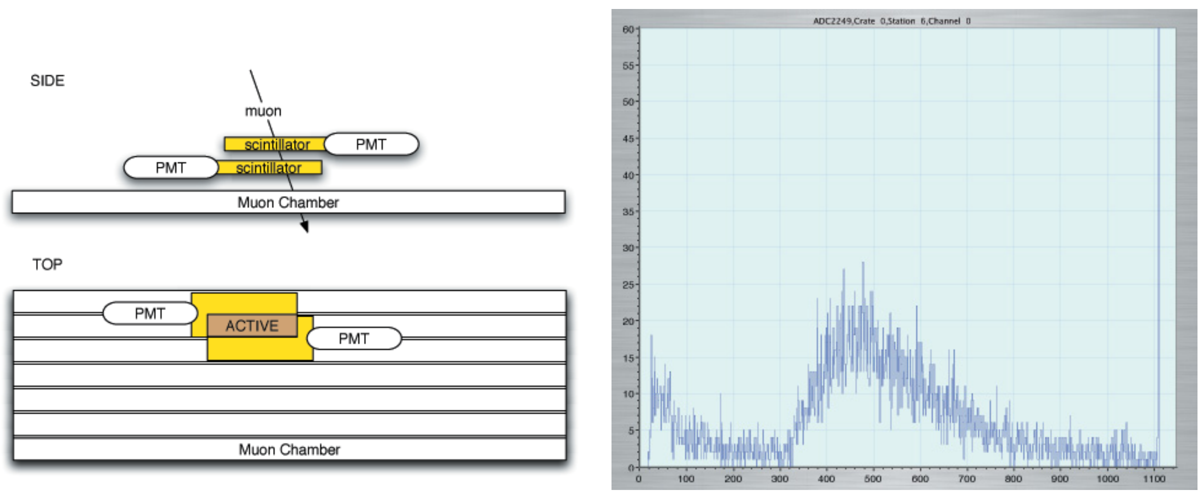

(a) (b)

Figure 1.6-2. (a) Scintillator paddle and muon chamber setup. (b) Muon spectrum from the scintillator paddles.

A scaled down version was assembled here at the University of Washington (see Fig. 1.6-2). A single channel of a muon chamber ran in coincidence with two scintillator paddles in order to verify the operation of the data acquisition system. Four half-hour runs were done in common-start single-word mode, at 4 nanosecond resolution, with a 4 microsecond window. Each channel would count up to 16 hits in a triggered event, which means multiple peaks generated in an event would all get counted. Data in Fig. 1.6-2 from an ADC connected to the PMTs verifies that triggers being generated are from muons. A clear peak centered at bin 479 is seen from minimum ionizing particles. A total of 6165 triggers were generated in a region above bin 300 indicating a muon rate of 51.3 muons per minute, approximately one third of the expected rate calculated from the 154 cm^2 of scintillator overlap region. Of the 6165 triggers generated there were 2992 TDC events with a measured accidental rate of 1 count per minute.

KATRIN

1.7 The CENPA contribution to the KATRIN neutrino mass experiment

T. H. Burritt, P. J. Doe, G. C. Harper, M. A. Howe, M. J. Leber, A. W. Myers, R. G. H. Robertson, B. VanDevender, T. D. Van Wechel, B. L. Wall and J. F. Wilkerson

This has been a very exciting year as construction activity on the KATRIN experiment rapidly moves towards a peak. Of the additional 12 M Euro required to increase the sensitivity of the experiment to 200 meV, 11 M have been secured and contracts have been released for the major components of the experiment. These include the window-less gaseous tritium source, the main spectrometer vessel and the building, which will house the experiment. Technical challenges in designing the gaseous source have resulted in delays but additional engineering resources have been identified and the first tritium runs are expected to begin in Fall 2008.

The US participants in the KATRIN collaboration propose to provide two crucial components of the experiment, the data acquisition system (DAQ) and the focal plane detector. To date the US contingent has supplied the data acquisition system that is being used to commission the pre-spectrometer and an electrode system in the pre-spectrometer that is used to reduce backgrounds. Both will provide important benchmarks for the final DAQ and the electrode system being designed for the main spectrometer vessel.

Activity on the US side has also been intense. Joseph Formaggio accepted a tenure track position at MIT and has taken with him the responsibility to provide the detector calibration system and the active veto and shield. This expansion of the US KATRIN contingent is a very positive move but now places an emphasis on management. Keith Rielage accepted a position at the Los Alamos National Laboratory. We are fortunate to welcome a new post-doctoral member to the collaboration, Brent VanDevender. The UW/CENPA will remain the lead institute in the US collaboration, housing both the spokesperson and the project manager.

In July 2005 we submitted to the KATRIN collaboration the Detector Design Document which laid out the design solution to meeting the needs of the focal plane detector and DAQ. This design is shown in Fig. 1.7-3. Since then we have been engaged in R&D to further refine the design. This R&D is scheduled to be completed in July 2006 and production of the fabrication drawings will begin.

In October 2005 we submitted to the DOE a proposal for funding the US contribution to the KATRIN experiment. This has been circulated for scientific review. At the time the DOE strongly encouraged us to formulate a Project Execution Plan (PEP). This PEP underwent review in January and the very helpful suggestions for improvement are being incorporated in the plan.

Central to the success of the US effort is the focal plane detector itself. This consists of a 10-cm diameter PIN diode array of several hundred pixels. A detector of this size, coupled with our requirement of a thin (50 nm) dead layer on the entrance window is very unusual.

As a result, many of the manufacturers who have quoted on providing the array have included relatively costly R&D.

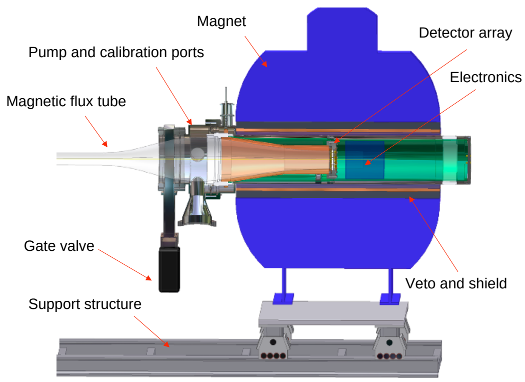

Figure 1.7-3. A cross-section showing the main components of the focal plane detector.

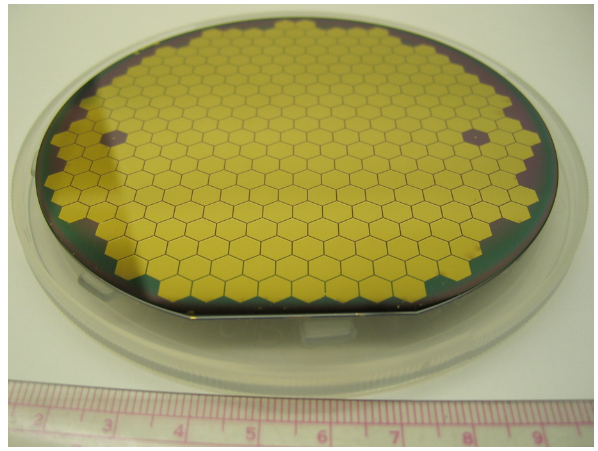

Figure 1.7-4. The prototype PIN diode array from WTC showing the hexagonal pixel shapes.

We are working with the manufacturers to measure the thickness of the dead layer using our electron gun at UW. One exciting development is the discovery that the Washington Technology Center (WTC) on the UW campus has the capability of manufacturing such detector arrays. We have contracted with WTC to provide three prototype arrays for study, the first of which is shown in Fig. 1.7-4.

The identical hexagonal shape of each pixel allows pixel-to-pixel comparison to ensure there is no variation in performance across the face of the detector. The final array will employ a dart board pixel arrangement which better addresses the physics needs. If successful the WTC effort promises considerable cost savings. The focal plane detector system is a complex apparatus that is a critical component in the success of the KATRIN experiment. Providing a commissioned detector and DAQ in time for the beginning of tritium data taking in fall 2008 will be a challenge that will draw heavily on the talents of the CENPA support staff.

1.8 The design of the KATRIN detector system

T. H. Burritt, G. C. Harper, M. J. Leber, R. G. H. Robertson, B. VanDevender, B. L. Wall and J. F. Wilkerson

In July 2005, with the release of the Detector Design document, the fundamentals of the design of the focal plan detector system were established. This enabled detailed design of the detector system to proceed. The main components of this design are shown in Fig. 1.8-1.

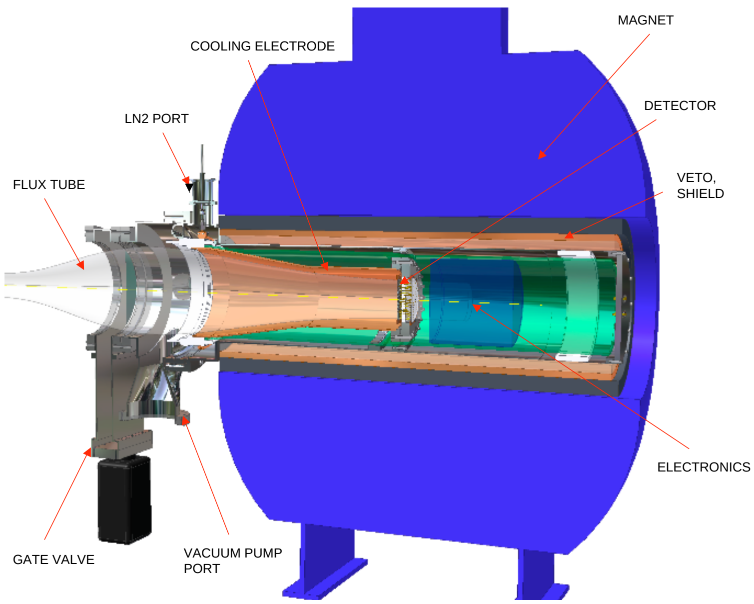

Figure 1.8-1. Cross-sectional view of the focal plane detector system showing the main components.

The detector housing is located inside the 40 cm diameter bore of a 3 to 5 tesla superconducting magnet which focuses the electrons from the beta decay onto the face of the detector. Also housed inside the bore of this magnet is an inert shield of lead and OFHC copper used to reduce background radiation and an active veto of plastic scintillator to register cosmic ray muons. The inert shield and active veto will be designed and manufactured by MIT. In order to gain easy access to the detector housing the magnet is mounted on a rail support structure that allows both the magnet and the veto system to be simply slid aside. In addition, this support structure allows the position of the magnet to be adjusted with respect to the detector in order to center the magnetic flux tube on the face of the detector. Details of the detector vacuum housing are shown in Fig. 1.8-2.

The detector housing contains two levels of vacuum. The extreme high vacuum of 10^{-11}mbar contains the detector and may be separated from the main spectrometer by a 250 mm gate valve. This gate valve allows the detector system to be operated independently of the rest of the experiment if so desired. To reduce electronic noise, the detector, its support structure and preamplifiers operate at $\approx$ 120K and therefore are surrounded by an insulating, medium vacuum, of $\approx 10^{-6}$ mbar. The detector and front-end electronics are mounted at the end of a conical copper electrode attached to a cylindrical ceramic insulator. This ceramic

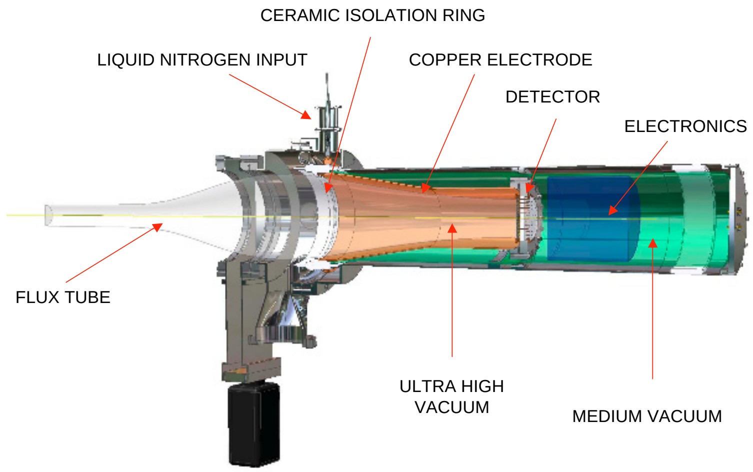

Figure 1.8-2. Details of the detector vacuum housing and cooling.

insulator is cooled by liquid nitrogen. A total of 10 W of heat must be removed from the detector and electronics. The ceramic insulator is attached to the ultra high vacuum chamber which contains the pumping ports and port to insert calibration sources and an electron gun which can be swept across the face of the detector to calibrate individual pixels with a variable, mono-energetic electron beam. If low energy radioactive backgrounds prove to be higher than acceptable it is possible to apply post acceleration to the electrons, raising them above the radioactive background. This is achieved by applying up to 30 kV to the copper electrode, detector and electronics. These backgrounds come principally from materials in the immediate surrounds of the detector such as the detector mount, the electrical connections to the individual pixels and the vacuum signal feed-through. To control these backgrounds we are working closely with manufacturers and assaying all materials to be used in construction. Another design challenge that arises due to the use of high voltages in intense magnetic fields is the possibility of enhanced ExB breakdown, even at the extreme levels of vacuum surrounding the detector and electrode. R&D into the questions of radioactive backgrounds, custom components such as ceramic insulators and feedthroughs will continue into July after which it is expected that the design will be frozen and fabrication drawings will be produced.

1.9 Electron gun for profiling silicon detectors for KATRIN

P.J. Doe, G. C. Harper, B. Kuffner* and J. A. Mitchell

The monoenergetic electron source developed in 2003[1] to profile electron backscattering with respect to incident angle of the large area silicon detectors to be used in the KATRIN experiment has been extensively modified to accommodate large (10 cm diameter) multi-pixel detectors. The apparatus uses an electron gun and an einzel lens that were previously translated via an external UHV X-Y translator. There is also an oil-free pumping system,[2] and the associated stand, diagnostics, power supplies, and sample chamber. The sample chamber has been completely redesigned.

The gun produces low energy (of order 1 eV) electrons by UV photoemission from a stainless steel surface. A UV grade silica fiber and hypodermic needle collimator direct photons from a mercury arc UV lamp onto a 1 mm diameter spot on the emission surface. The electrons are accelerated through a potential that can be varied up to -30 kV. The electron beam is focused to a 1 mm diameter spot on the device under test (DUT) 0.6 m from the emission surface by an einzel lens operating at about half of the accelerating potential. Electrostatic and beam transport studies of the gun and beam optics were been done using the ion optics program SIMION.[3]

It is now possible to scan the DUT under the electron beam in both transverse axes with an internal, vacuum-compatible X-Y translator table[4] having a range of ± 5 cm in each axis. The table may be rotated to any angle up to 60° with respect to the longitudinal axis. Cooling and noise-free pumping are provided by a small dewar of liquid nitrogen (LN_2). The boiled off vapor from the LN_2 is used to cool the detector. Two E-type chromel-constantan thermocouples are used to measure the temperatures of the DUT and the detector cooling ring.

All of the required parts have been procured and assembled. All of the utilities are accessible from the top 0.5 m diameter flange. The flange can be removed with an existing crane and placed on a work stand. The work stand allows the operator to rotate the flange 180° and clamp in place with no assistance to fully expose all of the serviceable parts of the assembly.

*Berufsakadamie Karlsrhue University of Cooperative Education, Karlsruhe, Germany.
[1]CENPA Annual Report, University of Washington, (2003) p. 65.
[2]Varian Vacuum Products, Lexington, MA 02421.
[3]SIMION 3D, version 6.0, David A. Dahl, Idaho National Engineering Lab, Idaho Falls, ID 83415.
[4]Newmark Systems Inc., Mission Viejo, CA 92691.

1.10 Developing a complete Geant4 simulation of the KATRIN detector region

J. A. Formaggio,* M. L. Leber, R. G. H. Robertson and J. F. Wilkerson

KATRIN is a next generation tritium beta-decay experiment with an expected sensitivity an order-of-magnitude better than previous experiments. To achieve this level of sensitivity, detector-related backgrounds must be limited to 1 mHz. To guide the detector design and understand the detector backgrounds, a complete Geant4 simulation is being developed. Muons, neutrons, and radioactive isotopes have been simulated, including the ^{238}U chain, the ^{232}Th chain, the ^{210}Pb chain, and ^{40}K.

Since the last annual report,[1] much progress has been made. More materials and their expected radioactive impurities have been added, including the connections between detector and mount, conflat^{TM} flanges, and insulators for the high-voltage electrode. A plastic scintillator records energy depositions and a time stamp, so simultaneous events from cosmic-ray secondaries in the beta detector can be vetoed. Although the simulation geometry is not complete, it can be used to guide the detector design. Copper shielding has shown as much as 80% higher rates from cosmic-ray secondaries than lead, so a pure lead or lead-copper combination will be used for shielding. A thicker detector has lower intrinsic noise, but may have a higher detection efficiency for background gammas. Fig. 1.10-1 shows the rate increase from thorium decays in the connections behind the detector, which can be as high as 15%. A greater effect will be from muon secondaries because only neutral particles, like photons, enter the high magnetic field region. Depending on the post acceleration voltage, a thicker detector may increase rates from muon secondaries as much as 80%.

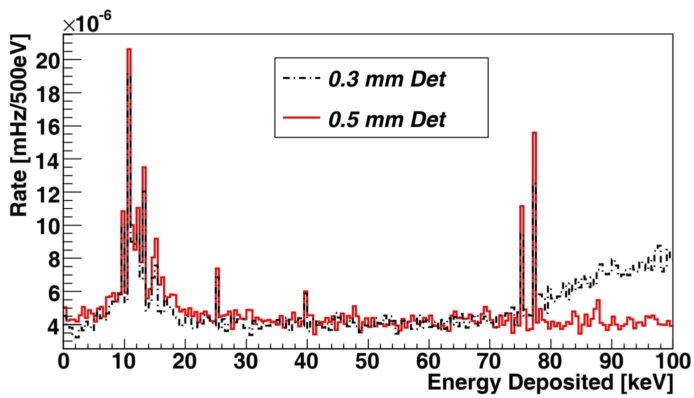

Figure 1.10-1. comparison of the background rates from the electrical connections behind the silicon detector for different thickness detectors.

Progress is being made toward a complete model for detector-related backgrounds in the KATRIN experiment.

*Presently at Massachusetts Institute of Technology, Building 26-568, 77 Massachusetts Ave, Cambridge, MA 02139.

[1] CENPA Annual Report, University of Washington (2005) p. 39.

1.11 Estimating background rates for KATRIN from cosmic rays ionizing the gaseous tritium source

J. A. Formaggio,* M. L. Leber, R. G. H. Robertson and J. F. Wilkerson

KATRIN's source is a 10 meter long tube filled with high purity tritium gas.[1] Electrons ejected from the gas molecules by cosmic rays could create a background to the beta decay measurement if they are in the energy region near the endpoint, 18.6 keV. Since these background electrons are created in the source, they have the same detection efficiency as beta decay electrons. Just like the beta electrons, only those created in the guided magnetic flux tube with an opening angle of 51 degrees will reach the detector. Using GEANT4, the background rate from these delta electrons has been calculated.

For this simulation, the source geometry is drastically simplified. A stainless steel tube, 1 cm thick walls, is filled with hydrogen gas. Muons,[2] high energy protons and neutrons,[3] and ambient neutrons[4] impinge on the tube and ionize the gas. The delta electrons produced in the simulation with the relevant energy and opening angle are counted and converted to a rate of ionization in the KATRIN source.

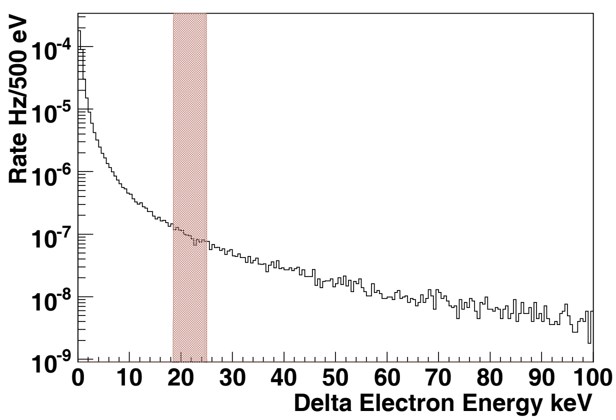

Figure 1.11-1. Rate of delta ray production in the source will be the background rate in the detector conservatively assuming perfect transmission. The lower limit on the energy window is from the main spectrometer voltage setting, the upper limit from the detector energy resolution.

Fig. 1.11-1 shows the spectra of ejected electrons, which falls like $\frac{1}{E^2}$, matching theoretical predictions. In the simulation the energy lost by the cosmic rays is consistent with the stopping power of hydrogen gas. The rate of delta ray production in the region of interest, 18.5-25 keV, is 1.33 ± 0.02 μHz. This is well below the design goal of 10 mHz background, and no shielding is necessary for KATRIN's source.

*Presently at Massachusetts Institute of Technology, Building 26-568, 77 Massachusetts Ave, Cambridge, MA 02139.

[1]KATRIN Design Report, (2004) http://www-ik.fzk.de/ katrin/publications/index.html.

[2]A. J. Da Silva, *Development of a low Background Environment for the Cryogenic Dark Matter Search,* Ph.D. dissertation, University of British Columbia, Vancouver, Canada.

[3]S. Eidelmann *et al.*, Phys. Lett. B **592** 1, 24 (2004).

[4]M. Yamashita, *et al.*, J. Geophys. Res. **71**, 16, 3817 (1966).

1.12 KATRIN preamplifier design and development

H. Gemmeke,* R. G. H. Robertson and T. D. Van Wechel

Two different charge sensitive preamplifier designs are currently under development by the CENPA electronics shop. One of the designs will be selected for use on the multi pixel Si PIN diode detector array at the focal plane of the KATRIN experiment. Since the preamplifiers will be cryogenically cooled, the goal is to minimize power dissipation. Another criterion is that the preamplifier design have low noise, with a goal of 600 eV FWHM. The first preamplifier is of a conventional design with a folded JFET cascode amplifier as the first stage. The second preamplifier is of a more unconventional design, a parametric amplifier.

The preamplifier design consisting of a folded cascode JFET input stage followed by a low power op amp second stage is nearly complete. For the cascode input stage a compromise has to be made between the output noise level and power dissipation. In general increasing the JFET current (Id) decreases the noise level. The noise level also decreases as the JFET's drain to source voltage (Vds) is increased. This effect is much weaker than that of the noise to current dependence. In the case of the folded cascode, another noise contributor is the current noise due to resistor Rd between the junction of the drain of the JFET and the emitter of the folded cascode PNP transistor, and the positive power supply. This resistor which sets the JFET current produces a noise current that is inversely proportional to the square root of resistor value. This implies that for a given power supply voltage and Vds, that if the value of this resistor is reduced to increase Id, to lower the FET's noise contribution, part of this reduced noise contribution is lost due to the increased noise contribution of Rd. Since the noise level is only loosely dependent upon Vds, it has been shown by circuit simulations that the best compromise if one desires to keep the supply voltage low for minimum power dissipation, is to set Vds to a low value such as between one and two volts so that for a given supply voltage, the value of Rd may be maximized. The lower Vds reduces the amplifier bandwidth somewhat, but since it is still over an order of magnitude greater than the Gaussian shaper's bandwidth, it is acceptable.

The proposed design has an overall preamplifier power dissipation of 84 to 90 mW, of which 72 mW is in the cascode stage and 12 to 18 mW is in the second stage op amp. The supply voltages are plus and minus 6 volts, with Vds set to 1.7 volts and Id at 10 mA. Pspice simulations with a detector capacitance of 15 pF predict that the noise level at the output of a 4-μS Gaussian shaper following the preamplifier is 564.8 eV FWHM at 300K and 453.1 eV FWHM, if the preamplifier is cooled to 200K. If Id is reduced to 5 mA, the total power dissipation is reduced by 30 mW, but the noise level increases to 605.6 eV FWHM at 300K and 490.5 eV FWHM at 200K. This folded cascode design also has potential use for the Majorana experiment and with modifications for Nanopore DNA sequencing. (See section 6.3.)

The main motivation for the parametric amplifier is that the first stage has much lower power dissipation than a conventional amplifier design. The disadvantage is in circuit com-

*Forschungszentrum Karlsruhe, Institut fur Prozessdatenverabeitung und Elektronik, POB 3640, 76021 Karlsruhe, Germany.

plexity. Parametric amplifiers are devices that provide amplification through the variation of a circuit parameter, in our case capacitance. The input stage of the parametric preamplifier has a varactor bridge consisting of a pair of reverse biased varicap diodes pumped in anti phase by a local oscillator(LO) signal. The junction of the varicap diodes is both the input and output of the first stage. The DC and low frequency input voltage appearing at the junction determines the degree of unbalance of the bridge with the pump voltage at the LO frequency developed at the diode junction being proportional to the degree of bridge unbalance. The detector is AC coupled through a coupling capacitor in series with an inductor acting as a low pass filter to the junction of the varicap diodes. Charge from the detector due to ionization events redistributes to the varicap diode junction producing a change in voltage at the diode junction modulating the pump voltage. The detector signal which is at a very high impedance, modulates the pump signal which is at a low impedance resulting in a large power gain. The pump voltage output is capacitively coupled to a second stage RF amplifier. The output of the second stage is transported outside of the cryostat to the room temperature environment where it is synchronously demodulated by a phase sensitive detector.

A prototype with a LO frequency of 200 MHz was constructed late last year as a proof of concept. It demonstrated that the concept works but had poor noise performance due to the poor impedance matching between the first and second stage. Also the power dissipation was quite high due to the use of a commercial broadband RF amplifier as a second stage. The new design currently under development will have a tuned MOSFET amplifier dissipating 6 mW for the second stage. Also using varicaps with a higher capacitance versus voltage slope and increasing the LO amplitude will help to improve the signal to noise ratio. The new design will use an active mixer for the phase sensitive detector, rather than the diode based Double Balance Mixer used by the prototype. A means of adjusting the relative phase shift between the LO and RF inputs of the mixer needs to be developed to compensate for circuit phase shifts and propagation delay.

Majorana

1.13 The Majorana neutrinoless double-beta decay experiment

J. F. Amsbaugh, J. A. Detwiler, P. J. Doe, A. García, M. A Howe, R. A. Johnson, K. Kazkaz, M. G. Marino, S. R. McGee, R. G. H. Robertson, A. G. Schubert, B. A. VanDevender and J. F. Wilkerson

Neutrinos continue to provide some of the most exciting opportunities in understanding our universe. Neutrinoless double-beta decay ($0\nu\beta\beta$) provides the physics community with the opportunity to build on our successes in understanding the neutrino and crafting a new standard model. Determining if neutrinos are Dirac or Majorana particles is one of the most important questions facing the physics community today. The Majorana experiment aims to answer this question. For the first time we can mount experiments that probe the neutrino mass region below the upper limits set by direct kinematical searches (tritium) and suggested by observational cosmology, while planning scaled approaches that can address the lower bounds of mass defined by the atmospheric and solar + reactor neutrino oscillation experiments.

Our proposed method uses the well-established technique of searching for $0\nu\beta\beta$ in high-purity Ge diode radiation detectors that play dual roles of source and detector. The technique is augmented with recent improvements in signal processing, detector design, and advances in controlling intrinsic and external backgrounds. Progress in signal processing from segmented Ge-diode detectors offers significant benefits in rejecting backgrounds, reducing sensitivity of the experiment to backgrounds, and providing additional handles on both signals and backgrounds through multi-dimensional event reconstruction. Development of sophisticated Cu electroforming methods allow the fabrication of ultra-low-background materials required for the construction of next generation detectors.

The envisioned Majorana experiment will consist of one or more modules containing 57 high-resolution intrinsic germanium detectors, each with mass $\sim$1.1 kg of Ge enriched to 86% in ^{76}Ge. The crystals will be deployed in an ultra-low-background electroformed Cu cryostat, located deep underground within a low-background shielding environment. Observation of a sharp peak at the $\beta\beta$ endpoint would quantify the $0\nu\beta\beta$ decay rate, demonstrate that neutrinos are Majorana particles, indicate that Lepton number is not conserved, and provide a measure of the effective Majorana mass of the electron neutrino.

The physics goals for the first phase of Majorana are to:

- Probe the quasi-degenerate neutrino mass region above 100 meV.
- Demonstrate that backgrounds, at or below 1 count/ton/year in the $0\nu\beta\beta$ - decay peak 4-keV region of interest, can be achieved that would justify scaling up to a 1 ton or larger mass detector.
- Definitively test the Klapdor-Kleingrothaus claim to have observed $0\nu\beta\beta$ - decay in ^{76}Ge in the mass region around 400 meV.

These goals are consistent with recent recommendations from the *DNP/DPF/DAP/DPB Joint Study on the Future of Neutrino Physics* and the conclusions on $0\nu\beta\beta$ reported by the Neutrino Scientific Assessment Group (NuSAG).

The Majorana Scientific Collaboration consists of about 100 scientists and 16 collaborating institutions from four countries with extensive experience in double-beta decay and ultra-low-background experiments. CENPA collaborators are currently involved in a number of research and development related projects as described in the following sections.

1.14 DAQ and SOH for Majorana

J. A. Detwiler, M. Howe, A. Myers, T. Van Wechel and J. F. Wilkerson

We have developed an initial conceptual plan for the Majorana data acquisition (DAQ) and State of Health monitoring (SOH). The DAQ systems include the digitization electronics, software management of the readout, and data storage. The SOH system encompasses hardware and software safety monitors and interlocks for detector and support systems, as well as electronics health and some data quality monitoring.

We drafted a list of tasks relevant to the implementation of the DAQ and SOH, and incorporated this list into the Majorana work-breakdown structure. We estimated the funds and labor necessary to complete each task based on price estimates for materials and services, and based on our experiences in previous experiments such as SNO. We identified several places where different options may allow for considerable savings or risk management. For example, the digitization electronics may be built in-house, or commercial systems may be purchased. Various points of interface with other Majorana systems were also identified and discussed among collaborators.

The DAQ and SOH plans and costing were incorporated into the Majorana reference design and the draft proposal was submitted to the DOE. We are in the process of refining that reference design to optimize cost and schedule versus physics impact of the experiment, and updating the proposal to reflect those refinements.

1.15 The Majorana sensitivity to excited-state double-beta decays of ^{76}Ge

S. R. Elliott,* V. M. Gehman,* K. Kazkaz, D.-M. Mei* and J. F. Wilkerson

The Majorana experiment[1] will be searching for neutrinoless double-beta ($0\nu\beta\beta$) decays of ^{76}Ge. The anticipated background levels in the Majorana detector are sufficiently low to allow for a search for two neutrino double-beta decays to an excited state of the daughter nucleus. Measuring the half life of this excited state two-neutrino double-beta (ES$2\nu\beta\beta$) decay will provide additional direction in the development of the theory behind calculating nuclear matrix elements.[2]

^{76}Ge is expected to decay to the first excited 0^+ state (also referred to as the "0_1^+" state) of ^{76}Se, with two accompanying cascade gammas with energies 563 and 559 keV. ^{76}Ge may also decay to the 2_1^+ state, with only one accompanying 559 keV gamma. While the phase-space factor for this latter decay is roughly an order of magnitude larger than that of the former, the matrix elements are relatively suppressed by roughly two orders of magnitude.[2] Thus decays to the 0_1^+ state are predicted to be more prevalent. Furthermore, from an experimental standpoint, it is reasonable to expect a search for a coincidence involving two cascade gammas rather than just one will offer greater background reduction capabilities. For these reasons, the Majorana experiment is focusing on decays to the 0_1^+ state.

The Majorana detector will consist of modules each containing an array of germanium crystals enriched to 86% ^{76}Ge. The array contains 3 layers of 19 crystals arranged in a hexagon, with four unique crystal locations per layer (see Fig. 1.15-1). We have performed preliminary calculations of the efficiency of this module to the ES$2\nu\beta\beta$ signal using MaGe, a GEANT4- and ROOT-based simulation framework collaboratively developed by the Majorana and GERDA[3] collaborations. Requiring a very simple 3-crystal cut, with two of the crystal energies being within 2 keV of 559 and 563 keV, the efficiency is calculated to be 0.983(1)%. The crystals may be segmented, though, to reduce the backgrounds to the $0\nu\beta\beta$ signal. One possible segmentation scheme involves 2 radial (i.e., "pie wedge") by 3 axial (i.e., "hockey puck") segments. Using a very simple 3-segment analysis that parallels the 3-crystal cut above, the efficiency is increased an additional 0.635(3)% to 1.618(3)% total. The efficiency of the module for this decay may be further increased with alternative analytical methods involving only energy cuts and relaxing the 3-crystal or 3-segment requirements. Such additional methods are currently under study.

The segmentation of the crystals may be higher, for instance up to 6×6 segments. In this case, the additional, simple 3-segment efficiency is 0.466(2)%, or 1.449(2)% total–a bit lower than in the 2×3 case. The reason for this is that with 6×6 segmentation, the individual segments have smaller volume, and while the gamma rays are therefore more likely to escape the segment in which the decay occurred, they are disproportionately less likely to deposit their full energy in a single segment. Relaxing the 3-segment requirement, however, may increase the efficiency of the 6×6 segmentation over that of the 2×3 scheme, as the driving

*P-23, MS H-803, Los Alamos National Laboratory, Los Alamos, NM 87545.

[1] http://majorana.pnl.gov.

[2] J. Suhonen and O. Civitarese, Phys. Rep. **300**, 123 (1998).

[3] http://www.mpi-hd.mpg.de/ge76.

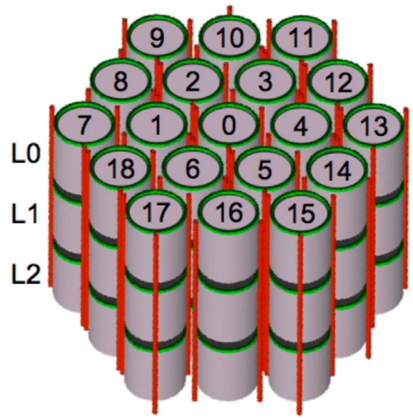

Figure 1.15-1. Simulation rendering of the Majorana detector module. There are four unique crystal locations per layer (typical crystal used in simulations are 0, 1, 7, and 8 in each of the three layers). The shielding, cryostat, and most of the support structure are omitted for clarity. The vertical bars are copper tubes comprising part of the support structure.

consideration then is only whether or not the gamma rays escape the segment in which the decay occurred, and the dependence on the photopeak efficiency of the gammas is reduced.

ES$2\nu\beta\beta$ decays are expected to have a half life 10-100 times as long as the half life of ground state $2\nu\beta\beta$ decays, 1.9×10^{21} years.[4] Assuming a half life of 10^{23} years, then, for the excited state decay, a single Majorana module will observe 25 such events in 8 months of live time. This live time requirement may be reduced when analysis methods to increase the signal efficiency are developed.

The backgrounds to the ES$2\nu\beta\beta$ decay come primarily from uranium and thorium in the germanium crystals, support structure, cryostat, and shielding, as well as ^{60}Co and ^{68}Ge in the crystals. At the anticipated levels of radioisotope contamination, the number of background events expected to survive the simple 3-crystal and 3-segment analysis cuts is only 0.002 counts over 8 months of live time. Thus this signal is essentially “backgroundless”. If more analysis cuts are developed to increase the sensitivity to the excited state signal, the backgrounds will have to be re-analyzed as well to calculate their level of contribution.

[4]H. V. Klapdor-Kleingrothaus *et al.*, Eur. Phys. J. A **12**, 147 (2001).

1.16 Development of simulation and analysis frameworks for Majorana

J. A. Detwiler, R. A. Johnson, K. Kazkaz, M. G. Marino and A. G. Schubert

Monte Carlo (MC) radiation transport simulation models have been developed for Majorana using MaGe, an object-oriented MC simulation package based on the Geant4 toolkit and optimized for simulations of low-background germanium detector arrays. MaGe is being jointly developed by the Majorana and GERDA[1] collaborations, using professional programming techniques in consultation with collaborators from the National Energy Research Scientific Computing Center (NERSC) at LBNL. MaGe defines a set of physics processes, materials, constants, event generators, etc. that are common to these experiments, and provides a unified framework for geometrical definitions, database access, user interfaces, and simulation output schemes in an effort to reduce repetition of labor and increase code scrutiny.

Our group has been instrumental in coding much of the backbone of MaGe, including the framework for handling general detector geometries, the list of simulated physics processes, and various event generators. We have also been involved in coding quality control, and have implemented several specific detector geometries within MaGe. We are in the process of validating the various physics processes simulated by MaGe in order to extend its applicability an increase confidence in MaGe results. These studies are discussed in more detail elsewhere in this Annual Report. We are also in the process of adding the capability to simulate pulse shapes generated by energy deposits in solid-state germanium detectors.

In order to organize the analysis of simulated and test data, and to prepare for analysis of physics data, we have proposed and begun to implement a software analysis framework for Majorana. The C++ framework is based on the ROOT data analysis toolkit, and is architectured with a "modular processing design", which standardizes computations performed at the event-loop level. In modular processing, the analysis is divided into several modules, each of which performs specific tasks at three different stages of data processing: at the beginning and end of the full analysis, at the beginning and end of each run processed, and at the event-by-event level. The initial implementation of this framework has been used to analyze background simulations for the Majorana reference design, and to study the background rejection efficacy of various detector options. We are in the process of optimizing the design of the framework and adding pulse shape analysis capabilities.

[1] The GERDA Collaboration, Nucl. Phys. B **143**, p. 567 (2005).

1.17 MaGe simulation of LANL clover detector with AmBe neutron source

A. G. Schubert

The Majorana and Gerda collaborations have jointly developed MaGe, a Geant4 and ROOT based simulation framework, to aid in the design and analysis phases of both experiments. Comparisons between experimental data and MaGe simulation results can be used to verify MaGe's performance. This report describes a MaGe simulation of an experiment performed at LANL.

The experiment used a detector consisting of four Ge crystals arranged in a clover configuration. The detector was surrounded by lead shielding, and an Americium Beryllium (AmBe) neutron and gamma source was located outside of the shield. A slab of polyethylene neutron moderator was placed within the lead shield, between the source and detector. Energy spectra were collected from the Ge crystals for various moderator thicknesses.

The experimental setup was modeled within MaGe. A comparison of experimental data and simulation results appears in Fig. 1.17-1. Overall agreement between the data sets helps to validate the MaGe package and verify calculations of experimental run time. Discrepancies between the locations of some peaks are currently being investigated.

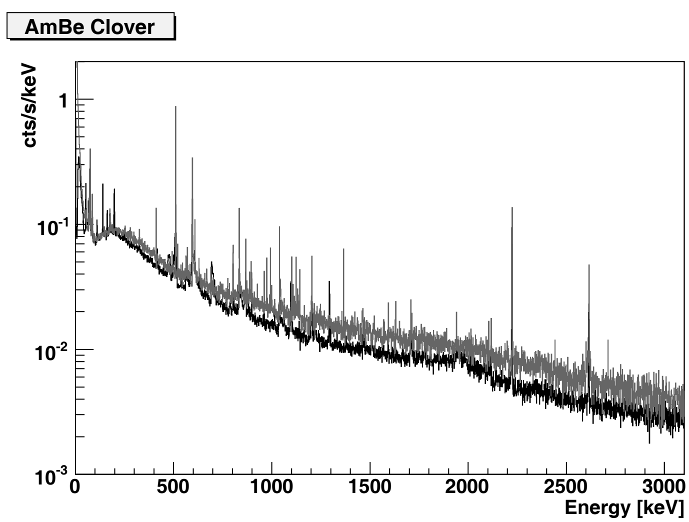

Figure 1.17-1. Comparison of experimental (black) and simulated (grey) energy spectra from a single crystal, for six-inch thickness of polyethylene moderator.

1.18 Simulation of the SLAC electron beam dump experiment using MaGe

M. G. Marino

Understanding the background created by neutrons involves the simulation of their creation, propagation, and interaction with the detector as well as the verification of all associated code. This paper presents work completed concerning the verification of neutron production and transport within the MaGe simulation package.

An experiment has been done at the Stanford Linear Accelerator Center (SLAC) which involved a high energy (28.7 GeV) electron beam incident upon an aluminum beam dump.[1] Neutrons were created mainly by photonuclear interactions initiated by bremsstrahlung photons from the decelerating electrons, and the neutron time-of-flight and energy spectra were measured outside a steel shield and a concrete shield of variable width. A detailed description of the setup of the SLAC beam dump experiment can be found in the reference cited. A 28.7 GeV electron beam was incident upon a cylindrical aluminum beam dump inside a shield housing with an opening to allow the beam to enter. A detector was placed laterally through the shields from the aluminum beam dump and the neutron energy and time of flight (TOF) spectra were measured for shield concrete shield widths of 9 ft, 11 ft, and 13 ft. Some results are shown in Fig. 1.18-1 (FLUKA and experimental data obtained from S. Roeslera *et al.*[2]).

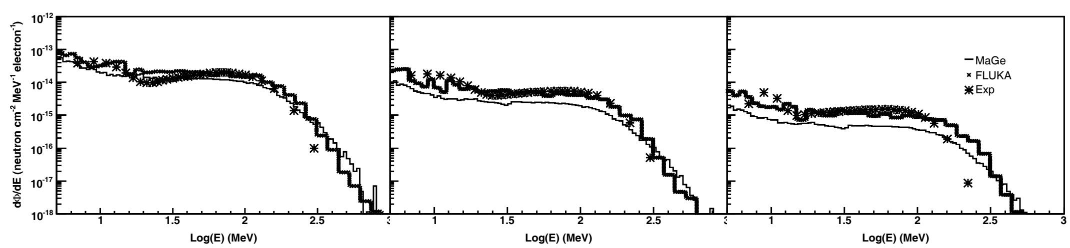

(a) Energy spectra.

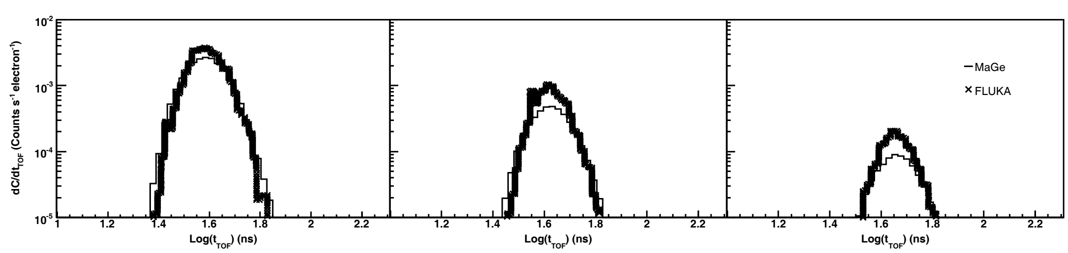

(b) TOF spectra.

Figure 1.18-1. A comparison of calculated and experimental energy and TOF spectra for three shield widths (L to R: 9 ft, 11 ft, 13 ft).

[1] S. Taniguchi *et al.*, Nucl. Instrum. Methods A, **503**, 595 (2003).
[2] S. Roeslera *et al.*, Nucl. Instrum. Methods A, **503**, 606 (2003).

1.19 Studies of α-contamination on high purity Ge crystals

J. A. Detwiler, R. A. Johnson, M. G. Marino and J. F. Wilkerson

The Majorana experiment will search for the neutrinoless double beta decay ($0\nu\beta\beta$) of ^{76}Ge $\rightarrow$ ^{76}Se using 60 kg modules of high purity germanium detectors enriched to 86% ^{76}Ge. The current lower limit on the half-life of this reaction in ^{76}Ge is 1.9×10^{25} years. A full understanding of our backgrounds is a necessary condition if we are to be successful in discerning such a small signal. We report on progress made on understanding surface contamination issues using MaGe, a Geant4 based Monte-Carlo simulation program for the Majorana and Gerda collaborations.

Each 60 kg module in Majorana consists of 57 close-packed 1.1 kg germanium crystals surrounded by a copper cryostat and various "small parts" such as copper support rods, teflon trays, and wiring. We came up with an algorithm to randomly sample any general surface in our simulation, as Geant4 currently has no satisfactory method for sampling the surfaces of complicated volumes. This algorithm was implemented into the MaGe package, and the results have been quite satisfactory. Fig. 1.19-1a shows randomly generated points that are uniformly distributed on the surfaces of a single crystal, support tray, and contact ring in a 60 kg module for Majorana.

Surface contaminants that may deposit energy into our region of interest(2039 ± 2 keV) include the ^{238}U and ^{232}Th radioactive decay chains. The decay daughters of Rn, ^{210}Pb especially, can be particularly problematic. ^{222}Rn is an airborne gas which quickly decays to ^{210}Pb. The chain ^{210}Pb$\rightarrow$^{210}Bi$\rightarrow$^{210}Po$\rightarrow$^{206}Pb deposits a 5.3 MeV α particle from the ^{210}Po decay. If ^{210}Pb plates out on a surface, the long half-life (26 years) will produce a steady stream of 5.3 MeV α particles for a long time. The simulated spectrum in Fig. 1.19-1b is from ^{210}Pb plated out on all the inner surfaces of a 60 kg module.

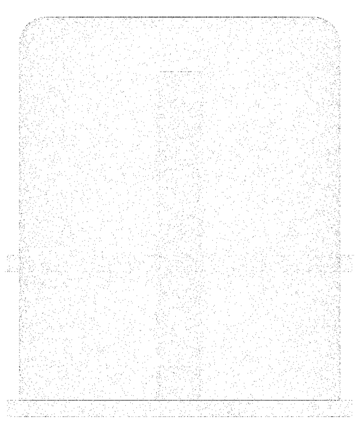

(a)

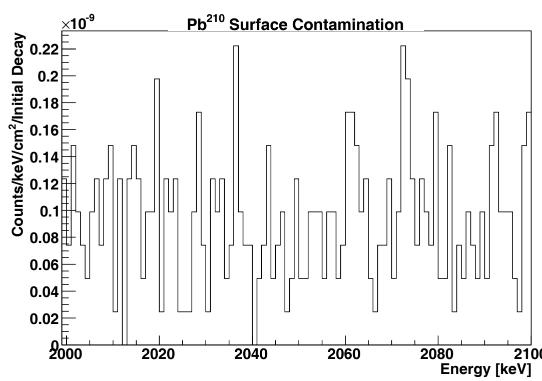

(b)

Figure 1.19-1. (a) Surface points randomly generated on the surface of a crystal, contact rings, and support tray. (b) ^{210}Pb contamination spectrum around the region of interest.

1.20 LArGe, liquid argon compton supressed germanium crystal

C. E. Aalseth,* J. F. Amsbaugh, P. J. Doe, M. H. Toups and J. F. Wilkerson

We have continued using the LArGe apparatus[1] to further understand background suppression in a high purity germanium crystal diode by identifying the Compton scattered gamma ray. This test apparatus consists of a 55 mm diameter by 53 mm P-type crystal suspended in a bath of liquid argon (LAr) with a minimum of 7 cm of LAr surrounding it. The LAr acts as an active shield, emitting scintillation light peaked at 128 nm. The scintillation light is wavelength shifted by a non-metallic visible light reflector, ESR[2], in order that it can be detected by a hemispheric 20 cm photomultiplier tube(PMT) in the LAr. The PMT signal is then used as an anti-coincident veto on the HPGe signal to eliminate events that deposit energy in both the crystal and LAr. The initial test run results were reported last year with background suppression consistent with 0.5 radiation lengths of LAr surrounding the HPGe.

During the subsequent run, the HPGe crystal exhibited high leakage current while biased. This is probably due to contamination of the crystal resulting from a leak to atmosphere in the crystal storage container. After several vacuum bake-outs the crystal performance was still unacceptable and it is now being refurbished by the manufacturer. A crystal replacement was not available for use.

While studying the PMT response without a crystal present, it was noticed that the reflector material acts both as a wavelength shifter and as a visible light guide. A quantitative estimate of the efficiency of these two processes could not be made using the existing apparatus. Modifications were therefore made to allow a summer student (M.T.) to investigate samples of light guide material coated with a wavelength shifter and examine the light guiding effect. A coating technique with polystyrene doped to about 10% TPB, tetraphenyl butadiene, and dissolved in toluene was used on samples of ESR and acrylic. PMT only spectra were collected with background only and an external ^{207}Bi source. Unfortunately, the results are inconclusive due to difficulties with the readout electronics and the investigation will be repeated.

Much of our effort this past year has been directed towards designing an apparatus, which will improve the efficiency of the Compton shield. A larger dewar, 87 cm ID by 137 cm tall has been acquired and will provide three radiation lengths of LAr shield around the crystal. A pressurized liquid nitrogen reservoir maintains the LAr in a liquid state while providing long periods of stable operation between filling the reservoir. To reduce sources of background, the HPGe crystal will be suspended in the argon using low background materials. The front-end components of the preamplifiers will be mounted close to the HPGe to optimize the noise performance. Four PMTs in the LAr will collect the light that has been wavelength shifted and reflected by ESR material, similar to our current apparatus. The crystal handling components are finished and the cryogenic components construction will begin soon.

*Pacific Northwest National Laboratory, Richland, WA 98352.

[1] CENPA Annual Report, University of Washington (2005) p. 46.

[2] also known as VM2000, from 3M Corp.

1.21 Thermal modeling of the MEGA cryostat cooling

J. F. Amsbaugh and D. Nikic*

The Majorana double beta decay[1] experiment has a multiple HPGe crystal prototyping and demonstration project known as Multiple-Element Gamma Assay or MEGA.[2] MEGA makes use of a very high purity electroformed copper cryostat to reduce radioactive background. The design can accommodate up to 8 copper inner cans(IC), each containing a pair of HPGe crystals, on a cooling plate (CP) ring inside an annular vacuum insulated cryostat. The CP is cooled by a long coaxial cold finger exiting the side of the annulus. A LN2 tank removes heat from the far end of the cold finger. To minimize background contributions from materials near the crystals, no black body (BB) radiation shields between the cold parts and the warm cryostat walls are used. The copper IC surrounds and cools the crystals. It also absorbs BB radiation from the cryostat wall. Sufficient heat conductance to the LN2 is required to keep the temperature below the HPGe's maximum operating temperature.

We studied the cryostat thermal performance using ANSYS finite element analysis software[3] by first calculating the maximum steady state temperature rise of the ICs as they conduct the absorbed BB radiation to the CP held at a 100K boundary condition (BC). This is shown in column ΔT_{IC} in Table 1.21-1. Next we calculated the maximum temperature rise in the CP and cold finger assembly as it conducts the IC heat loads into the LN2 (80K) with BB radiation and thermal contact conductivities accounted for. This is shown in column ΔT_{CP} in Table 1.21-1. The maximum temperature of the IC's is obtained by adding the two delta T's to the liquid nitrogen boiling point (80 K) to get the temperature given in column Temp. in Table 1.21-1. Solutions were obtained for copper emissivities, $\epsilon = 0.01, 0.05, 0.1, 0.2$. Finally, transient cool-down calculations of the previous model starting at 300K and modeled 96 or 192 hours were done. These results (not reported) are for an empty model since HPGe crystal heat capacity was not included but are consistent with the steady state calculations, verifying good convergence.

The material properties and contact conductivities ($IC = 7000 W/m^2K$ and $CF = 1500 W/m^2K$) used were typical for smooth OFHC copper. The ϵ of polished copper[4] ranges from 0.04 to 0.01and lightly oxidized is about 0.2.

ϵ	ΔT_{IC}	ΔT_{CP}	Temp.
0.01	0.48 K	5 K	86 K
0.05	2.4 K	26 K	109 K
0.1	4.8 K	52 K	137 K
0.2	9.6 K	105 K	195 K

Table 1.21-1. Steady State ANSYS results.

Further study and comparison with cool down data is needed, but the temperature results shows that copper surface ϵ and the contact conductivities need to be carefully considered and optimized. We have also accomplished our goal of gaining experience using ANSYS.

*Presently at Boeing Company, Seattle, WA.
[1]Information available online at http://majorana.pnl.gov
[2]K. Kazkaz *et al.*, IEEE Trans. Nucl. Sci. **51**, 1029 (2004).
[3]ANSYS Inc., Canonsburg, PA 15317.
[4]Y.S. Touloukian and D.P. DeWitt, *Thermophysical Properties of Matter*, Vol.7 Thermal Radiative Properties, p.136, IFI/Plenum, New York, 1970-

1.22 Monte Carlo simulation studies of the LoMo counting facility

J. A. Detwiler, J. A. Formaggio,* R. A. Johnson, M. G. Marino, S. R. McGee, A. G. Schubert and J. F. Wilkerson

Researchers at Pacific Northwest National Laboratory (PNNL) and the University of Washington (UW) have been collaborating on the design of an ultra-low-background counting facility to be constructed at Lower Monumental Dam (LoMo) on the Snake River in Eastern Washington State. Monte Carlo (MC) radiation transport simulation models were developed for a LoMo prototype screening detector and for the existing 329/17A Ultra-Low-Background screening detector (17A) using MaGe,[1] an object-oriented MC simulation package based on the Geant4 toolkit and optimized for simulations of low-background germanium detector arrays. MaGe is being jointly developed by the Majorana and GERDA[2] collaborations.

System performance studies were performed with the PNNL 17A detector, since the LoMo cryostat and crystal design is still at the conceptual stage. These initial studies were based on several short calibration runs taken with the 17A detector using ^{60}Co and ^{22}Na sources. The agreement between MC and data was very nice over almost the entire energy scale. Efficiencies and sensitivities for standard sample geometries were calculated for the 17A detector and compared with data where available. MaGe's arbitrary sample geometry framework allows for such calculations to be performed for any given sample.

Copper purity requirements for the LoMo depth were assessed with an analytical calculation based on the method outlined in Heisinger *et al.*[3] for estimating the spallation production of radioactive isotopes in underground experiments. The total activity of all radioactive spallation products at LoMo depth was found to be 290.4 μBq/kg, where most of the activity is from ^{57}Co, ^{58}Co, and ^{60}Co. The equivalent activity for intrinsic ^{238}U and ^{232}Th in the copper was found to be 23.4 and 71.5 μBq/kg, respectively. Efforts to verify cosmogenic activation physics in MaGe are ongoing so that these calculations can be backed-up with full end-to-end MC simulations.

For the LoMo geometry, ^{238}U and ^{232}Th decay chains were simulated in the copper can and coldplate surrounding the crystal, and in the passive lead shielding. These simulations indicated that backgrounds from lead impurities are about an order-of-magnitude lower than those from the copper at LoMo depths, and hence are not large enough to warrant an inner layer of ancient lead or high-purity copper. The ambient γ radiation at the LoMo site was measured by PNNL researchers and simulated with MaGe. This work indicated that no more than 10 inches of lead is needed to reduce the external γ background below the levels expected from cosmogenic activation of copper. These studies implied that significant cost savings could be obtained with a simplified passive shielding design without impacting the physics. However, further studies on the shielding of direct cosmogenic backgrounds, particularly backgrounds from spallation neutrons, will need to be performed when the μ-nuclear and hadronic physics in MaGe have been verified.

---

*Presently at Massachusetts Institute of Technology, 77 Massachusetts Ave, Cambridge, MA 02139.

[1] The Majorana Collaboration, Nucl. Phys. B **143**, p. 544 (2005).

[2] The GERDA Collaboration, Nucl. Phys. B **143**, p. 567 (2005).

[3] B. Heisinger *et al.*, Earth Planet. Sci. Lett. **200**, p. 345 (2002).

2 Fundamental Symmetries and Weak Interactions

Torsion Balance Experiments

2.1 Torsion balance search for spin coupled forces

E. G. Adelberger, C. E. Cramer and B. R. Heckel

We have completed a year-long search for new spin-coupled forces using our second-generation spin pendulum.[1] The spin pendulum, a net spin dipole containing approximately 6×10^{22} polarized electron spins, rotates about its fiber axis at a constant angular velocity. Consequently, its affinity for a preferred direction in space (or lack thereof) appears as a modulation of its angular position at the rotation frequency. The amplitude of this modulation is itself modulated both daily and annually as the orientation of the fiber axis changes with the earth's rotation and orbit around the sun. Analyzing data taken over thirteen months for signals modulated at solar or sidereal periods, we constrain the energy required to flip a spin in a hypothetical spin-coupled field to be less than 10^{-21} eV. Throughout the year, we performed systematic tests to measure the sensitivity of our apparatus to disturbances caused by tilt, temperature, magnetic fields, and local gravitational gradients. No significant corrections to the data had to be applied.

The constraint on spin-coupled forces can be interpreted as a limit on possible simultaneous Lorentz and CPT violation as described by Colladay and Kostelecký[2] as well as coupling to an astronomical source via pseudoscalar bosons[3] or massless bosons constrained only by rotational and translational invariance.[4] In the Kostelecký framework, we provide an upper limit on the CPT-violating parameter $|\tilde{b}^e| \leq 6.7 \times 10^{-21}$ eV that should be compared to the benchmark value $m_e^2/M_{\mathrm{P}} = 2 \times 10^{-17}$ eV, where m_e and M_{P} are the electron and Planck masses, respectively. Fig. 2.1-1 shows our limits on pseudoscalar boson coupling compared to the previous results reported by Youdin *et al.*,[5] Ni *et al.*[6] and Wineland *et al.*[7]

[1] CENPA Annual Report, University of Washington (2004) p. 7.
[2] D. Colladay and V. A. Kostelecký, Phys. Rev. D **55**, 6760 (1997).
[3] J. E. Moody and F. Wilczek, Phys. Rev. D **30**, 130 (1984).
[4] B. A. Dobrescu and I. Mocioiu, private communication.
[5] A. N. Youdin *et al.*, Phys. Rev. Lett. **77**, 2170 (1996).
[6] W. T. Ni *et al.*, Phys. Rev. Lett. **82**, 2439 (1999).
[7] D. J. Wineland *et al.*, Phys. Rev. Lett. **67**, 1735 (1991).

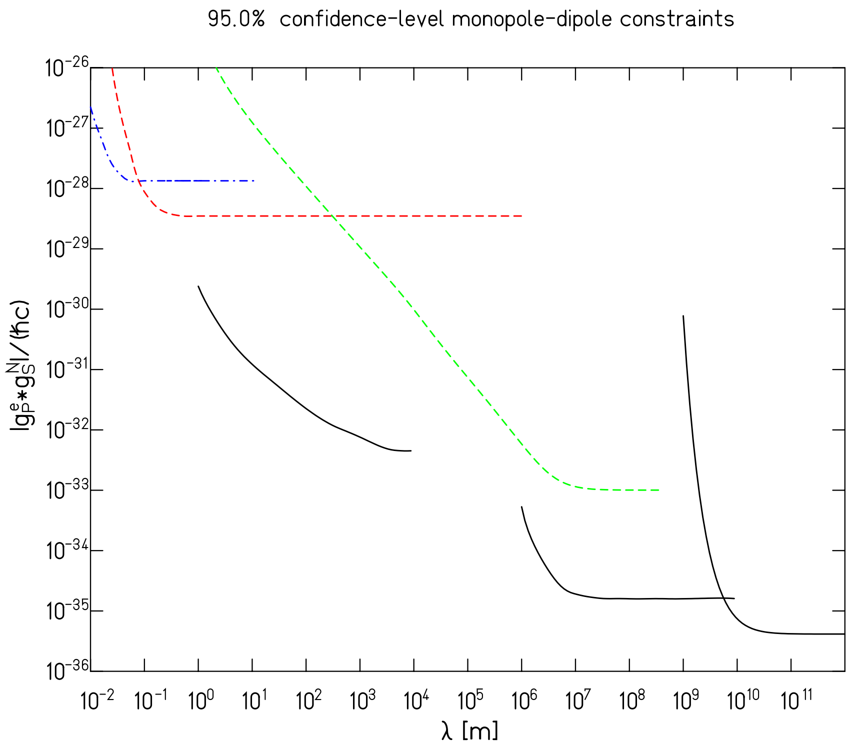

Figure 2.1-1. 2σ upper limits on $|g_P^e g_S|/(\hbar c)$ as a function of interaction range λ for the potential $V(r) = -\frac{g_P^e g_S}{8\pi m_e c}\sigma_e \cdot \nabla \frac{e^{-r/\lambda}}{r}$. Our results, previous work by Youdin *et al.*, Ni *et al.* and Wineland *et al.* are indicated by solid, dashed, dash-dotted and long sloping dashed lines, respectively. We do not give constraints for 10 km $< \lambda < 10^3$ km because integration over the terrestrial surrounding is not reliable in this regime.

2.2 Testing the weak equivalence principle using a rotating torsion balance

E. G. Adelberger, K-Y Choi, J. H. Gundlach, B. R. Heckel, S. Schlamminger,
H. E. Swanson and T. A. Wagner

We are using a torsion balance rotating with a constant angular velocity about its fiber axis to test the weak equivalence principle. Four titanium and four beryllium test bodies are mounted on the pendulum body in a dipole configuration. A violation of the equivalence principle would yield a differential acceleration of the two materials towards a source mass. Differential accelerations are detected as modulations of the angular position of the pendulum at the rotation frequency. This acceleration can be analyzed for a variety of source masses covering a range from one meter to infinity.

An equivalence-principle violating acceleration can be expressed as a Yukawa type interaction of a new composition dependent interaction, with a strength relative to the gravitational interaction (α) and an interaction range (λ). Of special interest for long range interaction are accelerations towards the sun and towards the center of the galaxy. The former would modulate our lab fixed acceleration with a daily period, the latter with a sidereal period.

In the past year we took two data sets, lasting 78 and 52 days. Before and after each data set we measured the gravity gradient fields from a nearby hill. In addition, we determined the gravity multipole moment of the pendulum and we performed several systematic tests to measure the sensitivity of our apparatus to disturbances caused by tilt, temperature and magnetic fields. It turned out that our first data set had a large susceptibility to a temperature gradient across the torsion balance. This problem was reduced significantly for the second data set, which was taken with a different fiber.

Using the measurements of the second data set we improved our previously published limit[1] on the equivalence-principle violation by a factor of five for local source masses. Fig. 2.2-1 shows the 2σ upper limit on new Yukawa type interactions coupling to the baryon number. The limiting systematic effect was a tilt induced signal.

Furthermore we tested the equivalence principle for astronomical sources, such as the Sun and the center of our galaxy, with a 12 times greater sensitivity than previous torsion balance experiments. We have measured a relative differential acceleration towards the sun of $\Delta a/a = (1.1 \pm 1.6) \times 10^{-13}$ (1σ uncertainty).

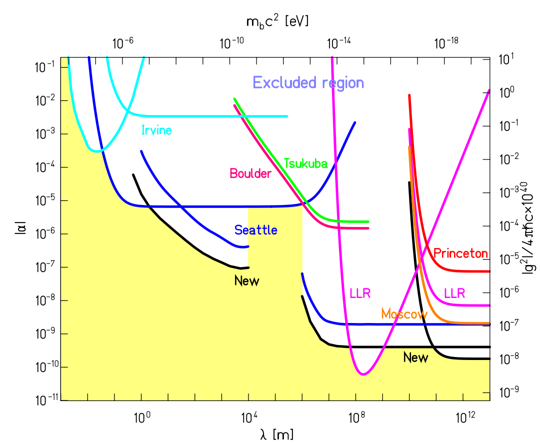

Figure 2.2-1. New 2σ limits on a Yukawa type force coupling to baryon number. The lines labeled "New" give the result of last year's data. The white region is now excluded from the parameter space.

[1] Y. Su *et al.*, Phys. Rev. D **50**, 3614 (1994).

2.3 Progress toward improved torsion fibers

J. H. Gundlach, C. A. Hagedorn and S. Schlamminger

We report here on continued efforts to fabricate improved torsion fibers for our LISA and small-force torsion balance experiments. As our experiments improve, we have found that one major obstacle to achieving greater sensitivity is the thermally generated torque noise from the torsion fibers themselves. The magnitude of the torque noise is proportional to the square root of the ratio of a fiber's torsion constant to its mechanical quality factor Q. We have made many efforts toward decreasing this ratio, primarily by increasing Q.

Furthermore, for our experiments, it is essential that our pendulums remain electrically neutral. Traditionally this has been achieved by using grounded conducting metallic wires as torsion fibers. In a quest to find higher quality factors, we have made fibers from quartz glass. The mechanical quality factor of quartz/fused silica is among the largest known. Quartz is a very good electrical insulator, making the problem of electrical grounding no longer trivial. We have refurbished a thermal evaporator that has a very large bell jar to permit the metalization of entire quartz fibers as they hang vertically.

In addition to allowing us to metalize fibers, the evaporator is an excellent multi-purpose vacuum chamber. We have installed, and continue to refine, a simple opto-electronic system that allows us to assess the Q of our fibers before and after coating. The evaporator's powerful turbo pump allows us to work at pressures markedly below 10^{-5} Pa, enabling us to work with residual gas pressures lower than those found in our small force experiments. These features, along with the user-friendliness of the bell jar, make it a useful test bed for new ideas.

With these systems in place, we are in a position to fabricate new fibers and quantify their properties. We have been able to make conducting fibers whose properties are slightly superior to those of our current tungsten fibers. Improvement is likely, and its extent is a topic of current research. If we are able to find a way to use unmetalized fibers, we should see at least a factor of ten improvement in our torque noise floor. We are investigating alternate methods of charge management to see if such an advance is possible for our torsion balances.

As our fibers have improved it has also become necessary to deepen our understanding of the effects of residual gas on our pendulum's Q. At present, the Qs of our small force experiments are dominated by losses in the fiber. Using our new Q measurement system, we have shown that, for some pendulum geometries, the system's Q will be dominated by gas damping if improved fibers are used. This result has important ramifications for future experimental design.

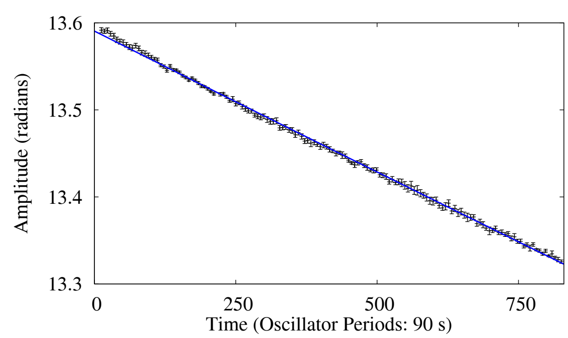

Figure 2.3-1. Excerpt from our data for an uncoated quartz fiber. The fitted curve is an exponential decay with Q = 130000. The tungsten fibers presently used in our operating experiments have $Q \sim 4000$.

2.4 Tests of the gravitational inverse-square law below the dark-energy length scale

E. G. Adelberger, T. S. Cook, B. R. Heckel, C. D. Hoyle, D. J. Kapner* and H. E. Swanson

For the past year we have been working to confirm or disconfirm the apparent short-ranged gravitational anomaly seen in the initial data of our 21-fold symmetric torsion pendulum.[1] With a thinner bottom attractor and modified apparatus we have completed two additional data sets, improved our modeling and analysis software, and explored numerous systematic effects. This search has not yielded any reasonable culprit to explain the discrepancy of the initial data set, however the bulk of the data now seem to confirm Newtonian gravity (see Fig. 2.4-1).

Progress is also being made on the "Wedge" pendulum,[2] which will be the next phase of our test of Newton's inverse-square law. The pendulum and attractor are made of $50\mu m$ thick rhenium foil with a 120-fold symmetric wedge pattern made by electric discharge machining. They are currently being cut by the instrument shop. The wedge pendulum will also get a number of apparatus improvements including a new drumhead type electrostatic screen that will improve the ease of clearing dust and an angle encoder for precise measurement of attractor rotation.

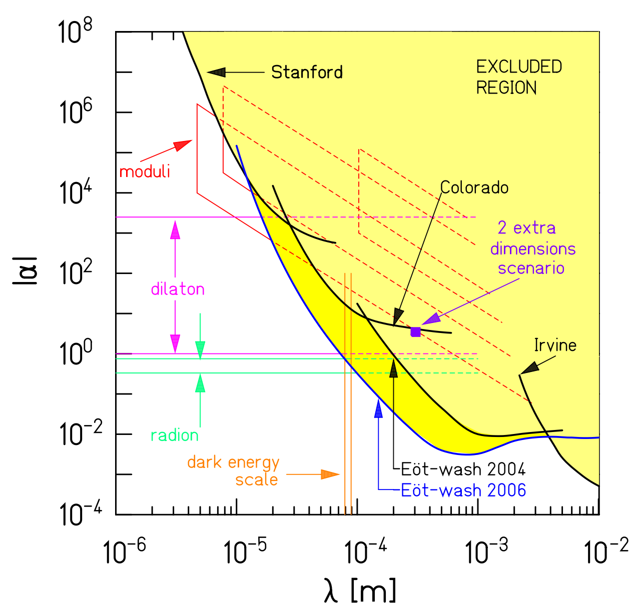

Figure 2.4-1. PRELIMINARY 95% exclusion limits on $|\alpha|$ and λ, the strength and range of a Yukawa potential. The line labeled "Eöt-Wash 2006" indicates the sensitivity of our most recent data set as compared to our previously published limits labeled "Eöt-Wash 2004".

*Presently at Kavli Institute for Cosmological Physics, University of Chicago, Chicago IL, 60637.
[1]CENPA Annual Report, University of Washington (2005) p. 13.
[2]CENPA Annual Report, University of Washington (2005) p. 14.

2.5 Small force investigations for LISA*

J. H. Gundlach, C. A. Hagedorn, B. R. Heckel, M. J. Nickerson, C. T. O'Rourke, S. E Pollack and S. Schlamminger

We are conducting low-noise force investigations for the Laser Interferometer Space Antenna (LISA)[1] being developed jointly by NASA and ESA for the study of gravitational waves from astronomical sources. Our work has concentrated on quantifying small forces which act on the proof masses housed within the LISA sciencecraft. Our measurements are carried out under similar operating conditions of LISA and within the relevant frequency band of 0.1 to 100 mHz. In this manner reliable models may be formulated which predict the performance and thereby direct the design of LISA. In the past year we have improved our existing low-noise torsion balance to better estimate these forces.

Our previous pendulum and field mass plate were both gold coated glass. To better simulate the LISA case of a Au/Pt proof mass and housing we have made a new pendulum and field mass out of conducting materials. Our new gold coated silicon pendulum is slightly larger than the old pendulum yielding a 1.7 increase in force sensitivity. The new opposing surface consists of two, electrically disconnected, gold coated pieces of copper placed a few hundred microns side-by-side. The two plates, together larger than the pendulum, simulate better the enclosed proof mass of LISA. A translation stage allows us to change the plate-pendulum separation by up to 10 mm. The current planned separation between the proof masses and housings in LISA is 4 mm.

Using the control electrodes installed last year we run the pendulum in electrostatic feedback so that the surface of the pendulum remains parallel to the surface of the plates. By changing the electrostatic potential on each plate and measuring the required torque needed to maintain the pendulum position we have determined the electrostatic contact potentials between each plate and the pendulum. Fig. 2.5-1 contains our results for the first few months of doing these measurements. We noticed a change in one plate of about 15 mV over the first month, but otherwise the two plates appear to have relatively constant contact potentials within 10 mV over three months of observation.

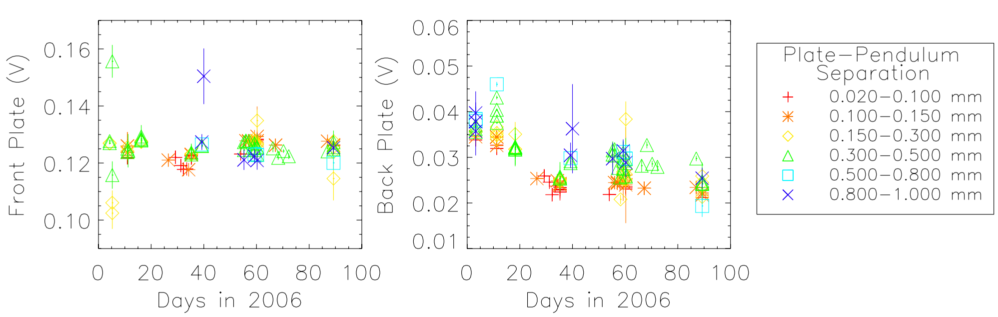

Figure 2.5-1. Plate-pendulum contact potentials during the first few months with our new pendulum and field mass bi-plate. Aside from some variation at early times, the contact potentials appear to be constant within 10 mV.

*Not supported by DOE CENPA grant

[1]http://lisa.jpl.nasa.gov

2.6 Progress on the torsion pendulum based axion search

E. G. Adelberger, B. R. Heckel, S. A. Hoedl, D. Schultheis and H. E. Swanson

Calculations indicate that a torsion pendulum search for the axion will offer an improvement of 10^{18} over the most recent measurement[1] for an axion mass of $\sim$ 200 μeV. The axion is the result of the hypothesized Peccei-Quinn symmetry and is a favored cold dark matter candidate.[2] The mass is constrained by the known flat geometry of the universe to be heavier than 1 μeV ($\lambda_a < 20$ cm), and is constrained by the neutrino flux from SN1987A to be lighter than 1000 μeV ($\lambda_a > 0.02$ cm). Note that microwave cavity searches probe for light axions (1.2 μeV $< m_a <$ 12.4 μeV). A torsion-pendulum based search is possible because the axion mediates a macroscopic pseudo-scalar potential between polarized and unpolarized fermions. By observing the motion of a germanium planar torsion pendulum (source of unpolarized fermions) position near the pole faces of an energized ferromagnet, we can observe such a force.

In the past year, we have constructed and evaluated three different electromagnet geometries, in addition to modeling and designing an appropriate cooling system to maintain a constant magnet temperature. In addition, we have developed a method for potting the magnet in a highly filled epoxy, enabling the magnet to operate at vacuum pressures near 10^{-7} Torr. The characterization of our first magnet assembly is complete, and a corresponding silicon pendulum, designed with the measured magnetic field gradients in mind, is in the process of fabrication. We intend to have a first publication of this experiment complete by the end of the calender year.

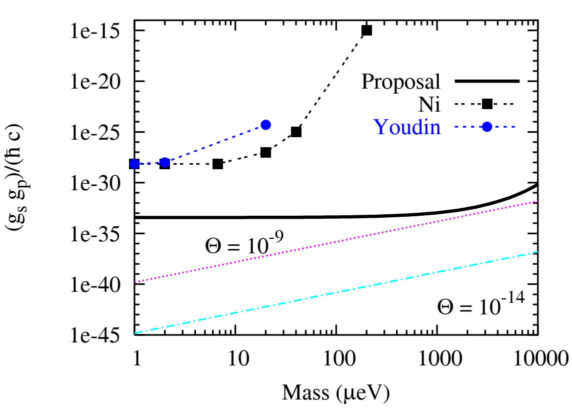

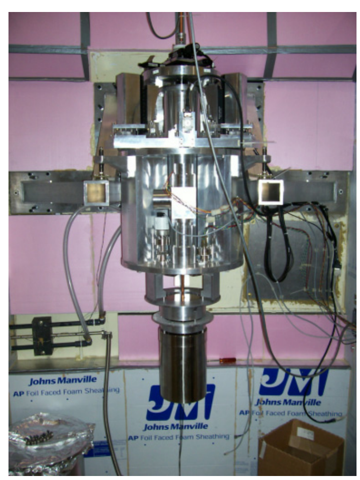

Figure 2.6-1. Our expected sensitivity to the axion electron-nucleon coupling as a function of the axion Compton wavelength compared with recent experimental searches and the expected coupling for different values of Θ_{QCD}; a picture of our axion-pendulum apparatus.

[1] W. T. Ni *et al.* Phys. Rev. Lett. **82**, 2439 (1999).

[2] L. J. Rosenberg and K. A. van Bibber, Phys. Rep. **325**, 1 (2000).

2.7 Eöt-Wash data acquisition development

H. E. Swanson and the Eöt-Wash Group

Data acquisition for the two rotating balances and the short-range balance has been ongoing for the last year, and no significant changes have been made to their respective computer codes or hardware.

A new data acquisition system has been assembled for the axion search apparatus. The hardware consists of a PC with a 2.4 GHz Athalon, 1 GB of RAM and National Instruments multifunction DAQ and GPIB interfaces (PCI-6229 and GPIB-USB-HS). We were able to reuse much of the software developed for the other instruments with the exception of the routines used to communicate with the DAQ hardware. When the short-range data acquisition system was upgraded we chose a National Instruments E-series DAQ board. The hardware interface used here is newer, provides a more useful mix of ADC, DAC and Digital I/O channels and is also less costly. It is unfortunately not compatible with the E-Series routines used in the short range system. We have developed a new set of software procedures to interface with the board's NI-DAQmx drivers.

The system is currently operational and has so far been used to investigate temperature stability in the apparatus environment.

2.8 Test of Newton's second law for small accelerations

K-Y. Choi, J. H. Gundlach, S. Schlamminger and C. D. Spitzer

One of the outstanding problems in astrophysics is the unexpected flatness of galactic rotation curves. Traditionally, dark matter has been introduced to solve this problem. A phenomenological solution explaining the rotation curves can be formulated by modifying Newton's second law. As early as 1983, M. Milgrom suggested such a modification, called MOdified Newtonian Dynamics (MOND).[1] Newton's second law was to be replaced by $F = m_g \mu(a/a_0)a$. The function $\mu(a/a_0)$ approaches one, and thereby restores Newton's second law, for accelerations much larger than the characteristic acceleration a_0. For accelerations smaller than a_0 the function reduces to $\mu(a/a_0) = a/a_0$.

A torsion pendulum can be used to test such a modification of Newton's second law.[2] The proposed modification would change the linear differential equation of motion to a nonlinear equation, without an analytic solution. We have programmed a numerical simulation using a realistic model of the pendulum to predict the torsional excursion as a function of time. We then fit the lowest frequency in this trace as a function of amplitude. The lowest frequency in such a model increases for smaller amplitudes as a function of a_0.

We used the Newwash torsion balance (see Sec. 2.2) to measure the frequency of the pendulum for small amplitudes. The pendulum, starting at rest, assumes on average an amplitude of approximately 100 nrad within one period. In order to measure at small amplitudes, we stopped the data collection after the pendulum has acquired a significant torsional amplitude. We then damped the pendulum and started a new run. By doing this many times we managed to get a reasonable distribution of amplitudes down to 20 nrad. We divided the recorded torsion angle as a function of time into 1600 s long sections. To each of the section, we fit the average amplitude and frequency of the oscillation. The results of the fits are shown in Fig. 2.8-1.

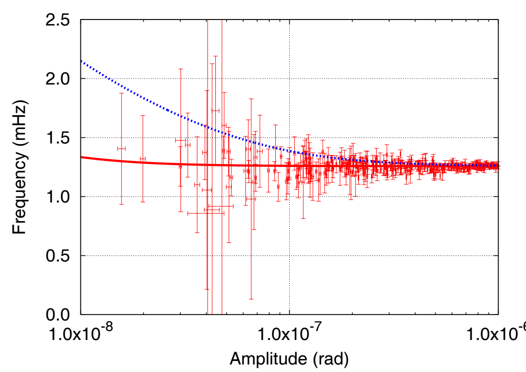

Figure 2.8-1. The measured frequency as a function of amplitude. The solid line is the best fit, yielding $a_0 = (7 \pm 14) \times 10^{-13}$ cm/s^2, the dashed line shows the predicted frequency for $a_0 = 10^{-11}$ cm/s^2.

From a very preliminary analysis of our data we get $a_0 = (7 \pm 14) \times 10^{-13}$ cm/s^2. This value is three orders of magnitude better than the previously published test[3] of F=ma and four orders of magnitude smaller than the required a_0 for a MOND fit of the galactic rotation curves. Current MOND scenarios require that no absolute accelerations are present. This condition cannot be obtained on earth for extended periods of time.

[1]M. Milgrom, Astrophys. J. **270**, 365 (1983).

[2]E. Fischbach encouraged us to perform the measurements described here.

[3]A. Abramovici and Z. Vager, Phys. Rev. D **34**, 3240 (1986).

2.9 Status of the APOLLO lunar laser ranging project*

E. G. Adelberger, C. D. Hoyle, H. E. Swanson, T. D. Van Wechel and the APOLLO Collaboration

Fundamental properties of gravity, including the Strong Equivalence Principle and $\dot{G}/G$, are best probed by the shape of the lunar orbit. APOLLO (Apache Point Lunar Laser-ranging Operation)[1] will measure this shape with unprecedented precision by detecting pulsed laser light (532 nm) returned from retroreflectors on the lunar surface. We aim for an order of magnitude improvement upon current measurements that characterize the lunar orbit at the 4 mm level.[2]

We have made much progress toward achieving "science-quality" data from APOLLO in the last year. All major mechanical work was completed and initial operation/acquisition software allowed for the first ranging operations in July, 2005 and the first detection of lunar return photons in October (see Fig. 2.9-1). To date, we have received several thousand lunar returns. This quantity of photons, collected in only a few hours of observation time, is equivalent to the number acquired over several years at other ranging stations. Additionally, the round-trip travel time of the photons agrees with the JPL lunar orbit prediction within several hundred picoseconds (corresponding to a distance uncertainty of only a few cm). The remaining hardware and software tasks required to achieve millimeter precision have recently been completed, and we are presently analyzing our first potential science-quality data.

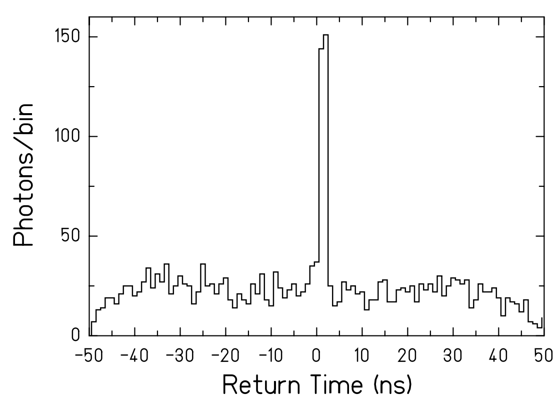

Figure 2.9-1. Return time histogram of the first lunar photons detected by APOLLO. The peak position and width are consistent with the JPL lunar orbit prediction.

In addition to these accomplishments, other key items completed in the previous year include development of an automated laser safety interlock system, as well as installing an infrared camera that will ensure that the beam does not intercept overflying aircraft. Finally, the Python/Tkinter data acquisition user interface software, developed here at CENPA, has achieved a mature state with many useful features that will allow remote operation of the entire system in the coming months.

*Not supported by DOE CENPA grant

[1] T. W. Murphy, *et al.*, Nucl. Phys. B, **134**, 155 (2004).

[2] J. G. Williams, S. G. Turyshev and D. H. Boggs, Phys. Rev. Lett. **93**, 261101 (2004).

2.10 APOLLO laser safety system*

E. G. Adelberger, C. D. Hoyle, H. E. Swanson and The APOLLO Collaboration

APOLLO, the lunar laser ranging program at the Apache Point Observatory (APO) operates a green (532 nm) pulsed laser with an average power of about 2 watts. This laser is classified as a class 4 vision hazard. The purpose of the safety system is two fold; to help prevent eye damage resulting from inadvertently looking directly into the laser beam or its reflections and to comply with the FAA requirement that the laser not be pointed at an aircraft in flight. The FAA has the further requirement that whenever the laser is active there will be two observers with the ability to immediately shut down the laser should they see any aircraft approach the general location of the beam.

There are spotter stations located on the catwalk on either side of the telescope. The spotters operate hand held kill switches that plug into weather proof outlets at each station.

As an additional safety measure we purchased a long wavelength infrared (LWIR) camera system that is able to detect aircraft in its field of view and provide a fast signal to shut down the laser. The camera has been mounted on the truss that supports the telescope's secondary mirror and bore sighted along the observing axis.

The safety system makes use of a spring loaded shutter that interrupts the laser beam before it leaves the enclosure. This shutter requires an active signal to open and is independent of the laser's electronics. Safe laser operation is imposed by requiring that the following conditions (interlocks) are satisfied before the shutter can be opened or remain open:

The door to telescope dome must be shut.
The telescope motor controller is not set to "emergency stop".
Neither Left nor right Spotter has activated a kill switch.
The LWIR camera's field of view remains clear.
APOLLO's control computer signals it's OK to range.

The operator's console is located in the telescope's control room. A key operated switch enables the shutter. The console has a diagnostic display showing the status of the interlocks and push buttons for opening and closing the shutter. There is a second operator's console located near the APOLLO apparatus in telescope dome.

The interlock logic is implemented in an Allen Bradley SLC500 Programmable Logic Controller.

*Not supported by DOE CENPA grant

Weak Interactions

2.11 The electron-capture branch of ^{100}Tc

A. Algora,* A. García, S. A. Hoedl, D. Melconian, H. Penttilä,† S. K. L. Sjue,
H. E. Swanson, S. Triambak and the IGISOL collaboration

Direct experimental measurement of the partial half life for the electron-capture decay of ^{100}Tc provides a value for the matrix element for neutrino capture by ^{100}Mo, an interesting candidate for solar neutrino detection. The same matrix element also enters into model calculations for the double-beta decay of ^{100}Mo.

We are in the process of completing the analysis of the measurement[1] of the ^{100}Tc(e,ν_e)^{100}Mo reaction. The electron capture is rare compared to the β-decay $^{100}\text{Tc}\rightarrow{}^{100}\text{Ru}+\text{e}^-+\overline{\nu}_e$, which happens >99.99% of the time. To determine the branching ratio, one must know both the total number of decays and the number of electron captures. The electron capture creates a K-shell vacancy in the ^{100}Mo daughter, which we detect via a subsequent x-ray emission. We are trying to understand some unexpected features in our γ-ray spectrum and their implications for systematic errors on our measurement. Currently we are developing a scheme to obviate the use of the peaks in the problematic γ-ray spectrum using the NaI detector that was next to our experiment.

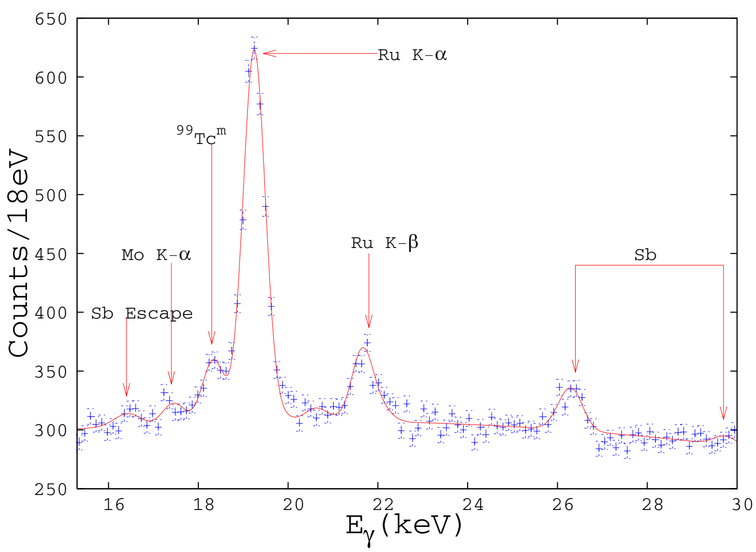

Figure 2.11-1. Spectrum of x rays from decay of ^{100}Tc.

This experiment is exceptionally difficult because the β-decay gives x-ray peaks with energies very close to the peaks from the electron-capture reaction. (See Fig. 2.11-1.) Over the last year, we've designed and proposed a new experiment using an ion trap and a new

*Institute of Nuclear Research of the Hungarian Academy of Sciences Debrecen, Hungary.
†University of Jyväskylä, Jyväskylä, Finland.
[1] CENPA Annual Report, University of Washington (2005) p. 5.

scintillator. The new scintillator would veto >95% of the βs, resulting in a clean spectrum with much smaller x-ray peaks from ^{100}Ru. The ion trap would completely remove the x-ray peak from ^{99}Tc^m, a contaminant from the reaction ^{100}Mo(p,2n)^{99}Tc. Fig. 2.11-2 shows a sketch of the proposed experimental setup. The pure ^{100}Tc beam from the ion trap goes into the cubic scintillator, which will veto >95% of the β-decays.

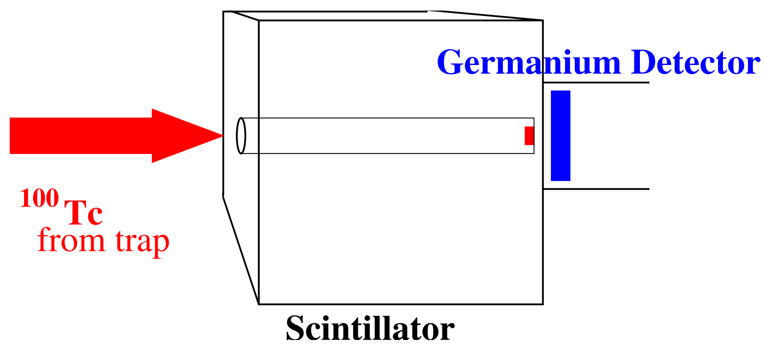

Figure 2.11-2. Setup for a proposed improved measurement.

2.12 Parity non-conserving neutron spin rotation experiment

B. R. Heckel, H. E. Swanson and A. Micherdzinska*

Data acquisition progress

Over this last year data acquisition development has centered on getting the program to control the apparatus. All elements of target control are now in place and the routine to configure the target has been developed.

In between data taking periods, when the target is being reconfigured, the magnetic field along the neutron beam will be measured. The main sequencer is awaiting the completion of the target change so is unavailable. We have implemented a state machine that sequentially positions the various fluxgate probes and switches them to a common readout module read by one of the ADC channels. When all probe positions are read they are logged to a file and the trim coil currents required to null the field are calculated and sent to their respective DACs.

Previously the sequencer generated a unique tag for each state entered in its database. This was changed so that identical states are now tagged the same. This simplifies using switching patterns to cancel slow linear and quadratic (or higher) variations in reactor beam intensity.

The noise performance of the gated integrators has been characterized using a current source. Initially a small fluctuating signal with an approximately 10 second period was observed on the current source. This was because the DAQ board itself determines when an ADC is read while the integrator reset signal was ultimately determined by the computer's clock. The time between the integrator's reset and the ADC reads varies periodically at the beat frequency of the two clocks resulting in a corresponding variation of the integrator's output due to small leakage currents. The integrator's reset signal is now synchronized to the DAQ board's clock and the resulting measured noise is about a picoamp for a full scale range of 10 nanoamps.

Experiment schedule and plans

The data acquisition system and much of the spin rotation apparatus has been moved from Indiana University to NIST. Construction of the polarized neutron beam line and installation of the polarimeter apparatus are currently underway. To test the apparatus, an initial measurement with room temperature D_2O targets is planned. This measurement will test the data acquisition system, characterize the polarized neutron beam, and provide a measure of systematic errors from small angle scattering. NaBr salt will then be added to the D_2O to measure the PNC rotation in Br. After these test runs, the targets will be replaced with liquid helium to begin the measurement of the PNC rotation in liquid helium. The D_2O runs are scheduled for the summer of '06, the helium runs should start in autumn '06.

*Department of Physics, IUCF, Bloomington, IN 47405.

2.13 Status of the ultra-cold neutron A_β experiment at Los Alamos

A. García, S. A. Hoedl, D. Melconian, A. L. Sallaska, S. K. L. Sjue and the UCNA collaboration

The Cabbibo-Kobayashi-Maskawa (CKM) matrix parameterizes the rotation between the weak and mass eigenstates of the quark families. If the Standard Model is complete, unitarity requires $V_{ud}^2 + V_{us}^2 + V_{ub}^2 = 1$; currently, this test fails at the 2.4σ level[1] which is suggestive of physics beyond the Standard Model. By far the largest element, V_{ud}, is known from measurements of the comparative half-lives, or ft-values, of nine superallowed $0^+ \rightarrow 0^+$ β decays, with theoretical uncertainties limiting the precision to which V_{ud} can be extracted. Being a much simpler system compared to complex nuclei, neutron β decay does not suffer from large theoretical uncertainties. However the precision of the experimental data must be improved for it to become a test of CKM unitarity. It is the goal of the Ultra-Cold Neutron Asymmetry (UCNA) collaboration to improve the measurement of the β-asymmetry parameter (A_β) which, when combined with the known lifetime, will provide a complementary measurement of V_{ud} with a precision that is comparable to that of the superallowed decays.

While at Los Alamos during our 2005 summer and fall run, we and the collaboration completed a number of development projects; among the highlights: the CENPA insert[2] was installed and functioned reliably throughout the run; the solid D_2 source was improved and characterized in greater detail; the UCN velocity distribution was measured; the guide system was built out to our final β-decay volume; and the β (MWPC + plastic scintillator) and cosmic-ray veto detectors were tested. We proved that UCN were being transported into the decay volume via flux and lifetime measurements with one of the solid-state detectors developed at CENPA.[3] This and other UCN production measurements unfortunately showed that our production and transport is still lower than we had expected. The expected β decay rate based on the UCN density in the decay volume was below the background level of ~ 1 Hz.

Based on these tests and Monte Carlo studies, the collaboration is in the process of making a significant overhaul of our system, including a new source and flapper/insert and improving the fabrication of the diamond-like carbon (DLC) coated quartz guides (replacing some with stainless steel). According to our models, the UCN production and transport should improve by two orders of magnitude in our next (May–Dec 2006) run, which should allow us to reach our goal. Development of the adiabatic fast-passage (AFP) polarizing magnet is nearing completion, so we also expect to have highly polarized UCN entering the decay volume. We should therefore be making preliminary A_β measurements by the fall of 2006.

We have recently installed the MIDAS data acquisition and PAW analysis programs on a local computer at CENPA which has allowed us to start analyzing the data of the last run in detail.

[1] J. C. Hardy and I. F. Towner, Phys. Rev. C **71**, 055501 (2005), and the Particle Data Group.
[2] CENPA Annual Report, University of Washington (2005) p. 7.
[3] CENPA Annual Report, University of Washington (2005) p. 8.

2.14 Monte Carlo calculations for experiments at LANL (UCNA) and the ILL

A. García, S A. Hoedl, D. Melconian, A. L. Sallaska and S. K. L. Sjue

Over the past year, we have completed testing our ultracold neutron monitor detectors at the Institut Laue-Langevin in Grenoble, France. These detectors are currently utilized in the ongoing UCNA experiment at Los Alamos National Labs. Intensive simulations of the two detector characterization experiments at the ILL and of the experimental setup in Los Alamos have been written and are currently in the polishing process.

The goal of our experiment in France was to characterize our detectors, which are solid state silicon detectors coupled with LiF or B/V foils that convert the neutrons into detectable charged particles. Our experiment consisted of two parts: a neutron time-of-flight measurement and a gravitational spectrometer. For our TOF, in order to qualitatively describe our detectors, we placed aluminum and stainless steel sheets in front of our converter foils to compare cutoff velocities, below which UCNs should be reflected and thus should not be seen in the detectors. Fig. 2.14-1 illustrates these features with a LiF detector.

The triangular data points represent the TOF for our bare LiF detector, which should have a UCN cutoff of 3.2 m/s. The box data points are our detector covered in aluminum, which has a cutoff of 3.22 m/s. Because these cutoffs are so similar, there should not be a very reduced signal between the two curves, which is not observed. However, there is a drastically reduced signal between the bare detector and the star data points, which display the measurements with a stainless steel covering. Stainless steel has a cutoff of 6.0 m/s so at longer times a great deal of the UCNs should be reflected, never reaching the detector, as is clearly seen in Fig. 2.14-1. Similar data exists for our boron detectors.

The second part of our experiment was the gravitational spectrometer, in which we change our detector height in order to provide different gravitational barriers to UCN, thereby altering the shape of the velocity distribution at our detectors. This setup has been rigorously modeled in order to quantitatively extract the cutoff velocities for each foil, which we hope to complete by the end of summer 2006. The results from these measurements are given in Fig. 2.14-2 as a function of net height gain and normalized to the counts seen at the low-

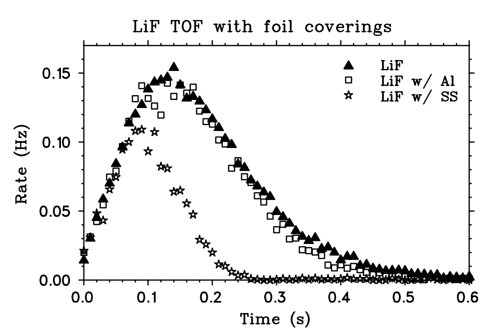

Figure 2.14-1. TOF comparison.

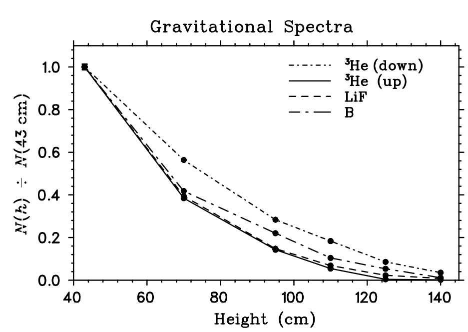

Figure 2.14-2. Gravitational spectrometer comparison.

est gain. Clearly, the most efficient is the calibrating helium detector in a position below the beam pipe, where the UCNs are accelerated to velocities higher than the cutoff for the detector's aluminum window. Because there is effectively no reflective barrier, the highest number of neutrons will be able to reach this detector. The B/V detector has the lowest, nonzero cutoff velocity (1.6 m/s theoretically) so it should be able to detect the next highest number of neutrons, which is clearly illustrated in this plot. Then the last two curves are not as distinguishable from one another because, as mentioned previously, LiF and helium (due to the aluminum window) have approximately the same cutoff. Therefore, qualitatively, our data is behaving as expected.

Lastly, we have written Monte Carlo simulations for our setup in Los Alamos as well. Currently, these include modeling of the motion of UCN through solid deuterium, passage through gravitational and magnetic fields, and quantum mechanical reflection and absorption from the guide surfaces. Our run in spring and fall 2005 produced data sets to understand our neutron production, including scans of our polarizer magnet from 0 to 7T, gravitational scans similar to the ones performed at the ILL, and measurements with different pressures of ^{3}He in certain sections of our system which should create another loss mechanism. All of these have been included in our models, which currently suggest that our diamond-like carbon guides have a much lower Fermi potential than expected. This is being rectified for our next spring run in 2006 by producing new guides with thicker DLC coatings and guides of highly polished stainless steel.

3 Nuclear Astrophysics

3.1 Astrophysical S-factor for the ^{3}He + ^{4}He reaction: energy loss and beam heating in the gas cell

C. Bordeanu,* N. Boyd,† A. Batchelor,‡ J. A. Mitchell, K. A. Snover and D. W. Storm

We continued the measurements, described last year,[1] of the resonance at 3.199 MeV (lab energy) in the ^{28}Mg(α,γ) reaction, in order to validate our technique for determining energy loss in the foil and gas of the target. Briefly, we made a ^{nat}Mg coated stopper for the gas cell. We ran the beam through the cell foil and gas as well as through the vacuum, onto this layer, measuring the beam energy for the thick target resonance. We described how, by measuring the shift in the resonance energy for different gas pressures, we could determine the energy loss in the gas and foil separately. We also described a preliminary measurement of the effect of beam heating on the gas density.

A new set of measurements, with careful monitoring of gas pressure and beam current, using different foils from the previous year, give us an energy loss of 160 ± 3 keV with 200 Torr ^{4}He gas in the cell, with a 600 nA beam. This result compares favorably with the 155 ± 4 keV reported last year.

We can study the change in density of the gas due to beam heating by studying the shift in resonance energy with beam current. If we assume energy loss is simply proportional to gas density ρ, then $\delta\rho/\rho = \delta E/\Delta E$, where δE is the shift due to heating, and ΔE is the energy loss at density ρ. Resonance curves measured using different beam currents with ^{3}He in the cell, give a change in density of $3.3 \pm 0.9\%$ between 200 and 600 nA, based on a shift in the resonance energy of 5.2 ± 1.4 keV. If we assume the change is proportional to the current, this gives a $5 \pm 2\%$ decrease in density at 600 nA compared to the case with no beam.

Then we fixed the accelerator energy at 3.845 MeV, the mid-point of the thick target resonance curve with 600 nA beam and 200 Torr gas pressure. Varying the beam current between 200 and 600 nA, we recorded the yield of the ground state gamma-ray per unit charge, shown in Fig. 3.1-1, which appears to be a linear function of the beam current. By using the slope of the resonance curve dY/dE and the change in yield with current, dY/dI, we can find $dE/dI = (dY/dI)/(dY/dE)$. Since the resonance curve was measured at a different time than the current dependence of the yield, we actually compute

$$\frac{dE}{dI} = \frac{\frac{dY_1}{dI}\frac{1}{Y_1(mid)}}{\frac{dY_2}{dE}\frac{1}{Y_2(mid)}},$$

where Y_1 are the values measured during the beam current variation, while Y_2 are measured during a sweep of the resonance curve, and $Y_i(mid)$ are the yields half way up the resonance,

*Presently at Horia Hulubei - National Institute for Physics and Nuclear Engineering, Department of Nuclear Physics (DFN 110), Str. Atomistilor nr.407, Bucharest-Magurele, PO Box MG6, Romania.

†Summer undergraduate helper, presently at University of British Columbia, Vancouver, Canada.

‡Undergraduate helper, presently at Amazon.com.

[1]CENPA Annual Report, University of Washington (2005) p. 54.

at $E = 3.845$ MeV with 600 nA. Then the fractional change in gas density due to beam current I is

$$\delta\rho/\rho = (\frac{dE}{dI}/\Delta E)I.$$

We find the yield changes by $42.3 \pm 5.9\%$ of the value at 600 nA, per μA of beam. From the resonance curves, we find that at 600 nA and 3.845 MeV, the yield changes by $4.1 \pm 0.4\%$ of the value mid way up the resonance curve, per keV. Combining these two figures, and using 160 keV for the energy loss in the gas at 600 nA, we find $\delta\rho/\rho = 3.9 \pm 0.6\%$ at 600 nA.

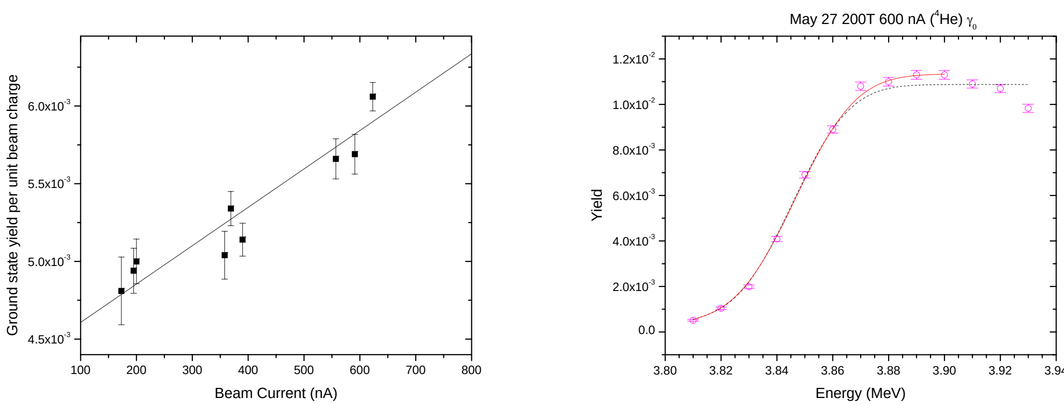

Figure 3.1-1. Yield dependence on beam current at $E = 3.845$ MeV, with linear fit, and corresponding resonance curve, with fits described in Ref 1.

This technique has several advantages over the repeated measurements of the resonance curve for various beam currents. First, the beam energy is not varied, avoiding possible shifts in the apparent beam energy due to the accelerator tuning. Second, the average beam current for each run can be determined accurately, while for the repeated resonance measurements, the current must be held to a constant value over the measurements that determine the resonance energy. Third, this technique is quicker and can be repeated to confirm results. Finally, the results obtained with this technique are more accurate than those obtained by repeating the resonance determination for different currents.

Because we expect to use a number of gas cell foils whose thicknesses will need to be measured, we built a device which uses a silicon PIN diode detector with a ^{148}Gd source to measure energy loss in foils. This device fits into the ^{7}Be scattering chamber, and we use the rotating arm to move the foil in and out of the space between the collimated source and detector. We can make several measurements on a given foil without breaking vacuum, and find we can measure energy loss for 3.183 MeV alpha particles with repeatability of better than 2 keV. We have measured the dead layer of the detector (see Sec. 3.4) which has a small effect on the measured energy loss in the foil. If we take a foil measured by the resonance technique, and use TRIM range values to determine the corresponding energy loss for the ^{148}Gd alpha particles, we find a value within 6 keV of the value measured directly for that foil.

3.2 Ge efficiency measurements and calculations for the ^{4}He + ^{3}He experiment

C. Bordeanu,* T. A. D. Brown, Y. Kharoti, J. Sibille,† K. A. Snover and D. W. Storm

We are using two Canberra 100% Ge detectors in our ^{4}He + ^{3}He experiment, Ge#2 for online counting the capture γ's during the irradiation, and Ge#1 for offline counting the 478 keV γ's from the ^{7}Be activity produced during the same irradiation.

Ge#2 efficiency calibration measurements were made with ^{137}Cs, ^{88}Y, ^{54}Mn, ^{133}Ba, ^{113}Sn and ^{203}Hg sources purchased from Isotope Products Corp., with activities in the range 1 - 5 kBq calibrated to a precision of 1.7 - 3.0% (99% CL). In addition, we used a ^{22}Na source made with the ^{23}Na(d,p)^{24}Na reaction to obtain the efficiency ratio for 1369 and 2754 keV γ-rays. A good fit was obtained to efficiency measurements at 25 cm using these sources and a fitting function $\epsilon(E) = aE^b(1 + cE)$; i.e. a power law expression with a small correction term represented by the c coefficient, thus determining the efficiency to better than $\pm$ 1% (1σ).

We also made an indirect check on the absolute Ge efficiency (or equivalently, the absolute source calibrations) by measuring the Ge#2 efficiency at 80 cm with the much hotter sources used in the ^{7}Be(p,γ)^{8}B experiment.[1] The hot ^{137}Cs source used in that experiment was cross-checked by comparison to a French ^{137}Cs source calibrated with different metrology. By measuring with the hot sources at 80 cm as well as the above ones at 25 cm and comparing the efficiency ratio to the ratio calculated from Penelope simulations (see below), we confirm the absolute calibration of the present (weaker) sources, particularly ^{137}Cs, to a precision of better than 1.5%.

For the ^{7}Be activity measurements, we will use Ge#1 in a close geometry inside a lead shield with 8" walls. The Ge#1 efficiency calibration at 478 keV was determined using a homemade ^{7}Be source (produced with the ^{10}B(p,α)^{7}Be reaction) whose activity we determined from measurements with Ge#2 at 25 cm. The Ge#1 efficiency so determined is $\epsilon(478\mathrm{keV}) = 0.125 \pm 0.001$.

For online counting of the prompt capture γ-rays, we plan to run at a mean source-to-detector distance of about 5 cm. For this calibration we have measured Ge#2 efficiency with the above sources located at the center of the gas cell, except for the ^{133}Ba source which is inappropriate at close distances due to multiline summing effects. To minimize summing corrections the sources used are all either single line or double line. The single line sources, ^{137}Cs, ^{113}Sn and ^{203}Hg, which have small summing corrections (due to coincident X-rays), were used to help decompose the double-line spectra into Compton and photopeak components. This information together with knowledge of the $\gamma - \gamma$ angular correlations allowed determination of double-line summing corrections of up to 1.06 with uncertainties of $\pm$ 0.01.

*Horia Hulubei - National Institute for Physics and Nuclear Engineering Department of Nuclear Physics (DFN 110) Str. Atomistilor nr. 407 Bucharest-Magurele, PO Box MG6, Romania.

†Summer 2005 REU student from Louisiana Tech, Ruston, LA 71272.

[1] A. R. Junghans *et al.*, Phys. Rev. C **68**, 065803 (2003).

We have also simulated the Ge detector response with the Monte Carlo code Penelope (Pendoses). The main purpose of these simulations is to calculate the lineshape of the capture γ-rays, including energy loss in the gas cell and Doppler spread, and to calculate the efficiency ratio for the extended gas cell source geometry relative to a point source.

We find that the simulated 25 cm Ge#2 efficiency is 0.94 to 0.99 times the measured efficiency, depending on energy. This agreement, which is good enough for our purposes, could presumably be improved by better knowledge of the Ge and other detector component dimensions. We've also measured the efficiency of Ge#2 at 5 cm with sources displaced longitudinally along the axis of the gas cell, and compared to Penelope with good agreement.

3.3 Completion of the measurement of ^{8}B beta decay

M. K. Bacrania, N. Boyd* and D. W. Storm

The setup and basic ideas of this experiment have been presented previously.[1] We have completed data taking and have obtained spectra of charged particles following the decay of implanted ^{8}B. These spectra cover two different energy ranges. The "high gain" spectrum covers the range from about 40 keV to about 1 MeV. It is calibrated as described in Sec. 3.4, and we expect to find the ground state decay of ^{8}Be in the range 75 to 120 keV, since 92 to 111 keV is deposited, including recoil, there is a 12 ± 3 keV pulse height defect associated with the two alpha particles, summing of the outgoing positron contributes a Landau distribution peaked at 8 keV, with a mean of 9.5 keV and standard distribution of 0.9 keV, and finally, the detector resolution is 7 keV. We obtained nearly equal amounts of data with ^{3}He in our gas cell, so ^{8}B was produced, and with ^{4}He in the cell, so we would have very similar primary beam backgrounds without producing a radioactive beam. The dominant feature of the "high gain" spectrum in either case is a broad peak centered around 180 keV, which we attribute to minimum ionizing radiation which both passes through the Si detector and triggers the scintillator. This radiation can come from cosmic rays or room background radiation, as well as from ^{8}B which may be deposited on collimators or other parts of the beam-line. Its rate is approximately 20 mHz, and it is present at nearly the same rate with or without beam. Spectra are shown in Fig. 3.3-1

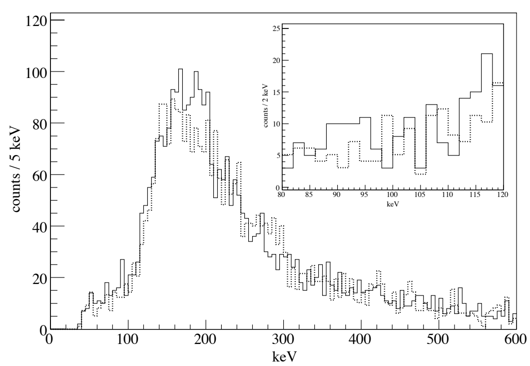

Figure 3.3-1. High gain spectrum with ^{8}B beam (solid) and background (dashed). The inset shows the energy region where the ^{8}Be ground state alpha particles would appear.

Combining data from a previous successful run with the one done this year, we find a small net excess of counts above background in the 75 to 120 keV region as well as in the region from 50 to 75 keV and the region from 120 to 140 keV. The adjacent regions represent an additional background which can be interpolated into the region of interest between 80 and 120 keV. In this region we find an excess of 86 ± 35 counts with an interpolated background of 40 ± 33, which gives a net of 46 ± 48 counts. This corresponds to a branching ratio of $2.3 \pm 2.5 \times 10^{-5}$ for the decay of ^{8}B to the ground state of ^{8}Be.

*Summer undergraduate helper, presently at University of British Columbia, Vancouver, Canada.
[1]CENPA Annual Report, University of Washington (2005) p. 55 and references therein.

3.4 Completion of the measurement of ^{8}B beta decay: Si detector response

M. K. Bacrania, N. Boyd* and D. W. Storm

We completed data taking and are in the process of final analysis of the search for the branch in the decay of ^{8}B to the ground state of ^{8}Be. In addition, we obtained calibrated data on the spectrum for the decay to the first excited state of ^{8}Be. We implant the ^{8}B in the detector so that we will be able to observe the two 46-keV alpha particles coming from the ^{8}Be ground state decay.[1] The total energy is actually 92 to 111 keV because of the recoil energy given the ^{8}Be by the beta decay.

We completed measurements scattering low-energy alpha particles into our detector, in order to determine the detector response. By using a very thin gold layer on a carbon target and scattering incident alpha particles backward to 100 degrees, we obtained a good mono-energetic source of alpha particles. We were able to operate the accelerator, with terminal ion source, to produce a beam energy as low as 90 keV. We determined dead-layer losses by rotating the detector about a vertical axis and measuring the change in alpha particle energy with angle. With eight different beam energies, we obtained data for alpha particles, after losses in the dead layer, of 48 to 380 keV. Comparing the peak position in the Si detector with peaks from ^{133}Ba photons, and correcting for the $0.984 \pm .008$ ratio[2] between the energy to produce a pair by alpha particles and by photons, we obtained the pulse height defect as a function of alpha particle energy. This is the energy that is lost to processes not producing charge collected from the detector. We found an energy dependence similar to that given in ICRU tables[3] but about 2 keV higher pulse height defect.

A long run with the ^{8}B beam was supplemented with runs with a ^{12}N beam produced by the same technique, but using a ^{10}B beam incident on our ^{3}He gas cell. The decays of ^{12}N to the 7.654 and 12.710 MeV states in ^{12}C produce three alpha particles with total energies of 379.4 and 5436 keV, respectively. The 7.654 MeV state decays by emission of a single alpha particle to the ^{8}Be ground state, while spin and parity require the 12.710 MeV state to decay by single alpha particle emission to the 3-MeV first-excited state of ^{8}Be. Correction of the 379.4 keV for recoil following beta decay involves adding a recoil spectrum of up to 5 keV. Correction for positron summing adds about 8 keV with a Landau tail at higher energy. Comparing the expected spectrum to the measured energy for the three alpha particles from the 7.654 MeV state decay using the calibration from ^{133}Ba, and apportioning the pulse height defect among them using the energy relations of Ref. 3, gives pulse height defects which agree with, or are a fraction of a keV lower than, those of Ref. 3.

For further analysis we will use pulse height defects from Ref. 3, with an additional uncertainty totaling 2.4 keV, to accommodate our measurements with incident alpha particles.

*Summer undergraduate helper, presently at University of British Columbia, Vancouver, Canada.

[1] CENPA Annual Report, University of Washington (2005) p. 55 and references therein.

[2] ICRU, Tech. Rep. 31 (1979).

[3] M. Berger, J. Coursey, M. Zucker and J. Chang, ESTAR, PSTAR, and ASTAR: Computer programs for calculating stopping-power and range tables for electrons, protons, and helium ions, an on-line database with machine-readable stopping power data from ICRU Technical Report 49 (1993). URL http://physics.nist.gov/Star.

3.5 Measurement of the ^{22}Na(p,γ)^{23}Mg reaction rate

J. A. Caggiano,* A. García, K. A. Snover and D. W. Storm

Orbiting gamma-ray observatories like the now decommissioned CGRO from the Comptel mission, and the recently launched INTEGRAL satellite have been used to detect unique gamma ray signatures from explosive events such as novae, supernovae, and gamma-ray bursts. These data are unique because they are tied to one particular isotope, in contrast to other observations which can not distinguish between individual isotopes of a given element. By understanding the production of a particular radioisotope, the explosive process that created it can be further understood. This process requires accurate nuclear physics data so that astrophysical models may be refined and modified to explain the observed gamma ray fluxes detected at these telescopes.

It remains a mystery why, for example, no ^{22}Na characteristic gamma rays (E_γ =1.275 MeV) have been observed in connection with specific, known explosions. Recently, a new level in the nucleus ^{23}Mg was identified at E_x=7.769 MeV (E_r=189 keV) and falls within the Gamow window for novae [Jenkins *et al.*, Phys. Rev. Lett. 92, 031101 (2004)]. The existence of this level may help to explain the absence of the characteristic gamma rays in observational data. The spin and parity of the level were tentatively assigned $9/2^-$, allowing $L = 1$ proton capture in novae. The present limits on the strength of this resonance ($\omega\gamma \leq$ 4meV) indicates it could be the dominant contributor to the burning of ^{22}Na. Hence, this resonance strength needs to be measured.

We have initiated a project to measure the strength of this resonance as well as others within 1 MeV of the proton threshold. We will use the high intensity ^{22}Na beam available at TRIUMF's ISAC to produce an implanted target of ^{22}Na and the CENPA accelerator to measure the resonance strength. We plan to implant stable ^{23}Na into a variety of carefully chosen candidate substrate materials, characterize the implanted targets using a strong proton resonance, produce the ^{22}Na targets/sources, and carry out the (p,γ) measurement.

In February of 2005, several metal foils were loaded with ^{23}Na at doses ranging from 0.2 to 2.0 mCi-equivalent ^{22}Na. The implantations were done at 30, 40, and 50 keV, the energies available at ISAC. Implantation was executed in the low energy part of the ISAC experimental hall. In order to produce uniformly-distributed layers of ^{23}Na, beam rastering was used with a 5mm diameter circular collimator placed just upstream of the target. By adjusting the parameters of the rastering program, a uniform distribution with sharp edges can be obtained.

In April of 2005, the three dimensional profile of some of these implanted targets were characterized. The profiles were measured using a strong ^{23}Na(p,γ) resonance at 309 keV. A beam of up to 1 particle - microamp singly-charged, molecular H_3 collimated to 1 mm diameter was delivered from ISAC to the DRAGON target position and BGO rates of known gamma rays were used to determine the resonance profile by stepping the beam energy in 2 keV/u steps. A two-dimensional translational motion stage was used to measure the lateral

*TRIUMF, 4004 Wesbrook Mall, Vancouver, BC, V6T 2A3 Canada.

profile by moving the target perpendicular to the beam.

In June 2005, a new target lid was fabricated and installed for the purposes of collecting the ^{22}Na at TRIUMF. A coil of LN2-cooled copper tubing was installed just upstream of the target to suppress carbon buildup on the substrates during collection, and to prevent migration of scattered ^{22}Na upstream. A 5mm diameter circular collimator was installed 5mm upstream of the substrate (target) ladder to limit the beam spot size on the targets. Following installation, one small (10μ Ci) target was fabricated in July 2005.

In October/November 2005, a beam of 25 pnA of ^{22}Na was used to make two target-quality sources of 300μCi and 185μCi. These targets will be used for testing detection apparatus and for the actual measurement.

At CENPA we will dedicate the 0° beamline for the resonance measurements.

4 Nuclear Structure

4.1 The $\mathcal{F}t$ value of the β-delayed proton decay of ^{32}Ar

E. G. Adelberger, M. Bhattacharya,* B. A. Brown,† M. W. Cooper,‡ A. García, T. Glasmacher,† V. Guimaraes,§ A. Komives,¶ P. F. Mantica,† D. Melconian, A. Oros,† J. I. Prisciandaro,† M. Steiner,† H. E. Swanson, S. L. Tabor,‡ S. Triambak and M. Wiedeking‡

As described in Sec. 2.13, unitarity tests of the Cabbibo-Kobayashi-Maskawa (CKM) mass-mixing matrix are a sensitive probe of physics beyond the Standard Model, currently limited by uncertainties in the theoretical corrections used to extract V_{ud} from superallowed $0^+ \rightarrow 0^+$ β decays. From the observed ft values, one defines a corrected $\mathcal{F}t$ value:

$$\mathcal{F}t \equiv ft(1-\delta_C)(1+\delta_R) = \frac{K}{G_F^2|V_{ud}|^2|M_{fi}|^2(1+\Delta_R)} \quad (1)$$

where $K/(\hbar c)^6 = 2\pi^3\hbar\ln 2/(m_e c^2)^5 = 8120.271(12)\times 10^{-10}$ GeV^{-4}, G_F is the Fermi coupling constant, $|M_{fi}|^2 = T(T+1)-T_3(T_3-1)$ is the matrix element of the decay, and the theoretical corrections are contained in δ_C, δ_R and Δ_R. Radiative corrections are separated in nucleus-dependent (δ_R) and nucleus-independent (Δ_R) terms. The isospin-breaking correction arises from two sources: mixing of 0^+ states due to charge-dependent forces (δ_{C1}), and radial overlap mismatch between the parent proton and daughter neutron states (δ_{C2}).

The $0^+ \rightarrow 0^+$ β-delayed proton decay of $T = 2$ ^{32}Ar is predicted to have $\delta_C = 2.0 \pm 0.4\%$, over three times larger than any of the nine precisely measured $T = 1$ cases, and is therefore an excellent case with which one may test theoretical models. With the half-life and Q_{EC} of ^{32}Ar recently measured to 0.2%, the superallowed branching ratio currently limits the precision of this nuclei's ft value to $\pm 7\%$.

To improve the superallowed branching ratio, an experiment was performed at the National Superconducting Cyclotron Laboratory where ^{32}Ar ions were implanted into the center of a silicon surface barrier detector, thick enough to contain all of the daughter protons. In addition to proton branches, the 0^+ excited states in ^{32}Cl can decay via γ emission and so the system was surrounded by an array of five HPGe detectors. By counting the number of proton decays observed in the Si detector and the number of γ decays from the HPGe detectors, and knowing the number of implanted ions, we are able to deduce the branching ratios of the decay. Over the past year, we have developed GEANT and PENELOPE simulations of this experiment, have nearly finished the data analysis, and have prepared a paper which will be submitted to Phys. Rev. C.

The final uncertainty on the superallowed branching ratio is $\pm 0.5\%$ which still limits the precision of the ft value, but is $15\times$ more precise than before. The limiting uncertainty of this experiment is the absolute γ efficiency of the HPGe detectors, which we are in the process of remedying (see Sec. 4.2).

*E-39 Von Braun Research Hall, University of Alabama, 301 Sparkman Drive, Huntsville, AL 35899.
†National Superconducting Cyclotron Laboratory, Michigan State University, East Lansing, MI 48824.
‡Department of Physics, Florida State University, Tallahassee, FL 32305.
§Department of Physics, University of Notre Dame, Notre Dame, IN 46556.
¶Department of Physics and Astronomy, DePauw University, Greencastle, IN 46135.

4.2 Measurement of the absolute γ branches in the decay of ^{32}Cl

C. Bordeanu,* A. García, J. C. Hardy,† V. E. Iacob,† D. Melconian, N. Nica,†
H. I. Park,† G. Tabacaru,† L. Trache,† S. Triambak, R. E. Tribble† and Y. Zhai†

As discussed in Sec. 4.1, the limiting systematic uncertainty in the measurement of the ft value of ^{32}Ar arises from the uncertainty in the HPGe γ efficiency. The γ decay of ^{32}Cl covers the same range of energies, and since $\approx 58\%$ of the time it is a daughter product of ^{32}Ar, a precise knowledge of these branches will provide us with an *in situ* calibration of our HPGe detectors.

We performed the experiment in the fall of 2005 using the fast tape-transport system at Texas A&M University. Our goal in this experiment is to measure the absolute γ branching ratios of ^{32}Cl to $\pm 1\%$, thereby reducing our dominant systematic uncertainty in the ft value of ^{32}Ar by a factor of five. The ^{32}Cl ions we implanted onto an aluminized-mylar tape and quickly moved between a plastic scintillator β detector and HPGe γ detector, using a coincidence between both detectors as our event trigger. The efficiency of the HPGe detector used has been measured[1] to $\pm 0.2\%$ up to 1400 keV; recently, our collaborators at Texas A&M have used ^{24}Al to extend this efficiency curve up to 7069 keV with $\pm 1\%$ precision.

We have a very clean data set, and have identified every significant peak in our spectrum (see Fig. 4.2-1), definitely identifying 8 new branches; we do not see two branches that were previously reported.[2] We have fit the ^{32}Cl peaks and determined their areas to $< 0.3\%$ statistical uncertainty; studies of systematic uncertainties and extraction of the β and γ branching ratios are nearing completion.

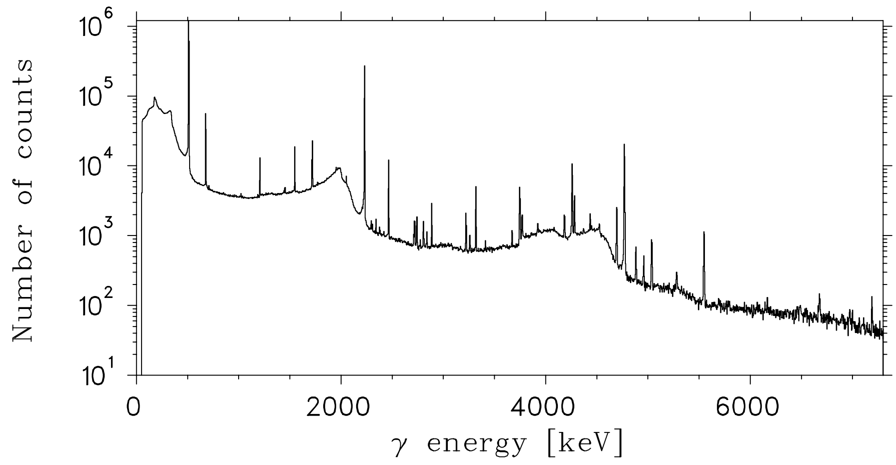

Figure 4.2-1. HPGe γ energy spectrum of the Texas A&M University data. The only significant background comes from ^{30}S at 677 keV; all others – nearly fifty in total – are from ^{32}Cl.

*Horia Hulubei - National Institute for Physics and Nuclear Engineering Department of Nuclear Physics (DFN 110) Str. Atomistilor nr. 407 Bucharest-Magurele, PO Box MG6. Romania.
†Department of Physics, Texas A&M University, College Station, Texas 77843.

[1] R. G. Helmer, *et al.*, Nucl. Instrum. Methods A **511**, 360 (2003).
[2] C. Détraz, *et al.*, Nucl. Phys. A **188**, 513 (1972).

4.3 $^{32}S(p,\gamma)$ and its importance in calibrating a ^{33}Ar beta-delayed proton spectrum

E. G. Adelberger, A. García, D. Melconian, H. E. Swanson and S. Triambak

In determining the $e^+ - \nu$ angular correlation from the decay of ^{32}Ar, energy calibrations are done using delayed proton groups[1] from the decay of ^{33}Ar. This is dependent on the precision of the excitation energies and widths of the states of interest in ^{33}Cl which are obtained from resonances in $^{32}S(p,\gamma)$.

Data from a previous measurement[2] show rough agreement of the excitation energies with tabulated values. However, the width of the second $J^\pi = 3/2^+$ excited state at $E_x \approx 3972$ keV in ^{33}Cl needs to be investigated further. An R-matrix fit to the delayed proton spectrum yields a width of ≈ 1 keV, whereas the $^{32}S(p,\gamma)$ spectrum shows a width of ≈ 7 keV. A previous $^{32}S + p$ experiment[3] reported a width of 5 ± 3 keV for the state of interest.

A direct and clean method of solving this discrepancy is by measuring excitation functions around that resonance using thin ^{32}S targets with $\Delta E \approx 1$ keV at $E_p \approx 1748$ keV. Preliminary tests show that targets made by evaporating Ag_2S on carbon foils create unnecessary background around the γ-energy we are interested in. Additional targets were made by evaporating a thin layer of Silver (≈ 120 Å) on a Gold foil and then evaporating a fleck of Sulfur at $\approx 210°$ C to make a thin Ag_2S target. These targets unfortunately are not stable when subjected to beams at $\approx 15\ \mu$A.

Plans to repeat the measurement using Sm_2S_3 and MoS_2 evaporated onto Gold foils are underway.

[1] E. G. Adelberger *et al.*, Phys. Rev. Lett. **83**, 1299 (1999).
[2] CENPA Annual Report, University of Washington, (2005) p. 59.
[3] M. M. Aleonard *et al.*, Nucl. Phys. A **257**, 490 (1976).

4.4 Mass of the lowest $T = 2$ state in ^{32}S: A test of the Isobaric Multiplet Mass Equation

E. G. Adelberger, A. García, S. A. Hoedl, D. Melconian, A. L. Sallaska, S. K. L. Sjue, H. E. Swanson and S. Triambak

We have completed a precision measurement of the mass of the lowest $T = 2$ state in ^{32}S as a test of the Isobaric Multiplet Mass Equation (IMME) using the ^{31}P(p,γ) reaction.[1] We made two independent measurements at different times. In the first measurement, data were taken with two HPGe detectors at $\pm$ 90° to the beam, and in the second measurement one HPGe detector was aligned at 0° to the beam, positioned at a much larger solid angle. The energy calibration for the former was based on a ^{56}Co source and the ^{35}Cl(n,γ) reaction while the 0° measurement was calibrated using the ^{56}Co source and the ^{27}Al(p,γ) reaction. We obtain the excitation energy of the lowest $T = 2$ state in ^{32}S to be $E_{\mathrm{x}} = 12047.96(28)$ keV, $\approx 7\sigma$ higher than the previously reported value,[2] which together with the best available results for the masses of other members of the $A = 32$ quintet shows a significant deviation from the IMME prediction $Q(\chi^2,\nu) = 0.001$. The fit results are shown in Fig. 4.4-1.

We investigated the possibility of isospin mixing with a nearby $T = 0$ level that could cause a shift in the $T = 2$ state of ^{32}S by ≈ 2.5 keV. This was done by looking for an isospin-violating $\Delta T = 2$, E2 transition from the $T = 2$ state to the first excited ($T = 0$) state as evidence for such mixing. The excitation function using the γ_1 yield showed the resonant contribution for such a transition consistent with zero.

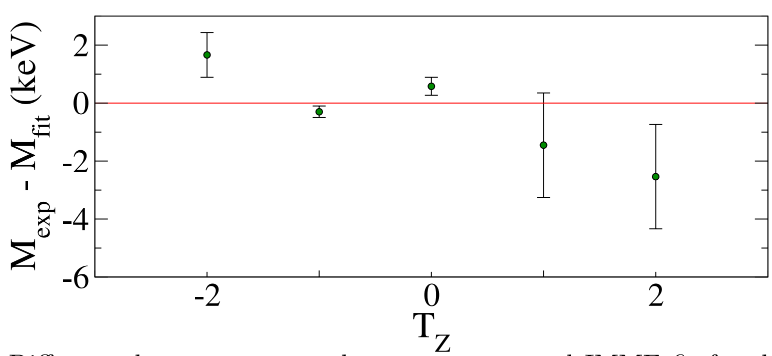

Figure 4.4-1. Difference between measured mass excesses and IMME fit for the $A = 32$, $T = 2$ quintet in keV

We however obtained an upper limit to this isospin violating branch to be 0.25%. As byproducts of this work we also obtain new results for relative γ branches from the $T = 2$ state in ^{32}S. We also measured excitation functions around the two closest $T = 0$ states at 11930 and 11869 keV using the γ_1 yield. The first resonance yielded an upper limit to the γ_1 width of 52 meV and the second resonance yielded a γ_1 width of 330(70) meV. Our results do not exclude either of these levels as a source of isospin admixture to the $T = 2$ state of interest.

---

[1] CENPA Annual Report, University of Washington, (2004) p. 58.

[2] M. S. Antony *et al.*, in *Proceedings of the International Conference on Nuclear Physics*, Berkeley, Lawrence Berkeley Laboratory, Berkeley, CA, Vol. 1 (1980).

5 Relativistic Heavy Ions

5.1 Opacity and chiral symmetry restoration in heavy ion collisions at RHIC: the DWEF Model

J. G. Cramer and G. A. Miller*

We have continued our work to develop a relativistic quantum mechanical approach to the analysis and prediction of pion HBT radii and spectra in RHIC Collisions. The work reported last year[1,2] fitted STAR $\sqrt{s_{NN}}$=200 GeV Au+Au central collision data on the pion spectrum[3] and HBT radii.[4] We have now investigated the extension of the distorted-wave emission function (DWEF) model to non-central collisions and to lighter systems. In particular, we have applied linear participant scaling by assuming that the geometrical space-time parameters of the model, R_{WS}, a_{WS}, and τ_0 are proportional to the number of participants in the collision, as estimated from Glauber model calculations. For the lighter systems, we have also scaled the dynamic emission duration parameter $\Delta\tau$ by $A^{\frac{1}{3}}$, where A is the atomic mass number of the colliding nuclei. This has allowed us to *predict* the HBT radii for the $\sqrt{S_{NN}}$= 200 GeV $Au + Au$ collisions and $\sqrt{S_{NN}}$= 200 GeV $Cu + Cu$ collisions as a function of centrality. We emphasize that these calculations were *not* fits, in that all parameters from the central $\sqrt{S_{NN}}$= 200 GeV $Au + Au$ fits were either frozen or scaled.

Fig. 5.1-1 shows these DWEF predictions for $\sqrt{S_{NN}}$= 200 GeV $Au + Au$ collisions as compared with the published STAR HBT radii. The upper (solid black) curve shows the fit to the most central (0-5% of total reaction cross section) collision data (red solid and circles). The other curves and points show centralities 5-10% (yellow dotted and plus), 10-20% (green short dash and triangle), 20-30% (aqua long dash and diamond), 30-50% (blue dot-dash and 5-star), and 50-80% (violet dot-dot-dash and 6-star) respectively. We note that the agreement between these predictions and data is very good, except for the most peripheral (50-80%) collisions, for which the physics assumptions of our model are questionable and the parameter extrapolations are most extreme.

Fig. 5.1-2 shows the predictions for $\sqrt{S_{NN}}$= 200 GeV $Cu+Cu$ collisions as compared with preliminary STAR HBT radii taken from conference proceedings. The upper curve shows the fit to central $Au+Au$ collisions for comparison. The lower curves and points show centralities 0-10% (red solid and circles), 10-20% (yellow dotted and +), 20-30% (green short dash and triangle), 30-40% (aqua long dash and diamond), 40-50% (blue dot-dash and 5-star), and 50-60% (violet dot-dot-dash and 6-star) respectively. Again we see very good agreement of predictions and data for the four most central collision groups, with diminished agreement for the most peripheral collisions, where the model assumptions are questionable and the parameter extrapolations are extreme.

---

*Department of Physics, University of Washington, Seattle, WA 98195.

[1] J. G. Cramer, G. A. Miller, J. M. S. Wu and J-H. Yoon, Phys. Rev. Lett. **94**, 102302 (2005).

[2] G. A. Miller and J. G. Cramer, ArXiv:nucl-th/0507004.

[3] J. Adams, *et al.*, Phys. Rev. Lett. **92**, 112301 (2004).

[4] J. Adams, *et al.*, Phys. Rev. C, submitted for publication, 2004; nucl-ex/0411036.

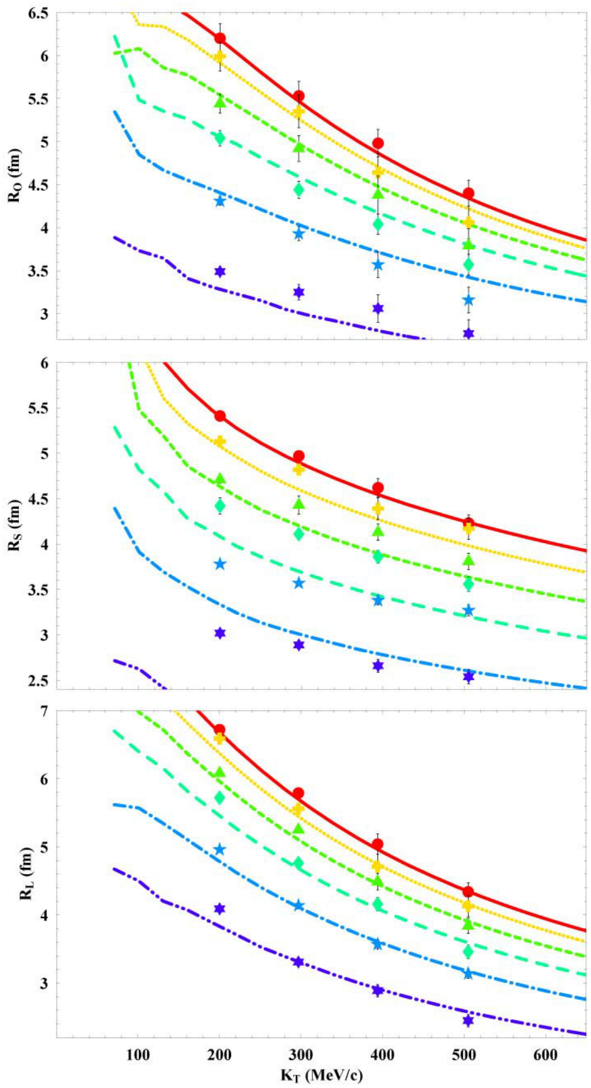

Figure 5.1-1. $Au + Au$ collision DWEF predictions vs. centrality at $\sqrt{S_{NN}}$= 200 GeV of HBT radii R_O, R_S,, and R_L; Centralities (high to low) are 0-5%, 5-10%, 10-20%, 20-30%, 30-50%, and 50-80%. See text for color, point, and line code.

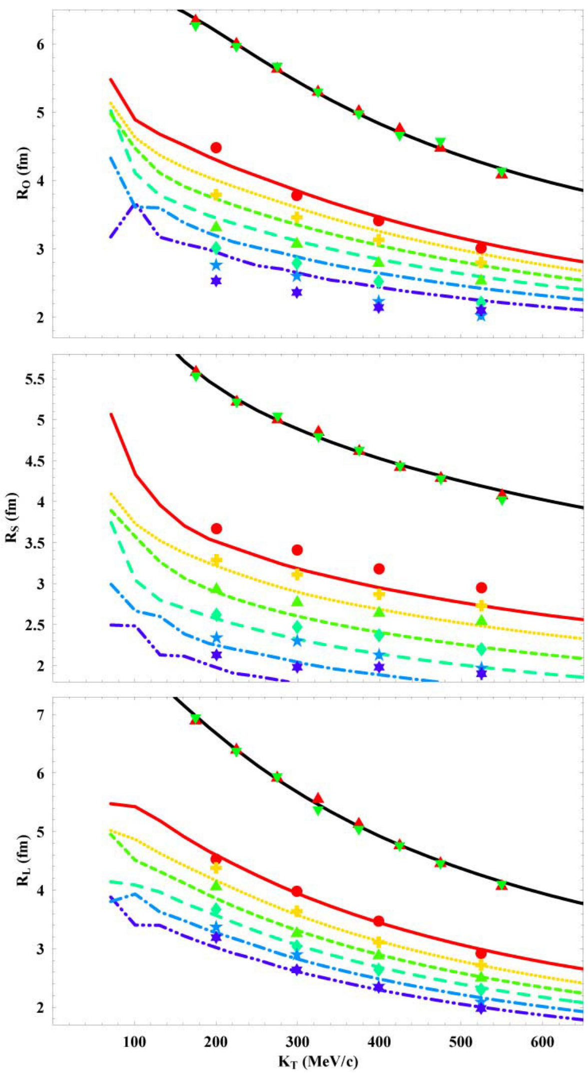

Figure 5.1-2. DWEF Predictions vs. centrality for $\sqrt{S_{NN}}$= 200 GeV $Cu + Cu$ collisions of HBT radii R_O, R_S,, and R_L; Upper curve and points show the central $Au + Au$ fit for reference. Centralities (high to low) are 0-10%, 10-20%, 20-30%, 30-40%, 40-50%, and 50-60%. Data are STAR preliminary. See text for color, point, and line code.

5.2 Using lattice-gauge predictions in DWEF calculations

J. G. Cramer and G. A. Miller*

In our recent work on development of the distorted wave emission function (DWEF) model, reported last year,[1,2] the temperature parameter used in the pion emission function was 222 MeV. This is an uncomfortably large value of temperature, high enough that pions would be expected to "melt" in such an environment and lose their identity. Further, some of our studies involved chemical potentials that were larger than the pion rest mass (139 MeV), a condition that might be expected to cause Bose-Einstein condensation of the system, since creation of new pions would add energy to the system. Therefore, we have undertaken to explore the extent to which the DWEF model requires such large values of these two parameters.

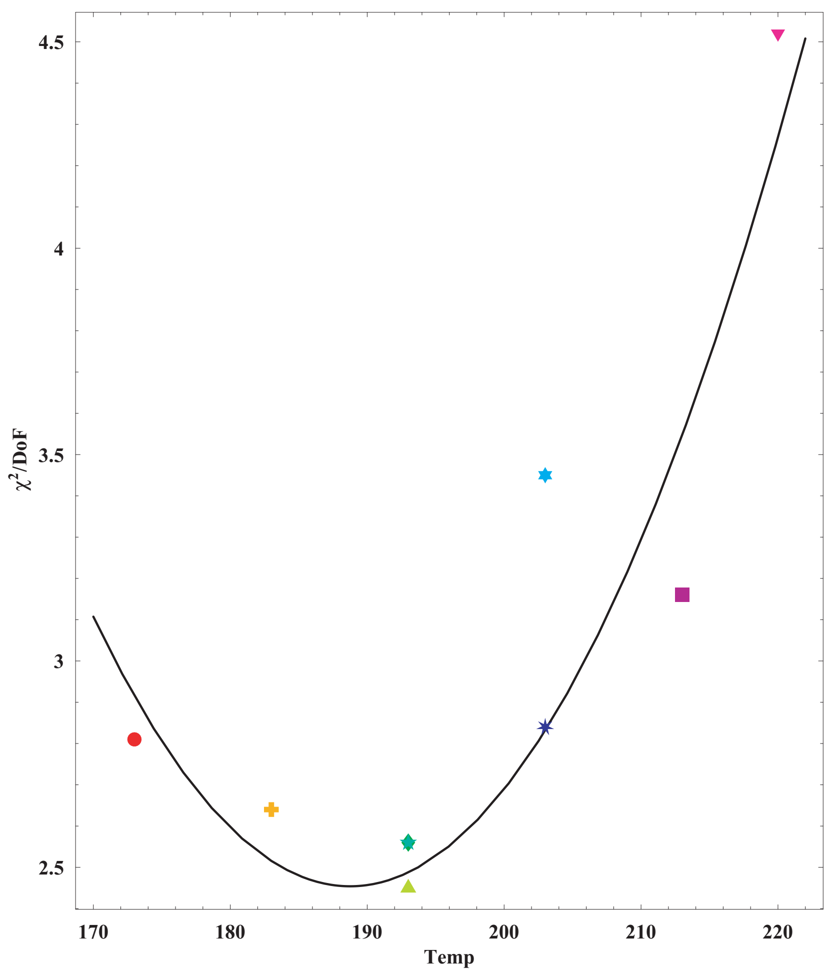

Figure 5.2-1. χ^2 per degree of freedom of nine fits to STAR $\sqrt{S_{NN}}$=200 GeV $Au+Au$ data

*Department of Physics, University of Washington, Seattle, WA 98195.

[1] J.Ġ. Cramer, G. A. Miller, J. M. S. Wu and J-H. Yoon, Phys. Rev. Lett. **94**, 102302 (2005).

[2] G. A. Miller and J. G. Cramer, ArXiv:nucl-th/0507004.

If one takes quite literally the expectation that the first pions are produced as massless objects as the strongly interacting quark-gluon plasma make a phase transition to a hadronic phase, then the emission function should have the temperature of the QGP transition, and the chemical potential should equal the free pion mass. Recent lattic gauge calculations reported at Quark Matter 2005[3] give the critical QGP transition temperature to be 193 MeV. Therefore, we adopted T=193 Mev and μ_π=139.57 MeV and searched for a new fit to the STAR $\sqrt{S_{NN}}$=200 GeV $Au + Au$ data. To our surprise, the fit with parameters fixed at these value was the best we have ever seen, with an overall χ^2 of 56.46 and a χ^2 per degree of freedom of 2.45. Further, subsequent searches in which the fixed temperature was set to values between 173 MeV and 220 MeV showed that there is a minimum in χ^2 at just the temperature value given by the lattice gauge calculation. This is shown in Fig. 5.2-1.

Fig. 5.2-2 shows the ratio of the parameters of eight other fits divided by the parameters of the T=193 MeV fit described above.

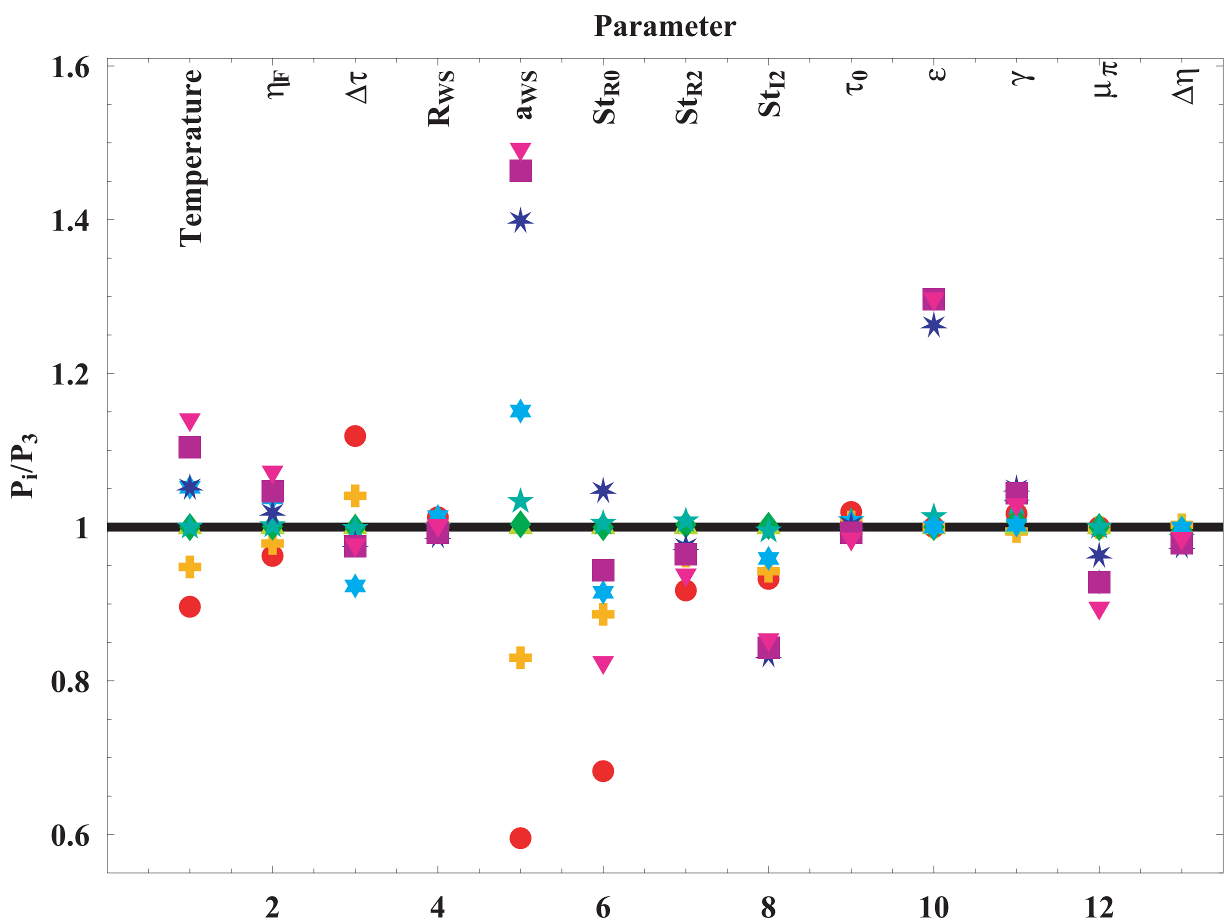

Figure 5.2-2. Ratio of the parameters of eight other fits divided by the parameters of the T=193 MeV fit described above

[3] S. D. Katz, ArXix:hep-ph/0511166.

5.3 Non-Gaussian HBT Correlations

J. G. Cramer and G. A. Miller*

Using our distorted wave emission function (DWEF) program with the best-fit T=193 MeV parameter set, as described above, we have calculated the detailed shape of the identical pion correlation functions predicted by the DEWF model and compared them with Gaussian distribution functions.

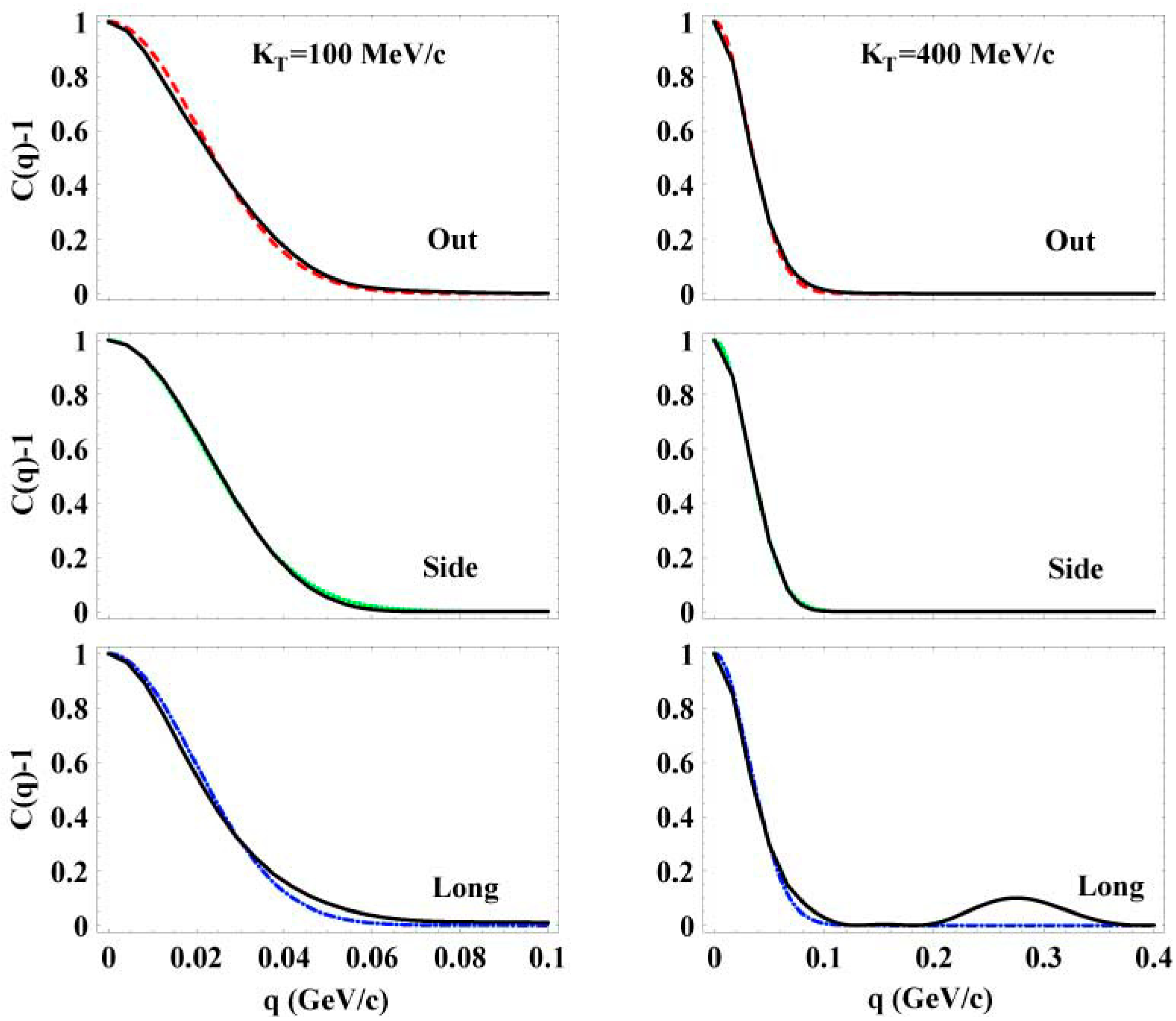

Figure 5.3-1. Predicted out, side, and long (top to bottom) correlation functions (solid black)and Gaussian fits (colored broken) at K_T= 158 and 316 MeV/c.

We find that there are significant deviations from Gaussian behavior in the predicted functions. However, we note that the curves match well at the "half-maximum" point, which is the point used in deducing the HBT radius in the DWEF search code. For this reason, we

*Department of Physics, University of Washington, Seattle, WA 98195.

expect that the DWEF code should perform well in predicting the HBT radii obtained from Gaussian fits that agree with measured correlation points in the half-maximum region.

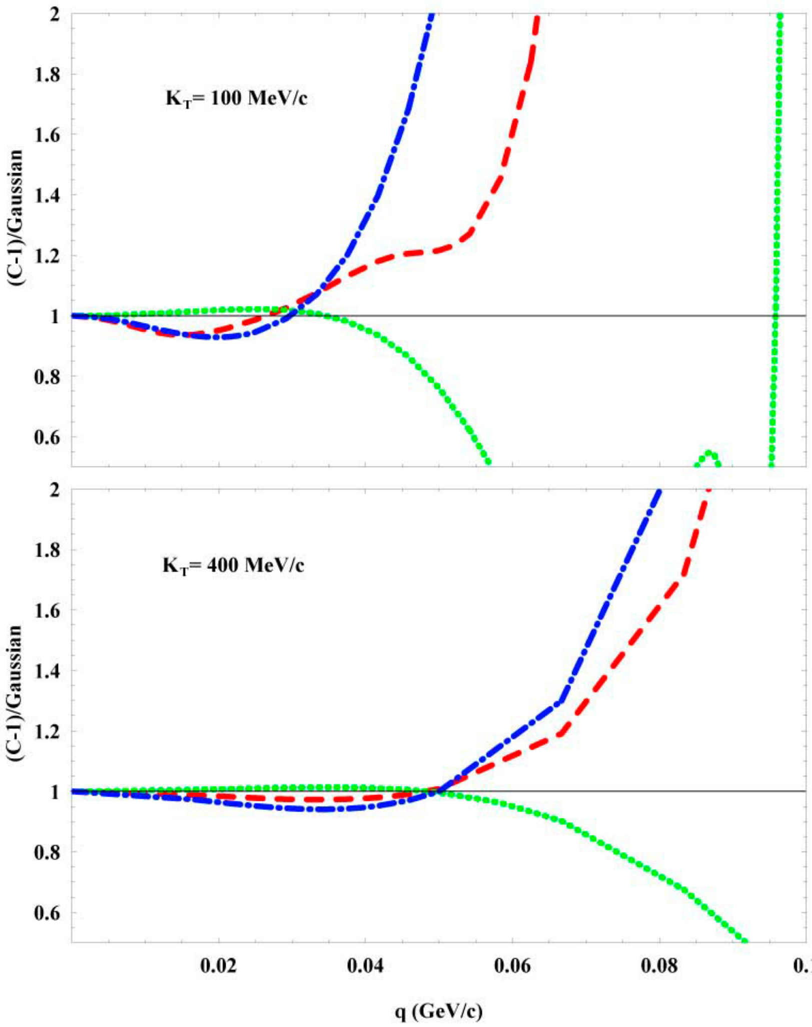

Figure 5.3-2. Ratio of Predicted out, side, and long correlation functions to Gaussian fits.

5.4 Studies of energy losses of fast charged particles

H. Bichsel

The review of "A method to improve particle identification in TPCs and silicon detectors" has been accepted for publication in Nuclear Instruments and Methods A. The paper is available at NIMA under "articles in print." A preprint is available at

http:/faculty.washington.edu/hbichsel

I have worked with several people on various aspects of the interactions of charged particles with matter.

- Prof. Z. Chaoui at University of Setif (Algeria): straggling of fast electrons.
- Dr. D. E. Groom at LBL (Berkeley): discussions about the energy deposition in hadron calorimeters.
- Dr. P. Christiansen at CERN: energy loss and energy deposition in the ALICE test TPC.
- Dr. Su Dong at SLAC: Practical methods of Monte Carlo simulations for Si detectors and achieving fast production of single collision cross sections for use in GEANT 4.

5.5 Summary of event structure research

T. A. Trainor

The main subject of this program is study of the colored medium produced in RHIC heavy ion (HI) collisions. Analysis of RHIC HI data has revealed complex correlation structures which motivated extensive analysis of p-p collisions and more recently of fragmentation functions in e^+-e^- collisions at PETRA and LEP. The common theme is low-Q^2 (small energy scale) parton collisions and fragmentation. The general topics we report here are

- e^+-e^- fragmentation functions and the beta distribution
- Fragmentation trends for identified partons and identified hadron fragments
- Scaling violations, the DGLAP equation and fragmentation energy dependence
- Angular correlations in p-p and A-A collisions at low Q^2 and non-perturbative QCD
- Precision centrality determination for A-A collisions
- Comprehensive survey of correlations in A-A collisions
- Correlations of identified particles in A-A collisions
- Web-based infrastructure for large-scale correlation analysis of RHIC data

The model-independent correlation analysis techniques which we developed for HI collisions revealed structure that we have since interpreted as fragmentation (jets) from parton collisions at the lowest energy scales ever observed ($Q = 1-5$ GeV). Low-Q^2 parton scattering in RHIC collisions is copious and produces much structure in the hadronic final state. Our study of the same phenomena in p-p collisions has led to a precise characterization of low-Q^2 fragmentation as a calibration for heavy ion studies. We have further extended the calibration effort by analyzing e^+-e^- fragmentation functions. We have introduced an improved model function which represents all e^+-e^- fragmentation functions more precisely and simply than conventional methods. The new representation allows us to extrapolate fragmentation functions to low Q^2 for comparison with our p-p and HI correlation measurements. Low-Q^2 parton (gluon) scattering and fragmentation emerge as both a production mechanism for and a probe of the colored medium in heavy ion collisions. Aside from their importance to the heavy ion program our recent results from analysis of e^+-e^- and p-p collisions may provide new experimental access to non-perturbative QCD and the hadronization process.

5.6 Describing fragmentation functions with beta distributions

D. T. Kettler and T. A. Trainor

We have plotted in Fig. 5.6-1 fragmentation function (FF) data for $\sqrt{s} = 14$, 44, and 91 GeV measured at the PETRA and LEP accelerators for unidentified hadrons from unidentified partons. In the first and second panels the FFs are plotted on momentum fraction x_p and logarithmic variable $\xi_p = \ln(1/x_p)$ respectively. These are the conventional variables used to describe fragmentation functions. Distributions on x_p emphasize the large-x_p (small-ξ_p) region where pQCD is expected to best describe data, where the naïve parton model would predict 'scaling' of a parton distribution (invariance on energy scale Q).

The logarithmic variable ξ_p (second panel) emphasizes the low-x_p (large ξ_p) region and better reveals the details of low-Q^2 fragmentation. The distribution is *approximately* Gaussian, with mode ξ_p^* and r.m.s. width σ_{ξ_p} predicted by pQCD. The fall-off at large ξ_p and maximum at ξ_p^* result from gluon coherence: parton showering is terminated when gluon transverse momenta fall below a characteristic momentum scale conjugate to hadron size. Measurement of the full fragment distribution below and above the mode is essential for a precise characterization of the fragmentation process.

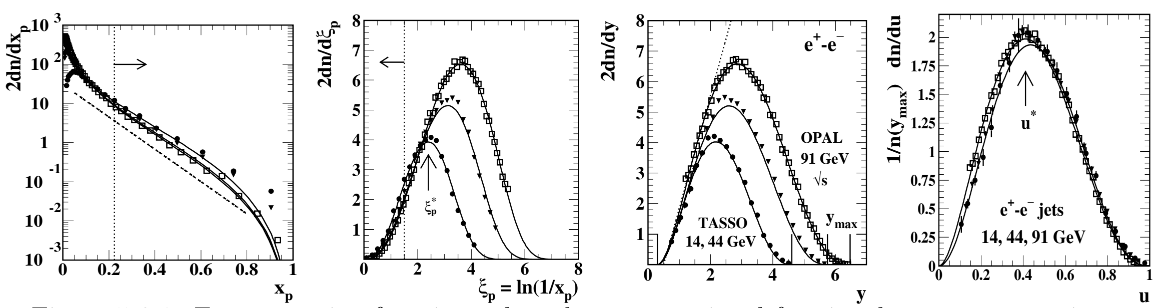

Figure 5.6-1. Fragmentation functions plotted on conventional fractional-momentum variables x_p and ξ_p and on the variables adopted for this analysis: rapidity y and normalized rapidity u.

In the third panel we plot the same data FFs on rapidity $y = \ln((E+p)/m)$. Distributions plotted on y exhibit an interesting feature. In the third panel we observe that the FFs for three energies have a common low-momentum limit $y_{min} \sim 0.35$ (vertical line). That observation is possible on rapidity because y has the well-defined limiting value 0 as momentum $p \to 0$, whereas conventional logarithmic variable ξ_p does not. Furthermore, the maximum rapidity (y_{max}) is determined by a strictly kinematic limit.

The new plotting format permits more precise study of FFs. For the independent variable we introduce normalized rapidity $u \equiv (y - y_{min})/(y_{max} - y_{min}) \in [0, 1]$. For the data normalization we note that fragmentation functions from e^+-e^- collisions can be factorized into dijet multiplicity $2n(y_{max})$ and a unit-normal form factor $g(u, y_{max})$, defining $D(u, y_{max}) = 2n(y_{max})\, g(u, y_{max})$. In the fourth panel we plot the three representative FFs transformed to normalized densities $g(u, y_{max}) \equiv 1/n(y_{max})\, dn/du$. $2n(y_{max})$ can be obtained from fits to data FFs, but the *shape* of $g(u, y_{max})$ also determines $2n(y_{max})$.

We observe that the form factor $g(u, y_{max})$ is well-described by beta distribution $\beta(u; p, q)$. The unit-normal beta distribution defined on $u \in [0, 1]$ is $\beta(u; p, q) = u^{p-1} (1-u)^{q-1}/B(p, q)$, with parameters p, $q \geq 0$ and beta function $B(p, q) = \frac{\Gamma(p)\,\Gamma(q)}{\Gamma(p+q)}$. That model function provides the solid curves in each panel, with model parameters (p, q) determined by the systematic trends on energy from our analysis (see Sec. 5.9) and transformed to each plotting space with appropriate Jacobians.

While we observe substantial 'scaling violations' on x_p or ξ_p (variation with parton energy scale Q^2) the distribution shapes on normalized rapidity u in the fourth panel are nearly independent of Q^2 or y_{max} over a substantial energy range. The small differences between data at different energies are however statistically quite significant. The differences in shape are determined by the energy systematics of the beta-distribution parameters (p, q) obtained in this analysis. Beta-distribution fits to data provide a precise description of the energy-scale dependence of FFs which includes *all* fragment momenta. This plotting format may distinguish more fundamental aspects of energy evolution of the fragmentation process (parton shower structure) from kinematic issues.

5.7 Identified hadron fragment distributions

D. T. Kettler and T. A. Trainor

Fragmentation functions (FFs) for identified hadrons as well as unidentified particles have been measured. Based on the abundances of the different hadron types in the process *unidentified parton → identified hadron* pions appear to be the dominant end-product of parton fragmentation. We have therefore defined a rapidity for unidentified hadrons by assigning the pion mass to all particle species. The other two significant fragment contributions are kaons and protons. To investigate the consequences of that procedure we consider identified-particle fragmentation data for three CM energies. In Fig. 5.7-1 we show data distributions $g(u, y_{max})$ and model functions $\beta(u; p, q)$ for identified charged pions $\pi^{\pm}$ (first panel) and kaons $K^{\pm}$ (second panel). The parton rapidity y_{max} was in each case determined using the assigned *hadron fragment mass.* The corresponding distributions for identified protons ($p,\bar{p}$) show similar behavior but with substantially larger statistical errors.

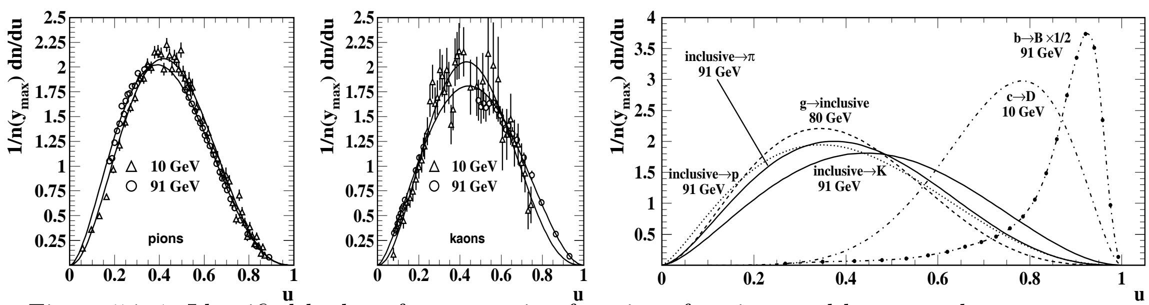

Figure 5.7-1. Identified hadron fragmentation functions for pions and kaons, and summary of fragmentation functions for identified partons and fragments.

Certain trends are notable: Proton fragments have the largest momenta but the smallest rapidities. When transformed to normalized rapiditity u the FFs for different fragment species are similar in shape but with significant differences. This is seen in the right panel and discussed further below. Unit-normal distributions $g(u, y_{max})$ for all species are well-described by function $\beta(u; p, q)$ and the variations between hadron types appear to be more significant than the variations with energy of a given type. This result establishes that the beta distribution is applicable to FFs for identified light meson and baryon fragments as well as to unidentified hadrons.

In the right panel we summarize fragment beta distributions for different fragment and parton types. We observe that the distribution mode tends to increase monotonically with increasing meson and parton mass. This is expected since a heavier meson should aquire a larger fraction of the parent parton's momentum. However, the proton peak mode for udsc (light-quark) jets is lower than the inclusive-hadron mode for gluon jets, and the proton distribution is significantly broader. The beta distribution generally describes the data well, except for the b-parton/B-meson data (the b → B curve is a spline fit to the data).

5.8 Fragment distributions from identified partons

D. T. Kettler and T. A. Trainor

We have observed that measured parton fragmentation functions (FFs) are well-described by the universal form $\beta(u; p, q)$, with shape parameters (p, q) generally depending on hadron fragment species and parton energy scale. We now consider the role of parton flavor in determining FFs. Normalized fragment distributions on normalized rapidity u are shown in Fig. 5.8-1 for unidentified hadrons from light-quark (udsc) jets (first), gluon jets (second) and b-quark jets (third) and for several parton energies in each case. Significant uncertainties in the lowest fragment momenta relative to y_{min} are indicated by horizontal error bars.

The best-fit beta distributions for $\sqrt{s}/2 = 45.6$ GeV udsc quark and 40.1 GeV gluon jets (data with the best statistics) are repeated as the dashed (β_{q}) and dash-dot (β_{g}) curves respectively in all three panels to provide a reference. Those results indate that the shape of the $g(u, y_{max})$ form factor depends more strongly on parton flavor than on energy scale in the energy interval studied. There is a substantial difference between quark and gluon jets at larger jet energies and a strong energy dependence of gluon jet shapes for smaller jet energies, evident in the second panel (the two solid curves correspond to ~ 5 and 40 GeV gluons).

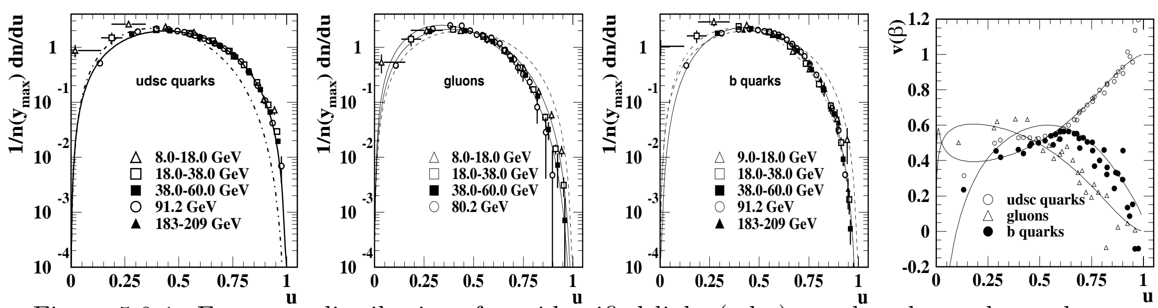

Figure 5.8-1. Fragment distributions from identified light (udsc) quarks, gluons, b quarks and a detailed comparison of b-quark fragments with those from udsc quarks and gluons.

In contrast to other cases, the b-quark data in the third panel are not well described by the beta distribution. We observe that distribution β_{q} (dashed curves) representing light fragments in udsc jets and distribution β_{g} (dash-dot curves) representing gluon jets appear to be limiting cases for all $\beta(u; p, q)$. We therefore define $v_{max} \equiv \ln(\beta_{\mathrm{q}} + \beta_{\mathrm{g}})$, $v_{min} \equiv -\ln(1/\beta_{\mathrm{q}} + 1/\beta_{\mathrm{g}})$ and normalized variable $v(\beta) \equiv (\ln \beta - v_{min})/(v_{max} - v_{min})$, with $v(\beta_{\mathrm{q}}) + v(\beta_{\mathrm{g}}) = 1$. We plot $v(\beta_{\mathrm{q}})$, $v(\beta_{\mathrm{g}})$ and $v(\beta_{\mathrm{b}})$ as the solid curves in the fourth panel along with corresponding data. We observe that the light-fragment distribution from b quarks (solid dots) coincides with $v(\beta_{\mathrm{q}})$ (and open circles) for $u < 0.7$, but diverges sharply from the quark-jet trend above that point and approaches gluon-jet trend $v(\beta_{\mathrm{g}})$ (and open triangles) as $u \to 1$. The b-quark fragment data were renormalized for this plot (reduced by 10%) to coincide with the quark-jet curve below $u \sim 0.7$. The initial data normalization is represented by the unit-normal beta-distribution fit (solid curve) with mode near 0.5. With this differential plotting format we confirm that b-quark light-hadron fragments are not well described by a beta distribution.

5.9 Parton energy dependence of fragmentation functions

D. T. Kettler and T. A. Trainor

By fitting e^+-e^- fragmentation functions (FFs) on normalized rapidity u with beta distribution $\beta(u;p,q)$ we provide a very compact representation of FF energy dependence. Dijet multiplicities $2n(y_{max})$ (y_{max} is the parton rapidity) can be obtained directly by integrating measured FFs. However, there is a direct correspondence between $2n(y_{max})$ and beta-distribution parameters $[p(y_{max}), q(y_{max})]$. We combine energy conservation within the cascade with the beta-distribution form factor to obtain $2n(y_{max}) = 1/\int_0^1 du\, x_E(u, y_{max})\beta(u;p,q)$, where $x_E(u, y_{max})$ is the energy fraction of a fragment with normalized rapidity u. Measured multiplicity trends on parton energy (or y_{max}) then provide tight constraints on the energy dependence of parameters (p,q).

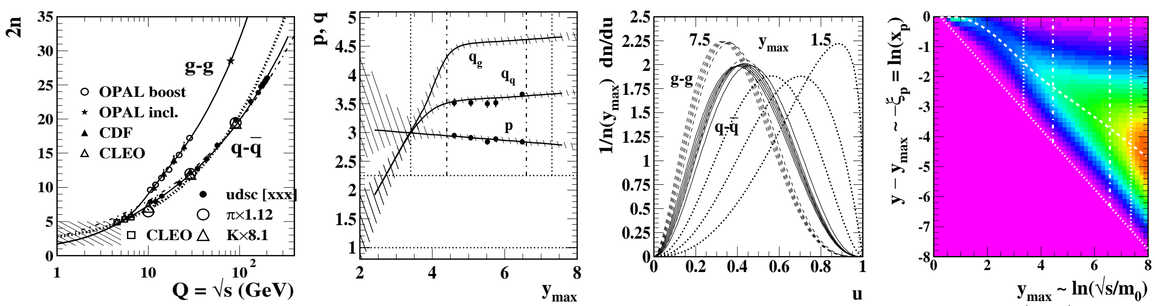

Figure 5.9-1. Energy dependence of dijet multiplicities $2n$, β-distribution parameters (p,q), beta distributions for a range of y_{max} and joint fragment distribution $D(y, y_{max})$.

The points in Fig. 5.9-1 (first panel) are measured di-jet multiplicities for g-g (gluon) and q-q̄ (quark) parton pairs. The solid curves correspond to integrals of the beta distribution, with our parameters (p,q) varied to fit the multiplicity data but constrained by (p,q) values from fits to fiducial FF data. In Fig. 5.9-1 (second panel) we show the energy dependence of parameters (p,q) which generated the solid curves in the first panel. The (p,q) curves summarize the energy dependence of light-quark and gluon fragmentation to unidentified hadrons in e^+-e^- collisions. The dotted vertical lines mark the limits of multiplicity measurements, while the dash-dot lines mark the limits of measured fragment distributions used in this analysis. The ten points represent fits to five fiducial fragmentation functions.

To the right of the first dash-dot line the parameters vary slowly with increasing energy scale. To the left of that line, the low-Q^2 region which motivated this study, the q parameters change rapidly. The multiplicity data require a sharp drop in the qs for both quarks and gluons, and a convergence of quark and gluon qs at the energy scale defined by the lower dotted line. The third panel shows beta distributions at a series of y_{max} values from 1.5 to 7.5 to illustrate variation of the FFs over a large energy range ($y = 8$ corresponds to $\sqrt{s} \sim 400$ GeV). We now have the components to construct a 2D fragment density in the form $D(y, y_{max}) = 2n(y_{max})\,\beta[u(y, y_{min}, y_{max}); p(y_{max}), q(y_{max})]$. In Fig. 5.9-1 (fourth panel) we show distribution $D(y, y_{max})$. The dashed curve is a 'locus of modes' (positions of maxima) of conditional slices on y with y_{max} fixed. Approach of that curve to the upper boundary ($y - y_{max} = 0$) corresponds to the approach of the dotted curves in the third panel to $u = 1$. This joint distribution is the basis for extrapolating FFs down to $Q \sim 1$ GeV ($y_{max} \sim 2$).

5.10 Scaling violations from beta-distribution fragmentation functions

D. T. Kettler and T. A. Trainor

Fragmentation functions (FF) plotted on x_p are approximately exponential (see Fig. 5.10-1 – third panel). So-called scaling violations (FF variations with parton energy scale Q) consist of an increasingly negative slope of the FF on x_p (the distribution 'softens') with increasing energy. Scaling violations are larger for gluon jets than for quark jets (greater color charge). To illustrate scaling violations in that conventional context we transform our parameterized FFs $D(y, y_{max})$ to $D(x_E, Q^2) = p/(E\, x_E) D[y(x_E Q), y_{max}(Q)]$. In Fig. 5.10-1 (first panel) we plot *conditional* distributions $D(x_E, Q^2)$ for $x_E = 0.02, 0.07, 0.15, 0.27, 0.41, 0.60, 0.81$ *vs* $Q = m_0 \cosh(y_{max})$ which precisely represents all LEP and HERA FFs. As an alternative fragment measure we introduce the *logarithmic derivative* $d \ln D(y, y_{max})/d \ln y_{max}$ plotted in Fig. 5.10-1 (second panel). That quantity reveals an underlying simplicity to the fragmentation process in the energy range best described by perturbative QCD (right of the dotted line).

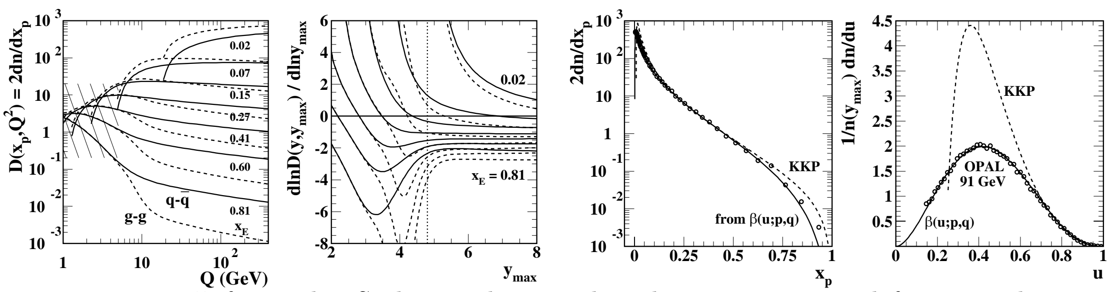

Figure 5.10-1. Left panels: Scaling violations plotted in a conventional format and as logarithmic derivatives. Right panels: Comparison of OPAL 91 GeV data and FFs based on beta distributions (solid curves) and scaling violations (dashed curves) in two plot formats.

Scaling violations are described by QCD theory in the form of the DGLAP equations

$$\frac{dD_i^h(\xi, s)}{d \ln s} = \frac{\alpha_s(s)}{2\pi} \sum_j \int_0^\xi d\zeta\, P_{ij}(\zeta)\, D_j^h(\xi - \zeta, s), \tag{1}$$

with $\xi_p = \ln(1/x_p)$, $\zeta = \ln(1/z)$, z the usual integration variable and $P_{ij}(\zeta)$ the Altarelli-Parisi splitting functions. In a typical study of scaling violations $D(x, s)$ is parameterized at several energy scales s with a model function, *e.g.* $D(x, s) = N\, x^\alpha\, (1 - x)^\beta\, (1 + \gamma/x)$. The DGLAP equations are used to evolve the model FFs between energy scales, varying $(N, \alpha, \beta, \gamma)$ with energy to best fit the data and emphasizing the region $x > 0.1$ where pQCD is most applicable. A typical result of that procedure, a KKP FF,[1] is illustrated in the last two panels of Fig. 5.10-1 where OPAL 91 GeV FF data (points), our corresponding beta distribution (solid curves) and the corresponding KKP FF (dashed curves) are compared. In the conventional context of the scaling-violations approach (third panel) agreement among data and models appears to be good. However, the same distributions plotted on normalized rapidity u in the fourth panel show that whereas the KKP FF (defined by fourteen parameters) adequately represents less than 10% of the fragments (for $x_p > 0.1$) our beta-distribution FF (defined by two parameters) describes 100% of the data down to $x_p = 0$, to few-percent accuracy.

[1] B. A. Kniehl, G. Kramer and B. Pötter, Nucl. Phys. B **582**, 514 (2000).

5.11 Correlations on transverse rapidity and fragmentation functions

D. T. Kettler, R. J. Porter and T. A. Trainor

Fig. 5.11-1 (first panel) shows SS-US correlations from 200 GeV p-p collisions plotted on transverse-rapidity space (y_{t1}, y_{t2}). We observe *soft* (smaller y_t) and *hard* (larger y_t) components. Pairs can also be separated on azimuth difference variable ϕ_Δ into *same-side* (SS) pairs ($|\phi_\Delta| < \pi/2$) and *away-side* (AS) pairs ($|\phi_\Delta| > \pi/2$). The 'soft' and 'hard' terminology is based on corresponding angular correlations. Hard-component angular correlations—a symmetric SS peak at the origin (jet cone) and AS ridge—are consistent with hard-scattered parton fragmentation or jets. We thus interpret the SS unlike-sign (US = $+-$, $-+$) hard-component peak at $y_t \sim 2.8$, elongated along $y_{t\Sigma}$ and running continuously into a small US soft component, as dominated by correlations among fragments from minijets.

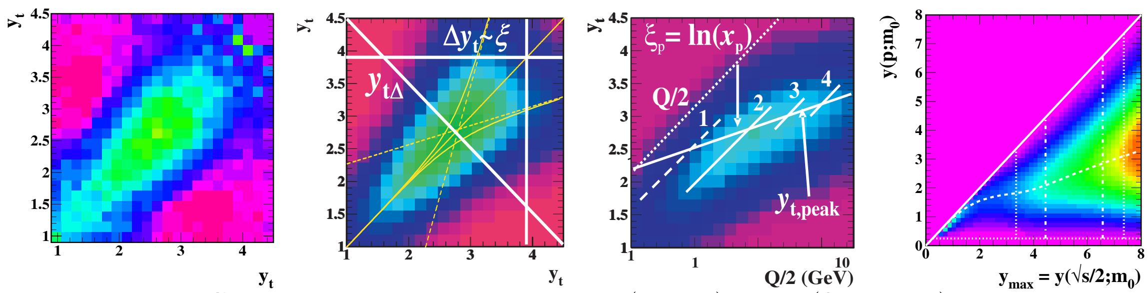

Figure 5.11-1. Correlations on transverse rapidity (y_{t1}, y_{t2}): data (first panel) and model (second and third panels) based on measured fragmentation functions (fourth panel).

Fig. 5.11-1 (second and third panels) shows a previous attempt to explain the origin of the correlation structure. The third panel sketches a joint distribution of parton fragments (on transverse rapidity y_t) *vs* parton energy scale $Q/2$ based on measured fragmentation functions (FF) in elementary collisions. The solid diagonal line suggests the locus of modes (peak positions) of FFs relative to parton energy (dotted line). Symmetrizing such a distribution to represent not fragment *vs* parton but fragment *vs* fragment leads to the second panel, which fairly represents the data in the first panel.

The data and qualitative sketch in Fig. 5.11-1 prompted the detailed study of LEP e^+-e^- FFs reported in previous articles. From that study we established a precise representation of all e^+-e^- FFs over a broad energy range. We used a parameterized beta distribution to construct a 2D fragment density on (y, y_{max}). The resulting 2D distribution $D(y, y_{max})$ is shown in Fig. 5.11-1 (fourth panel). The diagonal solid line represents the parton rapidity (y_{max}). The horizontal dotted line represents y_{min} (common lower bound for all FFs). The vertical dotted and dash-dot lines mark the energies bounding the measured FFs (dash-dot) and measured multiplicities (dotted) used to define the (p, q) representation. The dashed curve is a 'locus of modes' (positions of maxima) of conditional slices on y with y_{max} fixed. The approach of that curve to the solid diagonal line ($y = y_{max}$) corresponds to the approach of the FFs to a delta function representing 'fragmentation' of one gluon to one hadron (the low-Q^2 limiting case). Comparison of the FF surface distribution to the left of the lower dash-dot line with the sketch in the third panel indicates that the latter is indeed a fair representation of low-Q^2 parton fragmentation, now precisely characterized from FF data.

5.12 Angular asymmetry of low-Q^2 parton fragments and non-perturbative parton scattering and fragmentation

R. J. Porter and T. A. Trainor

We have introduced new analysis techniques that reveal jet correlations down to very low Q^2, where Q^2 is the negative invariant mass squared $(-q^2)$ of the four-momentum transfer between partons in a radiating color dipole. In the first panel of Fig. 5.12-1 we show inclusive correlations for p-p collisions at $\sqrt{s} = 200$ GeV on transverse rapidity $y_t = \ln[(m_t + p_t)/m_\pi]$, with transverse mass $m_t^2 = p_t^2 + m_\pi^2$. The large peak in the center we attribute to transverse parton fragmentation. The smaller peak at lower-left we attribute to longitudinal fragmentation. The grid defines a momentum cut space for an angular correlation analysis. Angular correlations from transverse fragmentation include a 'jet cone' or peak at the origin of angle space $(\eta_\Delta, \phi_\Delta)$ which is studied in the remaining three panels.

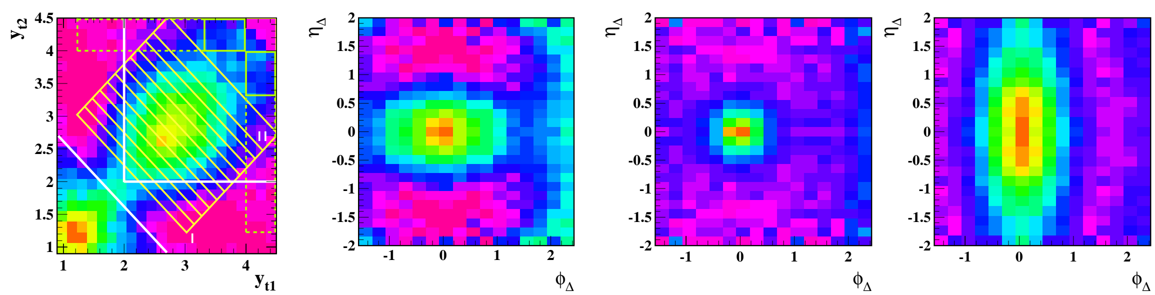

Figure 5.12-1. Left panel: p-p correlations on transverse rapidity space (y_{t1}, y_{t2}) used as a cut space for study of angular correlations. Right panels: Angular correlations from 200 GeV p-p (low and high Q^2, regions 1 and 11) and 130 GeV mid-central Au-Au collisions.

The right three panels show angular correlations on pseudorapidity and azimuth difference variables $(\eta_\Delta, \phi_\Delta)$ plotted in an exact 1:1 aspect ratio. The second panel shows the jet cone corresponding to region 1 of the first panel: the lowest-Q^2 parton collisions which produce correlated fragments interpretable as 'jets,' with a strong elongation in the ϕ_Δ direction not previously observed. The next panel shows the jet cone corresponding to region 11 of the first panel, with radius ~ 0.7 *nearly* symmetric and thus corresponding to pQCD expectations (there remains a small angular asymmetry favoring ϕ_Δ). The right-most panel is obtained from $\sqrt{s_{NN}} = 130$ GeV mid-central Au-Au collisions: strongly elongated in the η_Δ direction.

Both deviations from the pQCD symmetric jet cone, for low-Q^2 partons in p-p and minimum-bias partons in Au-Au mid-central collisions, are very interesting and signal possible new physics. In the case of central Au-Au collisions coupling of the parton fragmentation process to the longitudinal expansion of a colored medium could provide a mechanism for angular deformation. In the case of low-Q^2 parton interactions in p-p collisions we encounter an unanticipated phenomenon. The azimuth direction is strongly favored for parton fragments. That result suggests that at low Q^2 kinematic details of the parton collision, including the 'contact plane' defined by the collision of two spheres, may be relevant.

5.13 Precision centrality determination in A-A collisions

D. J. Prindle and T. A. Trainor

Because of the very strong centrality dependence of observed two-particle correlations we have pursued the development of precision centrality determination in A-A collisions based on the 'power-law' format: minimum-bias distributions on particle multiplicity, participant nucleon number and binary-collisions number all exhibit approximate power-law trends. Conventional centrality determination has typically been restricted to fractional cross sections in the range $0-80\%$. Fig. 5.13-1 (first panel) shows the nearly linear relation which connects $(n_{part}/2)^{1/4}$ to centrality measured by fractional cross section $1-\sigma/\sigma_0$. (Similar results pertain to the number of binary collisions in the power-law form $(n_{bin})^{1/6}$.) The solid curve is the *running integral* of the minimum-bias distributions on $(n_{part})^{1/4}$ which confirms that the power-law approximation (straight line in this context) is very good. The power-law format provides a simple means to parameterize centrality relations precisely. For the purpose of centrality determination the power-law Glauber-model curves at 200 GeV are well represented by linear expressions $(n_{part}/2)^{1/4} = 1 + 2.72\,(1-\sigma/\sigma_0)$ and $n_{bin}^{1/6} = 1 + 2.23\,(1-\sigma/\sigma_0)$. Monte Carlo Glauber results are thus represented precisely ($< 2\%$) by four numbers: exponents 1/4 and 1/6 and upper limits $n_{part,max}/2 = 3.72^4$ and $n_{bin,max} = 3.23^6$.

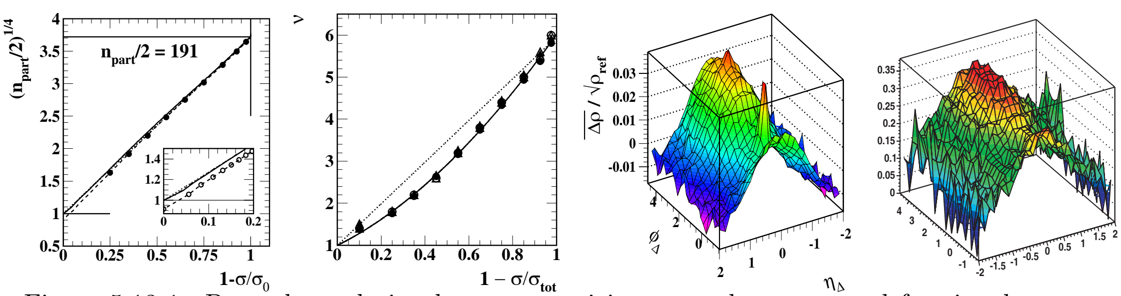

Figure 5.13-1. Power-law relation between participant number n_{part} and fractional cross section, path-length estimator ν, comparison between p-p and 90-100% central Au-Au data.

With precise expressions for $(n_{part}/2)^{1/4}$ and $n_{bin}^{1/6}$ *vs* fractional cross section established we can define participant path-length estimator $\nu = 2n_{bin}/n_{part}$, a geometric estimator defined in terms of *encountered nucleons* rather than a specific nuclear interaction, with limiting value 1 for peripheral A-A. Using the parametric expressions above we have

$$\nu = \{1 + 2.23(1-\sigma/\sigma_0)\}^6/\{1 + 2.72(1-\sigma/\sigma_0)\}^4. \tag{1}$$

Fig. 5.13-1 (second panel) shows $\nu(\sigma/\sigma_0)$ from Eq. (1) as the solid curve with maximum value near 6. The dotted line $1 + 5(1-\sigma/\sigma_{tot})$ provides a curvature reference. This result corresponds to σ_{NN} for 200 GeV N-N collisions. In the last two panels we compare soft-component ($p_t < 0.5$ GeV/c) angular autocorrelations for 200 GeV p-p collisions (third panel) with identified pions ($p_t < 0.8$ GeV/c) in the most peripheral (90-100% central) 200 GeV Au-Au collisions. The agreement of the two structures is excellent. This is the first direct comparison of such peripheral A-A collisions (90-100% – dominated by N-N) with p-p data and establishes the effectiveness of the power-law approach to centrality determination.

5.14 Two-particle correlations with identified particles

R.J. Porter, D. J. Prindle and T. A. Trainor

Over the past few years the dE/dx (specific energy loss) method of particle identification (PID) for the STAR TPC has become sufficiently reliable that we can use it in our correlation analysis to identify nearly pure samples of $\pi^{\pm}$, $K^{\pm}$, p and $\bar{p}$. The dE/dx PID method is reliable only over a limited momentum range, and some particle samples are contaminated by electrons in certain momentum ranges. Thus, addition of a time-of-flight PID system will be an important addition. Given the limitations of dE/dx PID we are now beginning to develop two particle correlations in conjunction to dE/dx PID as an initial exploration of correlations within the accessible momentum ranges as well as to prepare for more complete analysis with a TOF PID system.

The standard criterion for dE/dx PID is to require that a particle be within 2σ of the mean dE/dx value for a given species and outside the 2σ dE/dx band(s) for neighboring species. The $\pi^{\pm}$ band goes through a minimum at a momentum of just under 1 GeV/c and then passes through the $K^{\pm}$ and proton bands. This causes a gap in $\pi^{\pm}$ spectra, and we expect the higher-momentum part to have different correlation characteristics (and different physics) than the lower-momentum part. Thus we require $\pi^{\pm}$ and $K^{\pm}$ momenta to be less than 1 GeV/c.

For identified particles there may be a difference between π^{+}-p and $\pi^{-} - \bar{p}$. One of the code changes required was to place those pair types in separate histograms, not combine them as LS = $(++) + (--)$. We expect differences in the $y_{\perp}$ of π and protons, so for the unlike particle $y_{\perp} \times y_{\perp}$ histograms we keep track of the particle types and form an unsymmetrized two-particle distribution.

Currently, our various two-particle correlations codes have been modified to include a PID option and the code is being debugged. Issues arose due to the substantially different mean-$p_{\perp}$ ranges of the different particle types which have been resolved. We have run small data samples during the debugging phase. We are now preparing for a moderate-size check of the overall PID code prior to full production running.

5.15 CI and CD angular correlations in 200 GeV Au-Au collisions

M. Daugherity,* D. J. Prindle, R. L. Ray* and T. A. Trainor

Precision centrality determination over 100% of the A-A impact-parameter range becomes possible with new techniques described elsewhere in this report (see Sec. 5.13). Correlation measurements for peripheral A-A collisions out to very peripheral A-A ($\sim$ N-N) collisions are now possible (conventional methods fail beyond 80% fractional cross section). To confirm that capability we compare charge-independent (CI) and charge-dependent (CD) angular correlations measured in p-p collisions and in three centrality classes of Au-Au collisions at 200 GeV. Fig. 5.15-1 shows CI (top row) and CD (bottom row) angular correlations on pseudorapidity difference $\eta_\Delta = \eta_1 - \eta_2$ and azimuth difference $\phi_\Delta = \phi_1 - \phi_2$. The left panels are data from p-p collisions. The remaining panels are in order Au-Au centrality bins corresponding to fractions 90-100%, 60-70% and 5-10% of the total hadronic cross section. The 90-100% centrality bin should be dominated by N-N collisions according to a Glauber simulation.

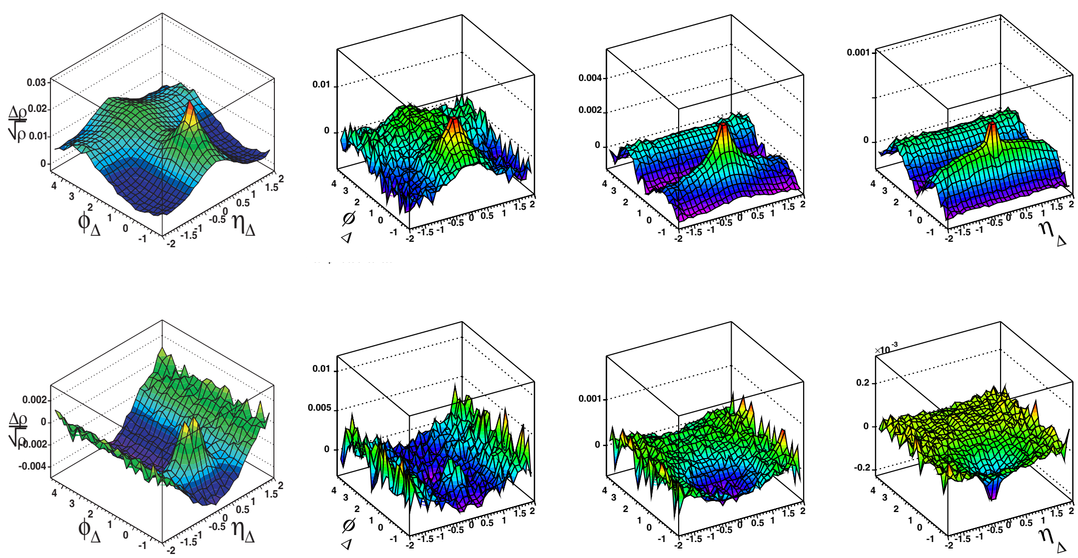

Figure 5.15-1. CI and CD angular correlations for p-p collisions (left panels) and 200 GeV Au-Au collisions. Centralities are 90-100%, 60-70% and 5-10% of total cross section.

We observe that the first two panels in each row are in excellent agreement, given slightly different pair-cut systems (*e.g.,* suppression of HBT or quantum correlations in Au-Au data) for the two analyses. The evolution of CI correlations with increasing centrality reveals the increasing amplitude of elliptic flow as a $\cos(2\phi_\Delta)$ sinusoid and strong elongation of the same-side ($|\phi_\Delta| < \pi/2$) minijet peak on η_Δ (minijet deformation). The evolution of CD correlations with increasing centrality reveals a dramatic change in net-charge correlations from 1D charge correlations on η_Δ in p-p collisions to a symmetric, large-amplitude and *highly-localized* 2D correlation on $(\eta_\Delta, \phi_\Delta)$ in Au-Au collisions, suggesting local charge conservation for hadron production from the 2D surface of a colored medium in central Au-Au collisions.

*Department of Physics, University of Texas, Austin, TX 78712.

5.16 Novel fluctuation and correlation analysis methods

D. T. Kettler, D. J. Prindle, R. J. Porter and T. A. Trainor

The complex structure of RHIC heavy ion and p-p collisions has driven major advances in correlation and fluctuation analysis methods. The most striking physical phenomenon that has emerged in our study of RHIC heavy ion collisions, and which we further pursue in p-p and e^+-e^- collisions, is fragmentation (color dipole radiation) from low-Q^2 parton collisions. Some of the novel techniques developed to study this new phenomenon are briefly described.

Joint angular autocorrelations Two-particle correlation analysis requires projection of the six-dimensional two-particle momentum space to viewable two-dimensional subspaces with as little information loss as possible. The joint angular autocorrelation makes it possible to reduce 4D two-point angular subspace $(\eta_1, \eta_2, \phi_1, \phi_2)$ to the 2D space of difference variables $(\eta_\Delta, \phi_\Delta)$ with no information loss *if* the full angular distribution is *stationary*, that is, does not depend significantly on sum variables $(\eta_\Sigma, \phi_\Sigma)$. We find that stationarity is a good approximation for nuclear collisions near mid-rapidity at RHIC energies.

Per-particle fluctuation measures There are many algebraic options for the definition of differential fluctuation measures. However, most possibilities can be ruled out on the basis of statistical bias and/or uninterpretable behavior. We have determined that interpretable fluctuation measures must be *per-particle* measures, that is, invariant under linear superposition in the absence of nontrivial correlation structure. An example is the scale-dependent variance difference $\Delta\sigma^2_{p_t:n}(\delta x) \equiv \overline{(p_t(\delta x) - n(\delta x)\,\hat{p}_t)^2}/\bar{n}(\delta x) - \sigma^2_{\hat{p}_t}$. If systems A and B have similar p_t correlation structure and are otherwise independent then $\Delta\sigma^2_{p_t:n}$ values for A, B and A+B will be the same. That property is essential for interpretable analysis of collision centrality dependence and energy dependence of $\langle p_t \rangle$ fluctuations for instance.

Inversion of fluctuation scale dependence We have determined the integral equation which connects fluctuation scale dependence to angular autocorrelations. By numerical inversion of fluctuation scale dependence we have provided physical interpretations of excess fluctuations in a number of cases where previously the mechanism was little understood. In the case of $\langle p_t \rangle$ fluctuations the corresponding p_t autocorrelations have revealed the new phenomenon of medium recoil in response to parton stopping in heavy ion collisions.

Transverse rapidity and normalized transverse rapidity We have introduced rapidity y and normalized rapidity u into the analysis of parton fragmentation in nuclear and e^+-e^- collisions. Use of relativistic momentum variables when momenta are hundreds of times the typical particle mass would seem to be recommended, but the conventional basis for momentum spectrum analysis has continued to be linear momentum variables p_t and x_p. Introduction of rapidities has greatly improved our understanding of event structure.

The beta distribution The conventional approach to modeling fragmentation functions on linear momentum fraction x_p leads to many-parameter model functions which typically describe only a small fraction of the total fragment distribution. We have determined that the two-parameter beta distribution $\beta(u;p,q) = u^{p-1}\,(1-u)^{q-1}/B(p,q)$ with $B(p,q) = \Gamma(p)\,\Gamma(q)/\Gamma(p+q)$ provides a natural and precise ($\sim 1\%$) description of fragmentation functions over 100% of the fragment momentum range and over a very large parton energy range.

5.17 GUI for submission and monitoring of STAR data analysis jobs

R. J. Porter and D. J. Prindle

Analysis of data recorded by the STAR detector is very complex. The analysis software is complex, the datasets are so large that we use special software tools to access them, and we run the analysis in parallel on many computers to get results in a reasonable time. We have many datasets taken in different running periods with different beams and different energies as well as comparable numbers of simulation datasets. Each dataset requires its own set of event and track quality cuts. In addition, event simulators require input parameters describing the initial conditions for each beam and energy combination. Assembling consistent information for a given analysis job is manageable, but processing many different datasets and keeping track of all the input information and analysis results has become very difficult. To help manage our analysis task we have developed a GUI which creates analysis jobs, monitors their progress, and archives enough information to be able to reproduce the analysis if necessary.

We describe an analysis job using an XML tree. A given tree can describe analysis of real data, GEANT, Hijing or Pythia datasets. Every one of these trees contains branches for

`jobControl:` overall job control such as input and output directories
`starSubmit:` for STAR `scheduler` information
`eventCuts:` event-wise cuts to ensure quality data
`trackCuts:` track by track cuts to ensure quality data
`pairCuts:` track cuts to ensure quality pairs
`doEStuctMacro:` information specific to this analysis such as centrality definitions, if this is a two-point correlation or a fluctuation analysis

Hijing and Pythia each have a second branch for their control parameters. To ensure that a description is complete we validate it against an XML Schema that we have written. The schema not only states what elements have to be present, but in many cases the values are restricted to allowable ranges.

The XML tree describing the job is transformed into a set of files using XSLT templates. Among the files we create are an XML file for use by the STAR scheduler, a cuts file containing the track and event quality cuts and a root macro that drives the data analysis. These elements are placed in a standard directory structure which the GUI creates. We also save the XML tree and EStruct source code for use in understanding the output later. The job output and log files are copied to this directory tree on job completion.

The visual interface to the XML tree is created by a tcl program. This program allows selection of a standard analysis job or the reading of an XML file describing the job. It creates a visual representation for each branch, containing entry widgets, comboboxes or buttons depending on attributes in the XML tree. Balloon help is available using attributes from the schema. When a change is made it is verified against the schema, showing whether the new value is allowable. When all required fields are set the job can be submitted, invoking the scheduler which checks for the location of the data and creates many csh scripts that can be submitted to a computer farm. Running analysis on a complete data set can require many hundreds of jobs on multiple computers in the farm. The progress and output of the jobs can be monitored via a tcl program. These tools take care of many of the book-keeping tasks, allowing us to concentrate on the data analysis itself.

5.18 Web interface for viewing histograms of data analysis

D. J. Prindle and M. Rodenburg

The correlation analysis of heavy ion collisions contains several aspects. We analyze data as a function of collision centrality, energy and beam species as well as compare real data with simulations. Two-particle correlation measurements include angular auto-correlations on difference variables $\eta_\Delta - \phi_\Delta$ and correlations on transverse rapidity $\mathrm{y}_\perp - \mathrm{y}_\perp$. It is useful to divide results into different charge combinations: like-sign, unlike-sign, charge-dependent and charge-independent, each of which may reveal a different physics issue. We can measure the $\eta_\Delta - \phi_\Delta$ auto-correlations using pair counting, but they can also be obtained by measuring fluctuations as a function of scale and performing a numerical inversion to autocorrelations. Together these combinations give us thousands of 2D histograms which we not only want to examine for trends but also share and discuss with persons at other institutions. To manage visual access to this complex data volume we have written a web interface that makes it easy to add to and view histograms in a directory structure. After a directory is established many persons can conviently select histogram subsets for viewing using our web browser.

Histograms to be browsed are put into a directory structure which has as descending levels the beam type and beam energy (e.g. CuCu62), a data type (e.g. Data or Hijing) and a data sub type (e.g. state of a simulation program – Hijing quench on or off). The histogram names consist of fields separated by underscores, the fields indicating the histogram type (e.g. fluctuations or 2-point correlations), whether it is number or momentum correlations, the charge combination, the centrality range, the $\mathrm{p}_\perp$ range and whether it represents errors or residuals or the measure itself by default. The html interface is generated by a javascript program that scans all directories from its base looking for all files that satisfy a defined pattern. The resulting html presents an interface showing all the directories, allowing the user to select one. On selecting a particular directory a javascript program generates a set of check boxes for selecting a subset of the available properties and a submit button that creates a page of all histograms within that directory which satisfy the selection. This allows convenient selection of e.g. AuAu200 charge-dependent momentum autocorrelations from fluctuation inversion for all centralities. To compare different data sets we can open other windows with the same selection criteria but from a different directory. The javascript program that generates the interface can be invoked from the top-level page at any time to scan for new histograms.

The 2D histograms are displayed in the form of gifs. To get information that is more flexible one can download the numerical histogram contents by clicking a button. It is also important to know where the histograms originate in order to check some aspect of the analysis or even redo it. An 'Analysis Trail' button displays a text file describing for example the centrality and $\mathrm{p}_\perp$ cuts, location of root analysis files, location of the inversion information, date of the analysis, etc. Currently, the text files are created by hand, but when the analysis software is modified to generate text files automatically those files will be used.

6 Electronics, Computing, and Detector Infrastructure

6.1 Electronic Equipment

G. C. Harper, J A. Mitchell, A. W. Myers, T. D. Van Wechel and J. A. White

The electronics shop personnel provided normal maintenance and repair on all laboratory electronics equipment in support of all experiments conducted at CENPA. The electronics shop also supported ongoing efforts at SNO, both from Seattle as well as on-site support at Sudbury, Ontario, Canada. Other projects undertaken by the electronics shop included the following.

1. Designed and built 2 temperature controlled racks with 2 NIM Bins and 1 CAMAC Crate for use in various experiments which required very stable electronics temperatures.

2. Upgraded the Terminal Ion Source high voltage power supplies to sealed/potted supplies.

3. Developed a new low noise/low power preamplifier for use in multiple experiments.

4. Designed a new Log Amp for the SNO MUX System.

5. Designed an 8 channel OR/Delay circuit for use in a new Muon detector to be installed at SNO.

6. Designed and built a High Voltage interface box to measure nanoamp currents in the Neutral Current Detectors at SNO.

7. Designed and built a 4 channel thermistor bridge circuit board for Gravity Experiments.

8. Developed a parametric preamplifier for use in the KATRIN experiment (development still in progress).

9. Provided support of the APOLLO experiment by modifying and adding functions to the Apollo Command Module circuit board FPGA which was developed here in 2003.

10. Populated two additional 32 bit GTID boards for possible use in KATRIN.

11. Populated Pulser Distribution boards for spares at SNO.

12. Designed and built a new Time-Base NIM Module for use in the ^{3}He + ^{4}He experiment.

13.Designed a 8 Channel NIM-TTL and 8 Channel TTL- NIM converter board for use in SNO and general use.

14. Designed and constructed a Dual purpose board with one section being an 8 input 2 output OR section and the other being a 1 input 8 output fanout section. This board is used in SNO as an interface between the shaper/ADC boards and the GTID Board as a ahaper lockout circuit.

6.2 Improvements to the ORCA DAQ system

J. A. Detwiler, M. A. Howe, F. McGirt,† J. F. Wilkerson and J. Wouters†

The Object-oriented Real-time Control and Acquisition (ORCA) system is an application software tool-kit that is designed for quickly building flexible data acquisition systems. In addition to being installed as the SNO NCD production DAQ system (see Sec. 1.4), ORCA is currently in use for several different development efforts including the KATRIN beta-decay experiment (see Sec. 1.6), detector characterization at University of Washington's Medical Imaging Lab, the Majorana double beta-decay experiment (see Sec. 1.12), and the SNO Muon chamber (MIT). Since ORCA has been extensively described in past CENPA Annual Reports,[1] only the most recent developments will be described here.

In the last year the number of hardware devices supported by ORCA increased substantially. New CAMAC cards added included the LeCroy 2228A TDC, LeCroy 3377 TDC, LeCroy 2132 high voltage controller, KineticSystems 3655 8-channel Timing Pulse Generator, LeCroy 3511 ADC, and the XIA digital gamma finder card. An IEEE1394 interface was developed for the control of FireWire devices including an Auger crate object, the Auger Second Level Trigger card, and the Auger First Level Trigger Card. Development work continues on these objects. In addition, RS232 support was added for the VXM stepper motor controller and the Newmark X/Y scanning platform controller. Finally, a major effort has started to develop the software framework to support compactPCI devices.

One big advance for ORCA was the addition of process control elements similar to the GORDO control system software.[2] Process control ladder diagrams are built by dragging elements from the object catalog into a process control container and connecting the elements into the desired logic configuration. Available elements include all common logic gates, flip-flops, one-shots, and counters. Input signals from digital I/O cards (such as the IP408) are fed into the ladder diagrams and the result is used to set digital output bits, post alarms, set run vetos, etc. Analog signals can also be monitored for out-of-band conditions which can be fed into the processing system.

In addition to the existing ORCA to ROOT capabilities, we are developing an ORCA to ROME interface which will allow users to leverage the power of ROME. ROME is a framework generator for event based data analysis that was developed for the MEG Experiment at PSI Switzerland. In the ROME environment, the experimenter defines the analysis framework for his experiment in an XML file. Out of this definition file, ROME generates all experiment specific classes of the framework. The experimenter only needs to add a small amount of custom code to have a full event building analysis package.

---

†Los Alamos National Laboratory, Los Alamos, NM 87545.

[1]CENPA Annual Report, University of Washington (2001) p. 83; (2002) p. 81; (2003) p. 70; (2004) p. 66; (2005) p. 85.

[2]CENPA Annual Report, University of Washington (1993) p. 89.

6.3 Single-molecule electrophoresis of RNA through a biological nanopore*

T. Z. Butler and J. H. Gundlach

We are continuing the development of a novel technique for the analysis of DNA/RNA at the single molecule level.[1] In this technique an external electric field drives DNA/RNA molecules through a nanometer-diameter protein pore. Translocation of a DNA/RNA molecule through the pore is observed as a transient obstruction of the ionic current flowing through the pore (Fig. 6.3-1). This technique may have the potential to be utilized in a low-cost, extremely fast DNA sequencing technology. It also constitutes a unique model system in which to investigate biologically relevant nanoscale processes.

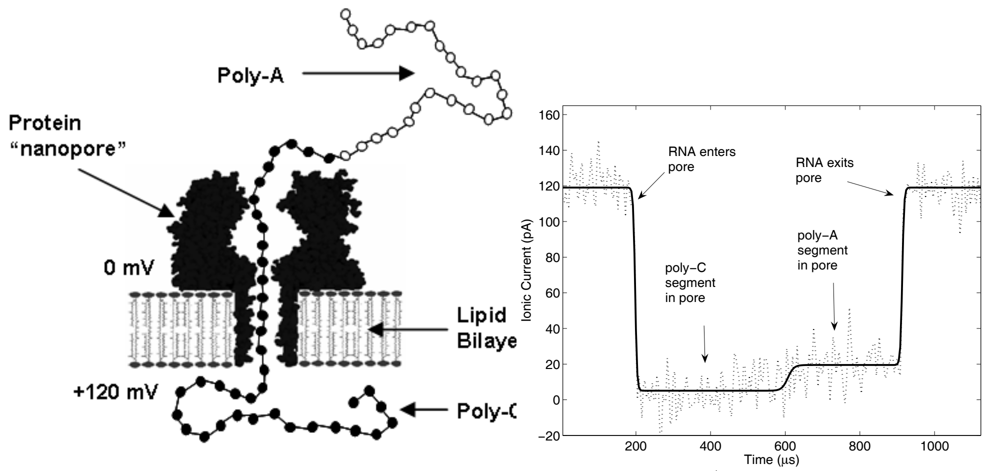

Figure 6.3-1. Schematic of electrophoretic translocation of a DNA/RNA molecule through a protein pore and an example of the resulting ionic current signal

Two distinct types of ionic current blockage signals are often observed in translocation experiments with homogeneous DNA/RNA molecules. It was hypothesized that the two possible orientations of a DNA/RNA molecule during translocation caused these two signal types. We tested this orientation hypothesis using diblock RNA molecules composed of a homogeneous adenine (poly-A) segment and homogeneous cytosine (poly-C) segment. The poly-C segment causes a deeper current obstruction than the poly-A segment, resulting in a bi-level signal during translocation (Fig. 6.3-1). The time-ordering of the bi-level signal indicates the orientation of the molecule during translocation. We conducted translocation experiments with four RNA constructs: A_{50}, C_{50}, $A_{25}C_{50}$ and $C_{50}A_{25}$. Classification and parameterization of each current obstruction signal enabled a quantitative comparison of the translocation characteristics of the four RNA constructs. The solid line in Fig. 6.3-1 shows the phenomenological fit function used to parameterize the translocation signal (dashed line). Our analysis confirmed the orientation hypothesis and revealed a number of additional orientation-dependent translocation phenomena.[2] Other work done on this project includes improvements to the experimental apparatus, preliminary experiments with alternative protein pores, and the development of improved electronics for ionic current detection.

---

*Not supported by DOE CENPA grant

[1]CENPA Annual Report, University of Washington (2004) p. 62.

[2]T. Z. Butler, J. H. Gundlach and M. A. Troll, Biophys. J. **90**, 190 (2006).

6.4 Laboratory computer systems

M. A. Howe, R. J. Seymour, H. E. Swanson and J. F. Wilkerson

This year had a lower rate of additions, upgrades and replacement of existing systems.

As AMD Athlon 64-bit processors have dropped in price, they have become our "$700 standard-issue" new-desktop configuration. For specialized applications requiring raw compute power, we use dual-processor AMD Opteron systems. One was purchased for John Cramer's work in RHIC simulation and analysis (see Sec. 5.1).

We have built another JAM-based data acquisition system for the ^{3}He + ^{4}He studies, using a Wiener PCI-CC32 system for CAMAC crate control. We encountered problems during the setup, wherein the Wiener PCI card caused addressing conflicts with a Compaq SR1550NX's ASUS K8S-LA motherboard's on-board video system. The "instant-fix" was to replace the host system with an eMachines T6216. When we can free up the Wiener hardware we will investigate further.

As hacking probes increase in frequency and sophistication, we have taken a more proactive defensive stance. We are now using DenyHosts (http://denyhosts.sourceforge.net) on our primary Linux systems to agressively block access by the more common password-cracking attacks within a few seconds of their initial probing. This has lowered the sniffer attempts from about 1000 per night per system to fewer than twenty. Compromised systems at other .edu sites are identified to their systems people.

To aid in Alejandro Garcia's and Manojeet Bhattacharya's analysis of ^{32}Ar (see Sec. 4.1), we have resurrected one of our 1988-era VAXstation 3200's to run our variant of the XSYS data acquisition/analysis program. Thus our "legacy" census has increased by one. Our DecStation 433au serves as the file server for the space-limited 3200. Occasional VMS Fortran programs are written to convert the various XSYS data and output formats to structures suitable for PC graphics and analysis programs' further processing. Some of those results appear in Sec. 4.1 of this report.

Similar data format conversion programs were written for the ^{32}Cl (see Sec. 4.2) work.

To assist the APOLLO laser-ranging studies, we have installed various lunar mapping and imaging programs, such as the Virtual Moon Atlas from http://www.astrosurf.com/avl/UK_index.html

Our computing and analysis facility consists of:
- A mix of Linux systems, RedHat v7.3 through v9.0 and Fedora Cores 3 and 4
- Twin dual-processor DEC/Compaq/HP Unix AlpherServer 4000s
- Three VMS/Vaxes and two VMS Alphas for "legacy" computing.
- The SNO, NCD, KATRIN and emiT groups rely upon Macintosh systems.
- One SunBlade 100 workstation serves CADENCE circuit design, analysis and layout duties.
- A VAXstation is the Linac and Vacuum systems' control and display system.
- Three desktop JAM acquisition and analysis systems, plus two laptops for taking to other installations.
- The bulk of CENPA's Windows-based PCs are behind a Gibraltar Linux-based logical

firewall using an automated setup procedure developed by Corey Satten of the University's Networks and Distributed Computing group. http://staff.washington.edu/corey/fw/

- Although not directly used by Lab personnel, we provide co-location services for the Institute for Nuclear Theory and the Physics Nuclear Theory group in the form of one VMS Alphastation 500. The Astronomy Department has located a 64-processor Xeon-based Beowulf cluster in our machine room. The cluster's work is described in Sec. 8.2 and Sec. 8.3 of this report.

7 Accelerator and Ion Sources

7.1 Ion sources, injector deck and accelerator crew training

G. C. Harper, J. A. White and D. I. Will

There was no significant development for our injector deck or its direct extraction ion source (DEIS) or its sputter ion source (SpIS). The image ion gauge controller on the injector deck was replaced.

CENPA relies on trained accelerator crews to assist our experimenters and assure a second head and pair of hands for everyone's safety (a two-person rule while operating the Van de Graaff and ion sources). Our policy is that all graduate students paid out of our DOE contract become competent accelerator operators. Two decades ago all incoming graduate students were trained by senior graduate students with great experience gained from many hours operating the machine for their own and others experiments. More recently the staff have come to supervise training as more graduate students work on non-accelerator projects.

Furthermore, the demands of research projects at other locations require weeks or months of time away from CENPA and so current graduate students crew for only two years. This leaves fewer graduate student crews here at any given time. We now must rely more heavily on paid undergraduate hourlies who often train during their second year at the university and typically give us at least two years of service. Most years we have at least one senior member of these undergraduates who can assist with some training while honing his skills as a teacher as well as his technical skills running our Van de Graaff and ion sources. As a backup when questions arise we have an extensive operations manual of over 150 pages which is revised at least yearly. As a further source of help some staff member is generally available by phone evenings, nights and weekends.

This past year two undergraduates and three graduate students have completed training. Another undergraduate and two graduate students are in training now. We also have four senior crews: two undergraduates who graduate this spring and two graduate students who will complete their two years of service soon. Finally, there are several older graduate students who take an occasional shift.

We expect crews to exercise good judgment and demonstrate competence in the following six areas: 1) sputter ion source (SpIS/860) startup, and tuning with the injector deck elevated to the low energy cup including switchover from the direct extraction ion source (DEIS) and installation of a new pellet; 2) DEIS startup, and tuning with the deck elevated to the low energy cup including switchover from SpIS/860 and installation of a new gas bottle and gas manifold pump/purge; 3) single-ended Van de Graaff operation with TIS startup and tuning from high energy cup to flap including use of nmr and energy stabilization; 4) tandem Van de Graaff startup and tuning of some beam from an injector deck ion source through the tandem to the flap including use of diagnostics and debugging of vacuum and interlock problems; 5) production of high radiation beams and proper safety and use of the CENPA radiation protection system; 6) documentation with crewsheets and the logbook of basic tuning data, plus logbook and email documentation of problems encountered.

7.2 Van de Graaff accelerator operations and development

J. F. Amsbaugh, G. C. Harper, J. A. Mitchell, A. W. Myers, T. D. VanWechel, J. A. White and D. I. Will

The tandem was entered 13 times this year. The terminal ion source (TIS) and the foil stripper were exchanged during three openings as were spiral inclined field tube #3 and the KN straight tube. The terminal computer was repaired during one tank opening and its fiber optic telemetry link was replaced. The tube gradient was changed during three openings. Idler bearings or charge pickup wheels were replaced during four openings. The RF source was serviced during two of the entries and terminal vacuum leaks were repaired during another two of the entries. The machine was entered three times to repair sparking problems from broken components in the column resistor string.

The nylon flange which holds the permanent solenoid magnets to the terminal ion source had been stressed and heated for years. It was warped to the extent that the vacuum joint at the bottom of the bottle would no longer seal reliably. This flange was replaced with a much stouter one made from G-10 fiberglass.

A rugged power supply scheme using adequate transient suppression and potted power supplies was installed last year[1] in the electrostatic deflector supply assembly. The same 24 VDC potted supply was installed in the terminal computer. These worked successfully since September 2004 with only one problem. The 24 VDC power supplies were working right at their current limits and would occasionally trip off. These would have to be powered down to restart. We replaced both of these with supplies of much greater current capacity.

The new GVM circuit utilizing a balanced demodulator was calibrated at higher voltages this year. The old calibration was done at about 3 MV terminal voltage because we were running single ended at the time. The new calibration was done at 7.5 MV terminal voltage and found to be within 2 kV of the previous calibration. The GVM is linear from 0 V to 10 MV. It has been used successfully with a 77 keV $^{4}He^{+}$ (69 kV terminal) beam and a 61.8 MeV $^{16}O^{+6}$ (8.8MV terminal) beam.

The high energy Faraday cup was repaired and the low energy turbomolecular pump was replaced this year. Clogged flow switches associated with the analyzing magnet, the switching magnet, and the low energy turbo were cleared or replaced. The 24 inch chamber on the right 30° beamline was completely refurbished to be used as a general purpose scattering chamber. The x-rays produced in the spiral inclined field tube #1 region now occur only in bursts while increasing the terminal voltage beyond about 6.5 MV but the level has been substantially reduced. The tandem and accelerator tube were at one time conditioned up to 8.8 MV this year.

During the 12 months from April 1, 2005 to March 31, 2006 the tandem pellet chains operated 2201 hours, the SpIS 431 hours, and the DEIS 409 hours. We did no molecular research using the deck only this year.

[1]CENPA Annual Report, University of Washington (2005) p. 88.

7.3 Physical plant maintenance, repairs and possible upgrade

B. J. Fulton, G. C. Harper, K. J. Higgins, A. W. Myers, H. Simons, D. W. Storm and D. I. Will

Our facility consists of three structures: the Van de Graaff building, the Cyclotron building, and the Cyclotron Shop building. Last year 313 work requests were placed for our structures: 154 for Van de Graaff, 98 for Cyclotron, and 61 for Cyclotron Shop. Maintenance and repairs to these are financed out of the University's indirect costs.

Of these 313 work requests, 306 were covered by contract overhead. Of these 306 requests more than half, 179, were placed by physical plant personnel as preventive maintenance. Another 36 requests were placed by physical plant staff who noted items in need of repair during routine inspection or preventive maintenance. CENPA staff placed 91 of these work requests for repair of failed or failing items.

The remaining 7 requests by CENPA staff hired services: transportation of the Department of Physics and Astronomy scissor lift needed here several times for research installations and repairs, recycling of refrigerant (freon) from research equipment, and estimation for replacement and planning purposes. These services cost $2,146.

As the result of decommisioning our superconducting linac booster some years back we now have 70 tons of excess chiller capacity plus reserve electrical power equal to several times our current peak usage. This cooling and power are available for modest costs of piping chilled water, running wires and conduit, plus purchase and installation of necessary fan coils and fire alarm upgrades. We already host Metate, a Beowulf cluster of 64 processors, for the Departments of Astronomy and of Medicinal Chemistry[1] (see Sec. 8.2). Recently the Institute for Nuclear Theory and the Department of Physics inquired as to CENPA's capacity to host a cluster of 250 to 500 processors (which we are able to do with the modest type of improvements listed above). The College of Arts and Sciences has expressed an interest in placing several small clusters at our facility and paid for budgetary engineering and estimation services.

[1]CENPA Annual Report, University of Washington, (2005) p. 86.

8 Outside Users

8.1 Studies of the low energy fission of the actinides using surrogate reactions

W. Loveland,* P. H. Sprunger* and A.Ṁ. Vinodkumar*

The nuclear fission process is both technologically important and because of its complexity, difficult to model with certainty. Among the measurable quantities in fission of technological importance are the prompt neutron spectra and multiplicities. The variation of these quantities with fragment mass division, nuclear excitation energy E*, nuclear composition (Z,A) and the fragment kinetic energy release offers insight into the partition of energy during the large scale collective motion of the scission process.[1] While the neutron multiplicities and spectra of some of the major actinides of interest to nuclear technology have been well-characterized, there is a paucity of data on the minor actinides. Accordingly we are engaged in an effort to characterize the fission properties of several minor actinides. Since we are generally interested in neutron emission from these nuclei, we are using reactions (surrogate reactions) other than neutron capture to induce fission.

In our first experiments at the CENPA, we formed the fissioning nuclei, ^{237}U, ^{238}U, ^{239}U, ^{236}Np, ^{237}Np, ^{238}Np, ^{240}Np and ^{239}Pu using surrogate reactions like (d,pf), (d,d'f), etc. We attempted to measure the fission cross section, mass-yield distributions, fission neutron multiplicities, and fission neutron spectra as a function of the excitation energy of these nuclei.

Our experimental setup is shown in Fig. 8.1-1. The incident deuteron beam strikes a thin (≈ 0.5 mg/cm^2) target of ^{238}U or ^{237}Np and emitted charged particles are detected in a three element counter telescope at 90° with respect to the incident beam. Fission fragments are detected by either Si strip detectors or arrays of individual surface barrier detectors. The time of flight and multiplicity of any coincident neutrons is measured using a series of BC501A liquid scintillators. By gating on the energy and (Z,A) of the emitted charged particles, excitation functions are deduced.

Our first run occurred in January-February, 2006. Data analysis is in progress.

*Department of Chemistry, Oregon State University, Corvallis, OR 97331.

[1] R. Vandenbosch and J. R. Huizenga, *Nuclear Fission*, Academic, New York, NY (1973).

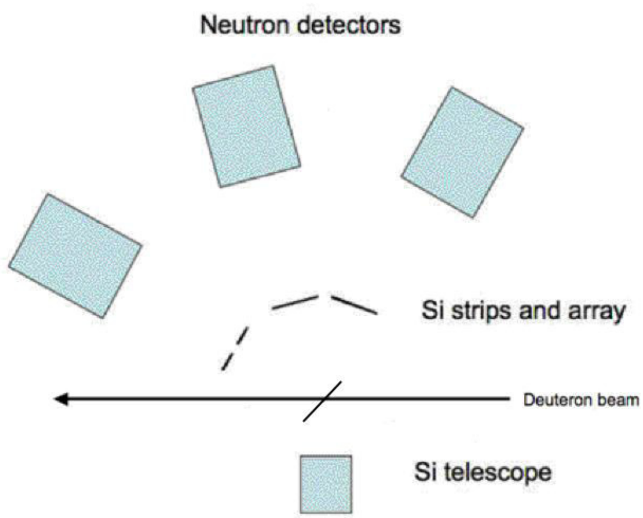

Figure 8.1-1. Schematic diagram of the experimental setup. An additional neutron detector is located out of the reaction plane above the target.

8.2 Department of Astronomy Beowulf cluster*

E. Agol,† V. P. Debattista,† C. J. Hogan,† N. A. Kaib,† T. R. Quinn,† R. Roskar,† J. H. Steffen‡ and K. Zurek‡

The 64-processor Beowulf cluster (metate) located at CENPA has been used by T. Quinn and collaborators in the Astronomy and Physics departments for both cosmological and planetary applications.

On the cosmological side Physics graduate student, K. Zurek, in collaboration with C. Hogan and T. Quinn has been calculating the generation of cosmic structure via a late phase transition of an axion field. These structures could be of interest for microlensing experiments, but numerical simulations of their non-linear collapse are needed to make predictions of their lensing properties.

Astronomy graduate student, R. Roskar, in collaboration with postdoc, V. Debattista, and T. Quinn, is simulating the evolution of the disks of spiral galaxies in the presence of bar instabilities. They are trying to understand the origin of breaks in the usual exponential disk structure.

Physics graduate student, J. Steffen, in collaboration with E. Agol, has been doing planetary orbit integrations in order to identify or constrain the secondary planets in known, transiting systems using a novel timing technique.[1]

Astronomy graduate student, N. Kaib, in collaboration with T. Quinn, is modelling the formation of the Oort Cloud in a realistic star formation environment. This work investigates the effect that the Sun's birthplace has had on the evolution and structure of the Oort Cloud.[2]

---

*Not supported by DOE CENPA grant

†Department of Astronomy, University of Washington, Seattle, WA 98195.

‡Department of Physics, University of Washington, Seattle, WA 98195.

[1] E. Agol, J.H. Steffen, *et al.*, MNRAS 359 567, (2005); and J. H. Steffen and E. Agol, MNRAS 364 96L, (2005).

[2] Kaib, N. & Quinn, T., 2006; *The Effect of the Sun's Early Environment on Oort Cloud Formation and Comet Showers*, [Abstract]; AbSciCon 2006, Washington, DC. Internat. J. Astrobiology, Supplement 1 (2006).

8.3 Molecular dynamics of proteins and peptides*

D. A. C. Beck,† V. Daggett,† D. O. V. Alonso,† A. Scouras‡ and G. W. N. White†

The Department of Medicinal Chemistry shares the CENPA co-located Beowulf Cluster "metate".

Dr. Valerie Daggett's lab in the Department of Medicinal Chemistry has been using the cluster to work on methods development projects and production work treating protein structure and dynamics. We use all-atom molecular dynamics (MD) simulations to calculate the dynamics of protein motion. This allows us to investigate a wide range of biological problems, including prion diseases (e.g., Mad Cow Disease), the protein folding problem, and the movement of a protein in its normal solvated biological environment. MD is especially useful where experimental probes of dynamics do not have the time resolution to describe rapidly occurring events.

Specific work:

- Replicate Exchange Molecular Dynamics (REMD) is a newer molecular dynamics method that purportedly improves sampling in MD simulations. George White, a recently graduated Ph.D. from the Biomolecular Structure and Design (BMSD) program, worked on the testing and development of REMD. The stability of the metate cluster made it practical for George to parallelize this method over many nodes.

- Peptides: Daigo Inoyama was an undergraduate student who has subsequently gone on to medical school. He used the cluster to simulate small peptides. In this case these were chains of five amino acids, rather than the chains of greater than fifty amino acids that generally form folded proteins. Because of their short chain length, short peptides remain dynamic and do not form the relatively rigid three dimensional fold of most proteins of fifty amino acids or more.

- Prion Protein: The prion protein is the pathological and infectious agent in a variety of neurological diseases including Bovine Spongiform Encephalopathy (BSE, a.k.a Mad Cow Disease) and Creutzfeld-Jakob Disease (CJD). The protein has benign and infectious forms, and they differ only in their fold or conformation. They are chemically identical. Alex Scouras, a Biochemistry graduate student in our lab, used the metate cluster to observe structural changes starting from the benign form of the prion protein.

---

*Not supported by DOE CENPA grant

†Department of Medicinal Chemistry, University of Washington, Seattle, WA 98195.

‡Department of Biochemistry, University of Washington, Seattle, WA 98195.

9 The Career Development Organization: year six.

M. K. Bacrania,* T. Butler, M. L. Leber, N. S. Oblath and L. C. Stonehill*

The Career Development Organization for Physicists and Astronomers (CDO)[1] at the University of Washington is a graduate student organization that helps physics and astronomy students find employment after graduation. Historically, CENPA has been very well-represented in the CDO's membership and leadership. Again, almost all active CDO members are CENPA graduate students. Building on previous years,[2] the CDO has organized the very successful Fifth Annual Networking Day event. In addition, the seminar series has continued and for the first time ever students were able to tour Boeing's industrial research labs.

The Fifth Annual Networking Day was held on November 1st, 2005. The Networking Day provides opportunities for students to make contacts outside academia and to present their research to interested employers. The focus of Networking Day is on allowing the students to present their strengths, which is different from a typical job fair, in which the employers are doing the majority of the presenting. This helps many companies that do not traditionally employ physicists to see the diverse skills that physics and astronomy students possess. Thirty students contributed talks, gave lab tours, and participated in the poster session. Twenty representatives from fourteen employers attended. As a result, at least one student secured a summer internship.

One goal of the CDO this year was to streamline the Networking Day planning process. After hosting this event for five years the format has converged, but each year a new CDO president, usually a CENPA student, has struggled with the responsibility of the planning. After meeting with the University of Washington Learning for Leadership Council (UWLLC), CDO has decided on a new leadership scheme. Networking Day will be planned jointly by the president and vice-president, who will each serve two-year terms. Thus one person will always have one year experience in the planning process. UWLLC also suggested meeting with business school students, which has lead to a "business plan" and documentation of the steps to plan a successful Networking Day.

The relationships fostered at Networking Day have led to more than just employment for UW students. Representatives from Systems Biology in Seattle, WA gave a seminar, "Systems Biology for the Physicist," for interested students. Boeing, a Networking Day attendee since inception, invited students to tour their research labs. Twenty graduate and undergraduate students spent the afternoon with the Boeing scientists visiting the flywheel energy storage system and linear accelerator laboratories. Both of these events exposed students to employment and research opportunities outside of academia.

*Presently at Los Alamos National Laboratory, Los Alamos, NM 87545.

[1] http://students.washington.edu/cdophys

[2] CENPA Annual Report, University of Washington (2005) p. 90.

10 CENPA Personnel

10.1 Faculty

Eric G. Adelberger	Professor	
Hans Bichsel	Affiliate Professor	
John G. Cramer	Professor	
Peter J. Doe	Research Professor	
Joseph Formaggio[1]	Research Assistant Professor	
Alejandro García	Professor	
Hartmut Gemmeke[2]	Visiting Scholar	
Jens H. Gundlach	Research Associate Professor	
Isaac Halpern	Professor Emeritus	
Blayne R. Heckel	Professor	
R. G. Hamish Robertson	Professor;	Scientific Director
Kurt A. Snover	Research Professor	
Derek W. Storm	Research Professor;	Executive Director
Thomas A. Trainor	Research Professor	
Robert Vandenbosch	Professor Emeritus	
William G. Weitkamp	Professor Emeritus	
John F. Wilkerson	Professor	

10.2 CENPA External Advisory Committee

Baha Balantekin	University of Wisconsin
Russell Betts	University of Illinois at Chicago
Stuart Freedman	UC Berkeley

10.3 Postdoctoral Research Associates

Cristina Bordeanu[3]	Thomas Brown
Jason Detwiler	Seth Hoedl
C.D. Hoyle	Daniel Melconian
Scott Pollack	Keith Rielage[4]
Stephan Schlamminger	Brent VanDevender

[1]Massachusetts Institute of Technology, Building 26-568, 77 Massachusetts Ave, Cambridge, MA 02139.

[2]Forschungszentrum Karlsruhe, Institut fur Prozessdatenverabeitung und Elektronik, POB 3640, 76021 Karlsruhe, Germany.

[3]Horia Hulubei - National Institute for Physics and Nuclear Engineering Department of Nuclear Physics (DFN 110) Str. Atomistilor nr. 407 Bucharest-Magurele, PO Box MG6. Romania.

[4]Los Alamos National Laboratory, Los Alamos, NM 87545.

10.4 Predoctoral Research Associates

Minesh Bacrania[1]
Ted Cook
Claire Cramer
Charles Hagedorn
Dan Kapner[3]
David Kettler
Frank Marcoline[4]
Kathryn Miknaitis[3]
Noah Oblath
Alexis Schubert
Laura Stonehill[1]
Smarajit Triambak
Brandon Wall
Ki-Young Choi[2]
G. Adam Cox
Charles Duba
Robert Johnson
Kareem Kazkaz
Michelle Leber
Michael Marino
Erik Mohrmann
Anne Sallaska
Sky Sjue
Matthew Swallows[5]
Todd Wagner

10.5 Research Experience for Undergraduates participants

Kathy Chaurasiya[6]
Hannah Gelman[7]
Meghan Mella[8]
Audrey Sederberg[9]
Jennifer Sibille[10]

[1]Los Alamos National Laboratory, Los Alamos, NM 87545.
[2]Ph.D., March 2006
[3]The Kavli Institute for Cosmological Physics University of Chicago, 5640 South Ellis Avenue, Chicago, IL 60637.
[4]No longer at the University of Washington.
[5]Department of Physics, University of Washington, Seattle, WA 98195.
[6]Department of Physics, Simmons College, 300 The Fenway, Boston, MA 02115.
[7]Department of Physics, Dartmouth, Hanover, NH 03755.
[8]Department of Physics, University of Northern Colorado Greeley, CO 80639.
[9]Department of Physics, Harvey Mudd College, Claremont, CA 91711.
[10]Department of Physics, Louisana Tech College, Ruston, LA 71272.

10.6 Professional staff

The professional staff are listed with a description of their recent major efforts.

John F. Amsbaugh	Research Engineer	Mechanical design, vacuum systems
Tom H. Burritt	Research Engineer	Construction SNO NCD's
Gregory C. Harper	Research Engineer	Electronic and mechanical design
Mark A. Howe	Research Engineer	Software for DAQ, control systems
Sean R. McGee	Research Scientist	SNO
R. Jefferson Porter	Research Scientist	STAR analysis
Duncan J. Prindle, Ph.D.	Research Scientist	Heavy ion software
Richard J. Seymour	Computer Systems Manager	
H. Erik Swanson, Ph.D.	Research Physicist	Precision experimental equipment
Timothy D. Van Wechel	Electronics Engineer	Analog and digital electronics design
Douglas I. Will	Research Engineer	Cryogenics, ion sources

10.7 Technical staff

James Elms	Instrument Maker
David Hyde	Instrument Maker
Allan Myers	Electronics Technician
Hendrik Simons	Instrument Maker, Shop Supervisor

10.8 Administrative staff

Barbara J. Fulton	Administrator
Kate J. Higgins	Fiscal Specialist

10.9 Part Time Staff

Brian Allen[1]
Asley Batchelor[1]
Owen Biesel
Corey Fredericks
Suzanne Hayward [1]
Yama Kharoti
Emily LeMagie
L. Peter Mannisto
Kamil Michnicki[1]
Jessica Mitchell
Michael Nickerson
Dejan Nikic[1]
Marissa Rodenburg
Daniel Schultheis
Mark Wehrenberg[1]
Joseph White
Jonathan Will

[1]Left during 2005.

11 Publications

11.1 Published papers:

"Event structure at RHIC from p-p to Au-Au," T. A. Trainor and the STAR Collaborators,* *Proceedings of 20th Winter Workshop on Nuclear Dynamics,* Trelawny Beach, Jamaica, March, 2004. Acta Phys. Hung. A **24**, 71 (2005).

"Analytic expressions for gravitational inner multipole moments of elementary solids and for the force between two rectangular solids," E. G. Adelberger, N. A. Collins and C. D. Hoyle, Class. Quant. Grav. **23**, 125 (2006).

"A transactional analysis of interaction-free measurements," J. G. Cramer, Found. Phys. Lett, **19**, 63, (2006), quant-ph/0508102.

"An electron transparent proton detector for neutron decay studies," S. A. Hoedl, J. Appl. Phys. **99**, 084904 (2006).

"Autocorrelations from fluctuation scale dependence by inversion," T. A. Trainor, R. J. Porter and D. J. Prindle, J. Phys. G **31**, 809 (2005).

"Experimental and theoretical challenges in the search for the quark gluon plasma: The STAR collaboration's critical assessment of the evidence from RHIC collisions," J. Adams and the STAR Collaborators,* Nucl. Phys. A **757**, 102 (2005), nucl-ex/0501009.

"The ^{7}Be(p,γ)^{8}B astrophysical S-factor," K. A. Snover, A. R. Junghans, E. C. Mohrmann, T. D. Steiger, E. G. Adelberger, J. M. Casandjian, H. E. Swanson, L. Buchmann, S. H. Park, A. Zyuzin and A. M. Laird, *Proceedings of the 8th Nuclei in the Cosmos Conference*, July 2004, Vancouver, BC, Nucl. Phys. A **758**, 685c (2005).

"Recent results from SNO and other solar neutrino experiments," R. G. H. Robertson, Invited Talk, *Proc. 8th Internat. Workshop on Topics in Astroparticle and Underground Physics International Conference*, TAUP 03, University of Washington, Seattle, WA, September, 2003, Nucl. Phys. Proc. Suppl. **138**, 243 (2005).

"Phi meson production in Au+Au and p+p collisions at $\sqrt{s_{NN}}$ =200 GeV," J. Adams and the STAR Collaborators,* Phys. Lett. B **612**, 181 (2005), nucl-ex/0406003.

"Autocorrelations from the scale dependence of transverse-momentum fluctuations in Hijing-simulated Au-Au collisions at $\sqrt{s_{NN}}$ = 200-GeV," Q. J. Liu, D. J. Prindle and T. A. Trainor, Phys. Lett. B **632**, 197 (2006).

"System size and centrality dependence of the balance function in A + A collisions at $\sqrt{s_{NN}}$ 17.2-GeV," C. Alt and the NA49 Collaborators, Phys. Rev. C **71**, 034903 (2005), hep-ex/0409031.

"Pion interferometry in Au+Au collisions at $\sqrt{s_{NN}}$ = 200 GeV," J. Adams and the STAR

Collaborators,* Phys. Rev. C **71**, 044906 (2005), nucl-ex/0411036.

"K(892)* resonance production in Au+Au and p+p ccollisions at $\sqrt{s_{NN}} = 200$ GeV at STAR," J. Adams and the STAR Collaborators,* Phys. Rev. C **71**, 064902, nucl-ex/0412019.

"Event-wise mean-p$_T$ fluctuations in Au-Au collisions at $\sqrt{s_{NN}} = 130$ GeV," J. Adams and the STAR Collaborators,* Phys. Rev. C **71**, 064906 (2005).

"Azimuthal anisotropy in Au+Au collisions at $\sqrt{s_{NN}} = 200$ GeV," J. Adams and the STAR Collaborators,* Phys. Rev. C **72**, 014904 (2005), nucl-ex/0409033.

"Incident energy dependence of p$_T$ correlations at RHIC," J. Adams and the STAR Collaborators,* Phys. Rev. C **72**, 044902 (2005), nucl-ex/0504031.

"Polarized neutron β-decay: proton asymmetry and recoil-order currents," S. K. L. Sjue, Phys. Rev. C **72**, 045501 (2005).

"Electron energy spectra, fluxes, and day-night asymmetries of ^{8}B solar neutrinos from measurements with NaCl dissolved in the heavy water detector at the Sudbury Neutrino Observatory," B. Aharmim and the SNO Collaborators,* Phys. Rev. C **72**, 055502 (2005), nucl-ex/0502021.

"Directed flow in Au+Au collisions at $\sqrt{s_{NN}} = 62$ GeV, J. Adams and the STAR Collaborators,* Phys. Rev. C **73**, 034903 (2006), nucl-ex/0510053.

"Upper limit of D^0 production in central Pb+Pb collisions at 158-A-GeV," C. Alt and the NA49 Collaborators,* Phys. Rev. C **73**, 034910 (2006), nucl-ex/0507031.

"Multiplicity and pseudorapidity distributions of charged particles and photons at forward pseudorapitity in Au + Au collisions at $\sqrt{s_{NN}} = 62.4$ GeV," J. Adams and the STAR Collaborators,* Phys. Rev. C **73**, 034906 (2006), nucl-ex/0511026.

"Measurement of the response of a Ga solar neutrino experiment to neutrinos from a ^{37}Ar source," J. N. Abdurashitov and the SNO Collaborators,* Phys. Rev. C **73**, 045805 (2006), nucl-ex/0512041.

"A search for periodicities in the ^{8}B solar neutrino flux measured by the Sudbury Neutrino Observatory," B. Aharmim and the SNO Collaborators,* Phys. Rev. D **72**, 052010 (2005), hep-ex/0507079.

"System-size dependence of strangeness production in nucleus-nucleus collisions at $\sqrt{s_{NN}} =$ 17.3-GeV, " C. Alt and the NA49 Collaborators, Phys. Rev. Lett. **94**, 052301 (2005), nucl-ex/0406031.

"Quantum opacity, the RHIC Hanbury-Brown Twiss puzzle, and the chiral phase transition," J. G. Cramer, G. A. Miller, J. M. S. Wu and J-H. Yoon, Phys. Rev. Lett. **94**, 102302 (2005), nucl-th/0411031.

"Ω^- and $\overline{\Omega}^+$ production in central Pb+Pb collisions at 40-AGeV and 158-AGeV," C. Alt and the NA49 Collaborators,* Phys. Rev. Lett. **94**, 192301 (2005), nucl-ex/0409004.

"Multiplicity and pseudorapidity distributions of photons in Au + Au Collisions at $\sqrt{s_{NN}}$ = 62.4 GeV," J. Adams and the Star Collaborators,* Phys. Rev. Lett. **95**, 062301 (2005), nucl-ex/0502008.

"Multi-strange baryon elliptic flow in Au+Au collisions at $\sqrt{s_{NN}} = 200$ GeV," J. Adams and the Star Collaborators,* Phys. Rev. Lett. **95**, 122301 (2005), nucl-ex/0504022.

"Erratum: Quantum opacity, the RHIC Hanbury-Brown Twiss puzzle, and the chiral phase transition," J. G. Cramer, G. A. Miller, J. M. S. Wu and J-H. Yoon, Phys. Rev. Lett. **95**, 139901 (2005).

"Hadronization geometry and charge-dependent number autocorrelations on axial momentum space in Au-Au collisions at $\sqrt{s_{NN}} = 130$ GeV," J. Adams and the STAR Collaborators,* Phys. Rev. Lett. **634**, 347 (2006).

"Distributions of charged hadrons associated with high transverse momentum particles in pp and Au+Au Collisions at $\sqrt{s_{NN}} = 200$ GeV," J. Adams and the STAR Collaborators,* Phys. Rev. Lett. **95**, 152301 (2005), nucl-ex/0501016.

"Solar neutrinos," R. G. H. Robertson, *Proceedings of Erice International School of Nuclear Physics: 27th Course*, Neutrinos in Cosmology, Erice, Sicily, Italy, Sept. 2005. Prog. Part. Nucl. Phys. **57**, 90 (2006), nucl-ex/0602005.

"Present status of the SAGE ^{37}Ar neutrino source experiment," J. N. Abdurashitov and the SAGE Collaborators,* *Proceedings of the 11th International Workshop on Neutrino Telescopes*, Venice, Italy, February 2005, Published in Venice 2005, Neutrino telescopes, 187 (2005).

"Conceptual design for a Deep Underground Science and Engineering Laboratory Cascades," W. Haxton, J. Wilkerson, R. A. Robertson and R. J. Guardia, in *Rapid Excavation Tunneling Conference Proceedings 2005*, Editors: J. D. Hutton and W. D. Rogstad, Published by Society for Mining, Metallurgy, and Exploration (2005).

"Proceedings of MIT Workshop on Correlations and Fluctuations in Relativistic Nuclear Collisions," G. Roland and T. A. Trainor, editors, Cambridge, MA, April 2005, J. Phys. Conf. Ser. 27, (2005).

Papers submitted or to be published 2006:

"The BNO-LNGS joint measurement of the solar neutrino capture rate in ^{71}Ga," J. N. Abdurashitov and the SAGE Collaborators,* accepted by Astropart. Phys., nucl-ex/0509031.

"A power-law description of collision centrality applied to Hijing-1.37-simulated Au - Au collisions at $\sqrt{s_{NN}}$ = 200-GeV," T. A. Trainor and D. J. Prindle, submitted to J. Phys. G, hep-ph/0411217.

"Identified hadron spectra at large transverse momentum in p+p and d+Au collisions at $\sqrt{s_{NN}}$ = 200 GeV," J. Adams and the STAR Collaborators,* submitted to Phys. Lett. B, nucl-ex/0601033.

"Forward neutral pion production in p+p and d+Au Collisions at $\sqrt{s_{NN}}$ = 200 GeV," J. Adams and the STAR Collaborators,* submitted to Phys. Rev. Lett., nucl-ex/0602011.

"Strangelet search at RHIC," J. Adams and the STAR Collaborators,* submitted to Phys. Rev. Lett., nucl-ex/0511047.

"Transverse-momentum p_T correlations on (η, Φ) from mean-p_T fluctuations in Au - Au collisions at $\sqrt{s_{NN}}$ = 200-GeV," J. Adams and the STAR Collaborators,* accepted by Phys. Lett. B, nucl-ex/0509030.

"A method to improve particle identification in TPCs and silicon detectors," H. Bischel, Nucl. Instrum. Methods in Phys. Res. A, in press.

"Precise study of the final-state continuum in ^{8}Li and ^{8}B decays," M. Bhattacharya, E. G. Adelberger and H. E. Swanson, Phys. Rev. C, in press.

"Mass of the lowest $T = 2$ state in ^{32}S: a test of the isobaric mass multiplet equation," S. Triambak, A. García, E. G. Adelberger, G. J. P. Hodges, D. Melconian, H. E. Swanson, S. A. Hoedl, S. K. L. Sjue and A. L. Sallaska, Phys. Rev. C, in press.

"Arguments for a 'U.S. Kamioka': SNOLab and its implications for North American underground science planning," W. C. Haxton, R. Holtz, P. Long and J. F. Wilkerson, to be submitted, nucl-ex/0604004.

11.2 Invited talks, abstracts and other conference presentations:

"The Eöt-Wash axion search," S. A. Hoedl, MIT Cosmology Seminar, Massachusetts Institute of Technology, Cambridge, MA, April 2005.

"Transverse momentum correlations in relativistic nuclear collisions," T. A. Trainor, D. J. Prindle and the STAR Collaborators, *Proceedings of MIT Workshop on Correlations and Fluctuations in Relativistic Nuclear Collisions*, G. Roland and T. A. Trainor, editors, Cambridge, MA, April 2005, J. Phys. Conf. Ser. **27**, 134 (2005).

"The equivalence of fluctuation scale dependence and autocorrelations," D. J. Prindle and T. A. Trainor, *Proceedings of MIT Workshop on Correlations and Fluctuations in Relativistic Nuclear Collisions*, G. Roland and T. A. Trainor, editors, Cambridge, MA, April 2005, J. Phys. Conf. Ser. **27**, 118 (2005).

"Correlations from p p collisions at $\sqrt{s}$= 200-GeV," R. J. Porter, T. A. Trainor and STAR

Collaborators,* *Proceedings of MIT Workshop on Correlations and Fluctuations in Relativistic Nuclear Collisions*, G. Roland and T. A. Trainor, editors, Cambridge, MA, April 2005, J. Phys. Conf. Ser. **27**, 98 (2005).

"The blind men and the quantum: testing quantum interpretations," J. G. Cramer, Invited popular-level lecture given at *NASA/AIP Physics for the 3rd Millennium: II*, Huntsville, AL, April 2005.

"The Eöt-Wash axion search," S. A. Hoedl, Northwest APS Section Meeting, University of Victoria, Victoria, BC, May 2005.

"The Majorana neutrinoless double-beta decay experiment," J. F. Wilkerson, Invited Presentation to the *Neutrino Scientific Assessment Group HEPAP-NSAC Sub-committee*, Gaithersburg, MD, May 2005.

"Digging Neutrinos: Pursuing Science Deep Underground," J. F. Wilkerson, Invited Colloquium, University of Washington Science Forum, Seattle, WA, June 2005.

"The Majorana Neutrinoless Double-Beta Decay Experiment," J. F. Wilkerson, Invited Talk, INT Workshop on Underground Science, June 2005.

"Solving the RHIC HBT puzzle," J. G. Cramer, Invited talk, presented at the *Workshop on Femtoscopy, RHIC/AGS Users Meeting*, Brookhaven National Laboratory, NY, June 2005.

"The Quantum handshake: A review of the transactional interpretation of quantum mechanics," J. G. Cramer, invited 1-hour lecture presented at the *Time-Symmetry in Quantum Mechanics Conference*, Sydney, Australia, July 2005.

"The Eot-Wash axion search," S. A. Hoedl, International School on Contemporary Physics, Ulaan Baator, Mongolia, August 2005.

"Low-Q^2 partons in p - p and Au - Au collisions," T. A. Trainor and the STAR Collaborators,* *35th International Symposium on Multiparticle Dynamics (ISMD 05)*, Kromeriz, Czech Republic, August 2005.

"Pion opacity, chiral symmetry restoration, and RHIC HBT," J. G. Cramer, Invited talk, *WPCF 2005*, Kromeriz, Czech Republic, August 2005.

"Chiral symmetry restoration, pion opacity, and the RHIC HBT puzzle," J. G. Cramer, Invited talk, presented at *ISMD 2005*, Kromeriz, Czech Republic, August 2005.

"The RHIC HBT puzzle, chiral symmetry restoration, and pion opacity," J. G. Cramer, Contributed paper, selected for oral presentation at *Quark Matter 2005*, Budapest, Hungary, August 2005.

"Mass of the lowest $T = 2$ state of ^{32}S and the isospin multiplet mass equation," S. Triambak, Talk at: RIA Summer School, Lawrence Berkeley National Laboratory, Berkeley, CA, August 2005.

"Mass of the lowest $T = 2$ state of ^{32}S", S. Triambak, A. García, E. G. Adelberger, G. J. P. Hodges, H. E. Swanson, S. A. Hoedl, S. K. L. Sjue and A. L. Sallaska, 12$^{\mathrm{th}}$ *International Symposium on Capture Gamma-Ray Spectroscopy and Related Topics*, Notre Dame, IN, September 2005, AIP Conference Proceedings, **819**, 607, (2006).

"Evidence for a chiral phase transition at RHIC," J. G. Cramer, York University, Toronto, Physics Colloquium, September 2005.

"Neutrinoless double beta decay - current results, future implications," J. F. Wilkerson, Invited Talk, *US - Japan Seminar on Double Beta Decay and Neutrino Mass Meeting*, Maui, HA, September 2005.

"Direct determination of neutrino mass with KATRIN," K. Rielage, Second Joint Meeting of the APS/JPS, Maui, Hawaii, September 2005, Bull. Am. Phys. Soc. **50**, 22 (2005), Session IWF1.

"^{7}Be + p and ^{3}He + ^{4}He fusion reactions and neutrino astrophysics," K. A. Snover, Invited talk, Second Joint Meeting of the APS/JPS, Maui, Hawaii, September 2005, Bull. Am. Phys. Soc. **50**, 23 (2005), Session IWG3.

"Search for right-handed currents in the β^{+} decay of laser-cooled, polarized ^{37}K," D. Melconian, Second Joint Meeting of the APS/JPS, Maui, Hawaii, September 2005, Bull. Am. Phys. Soc. **50**, 43 (2005), Session BB4.

"Mass of the lowest $T = 2$ state of ^{32}S," S. Triambak, A. García, E. G. Adelberger, G. J. P. Hodges, H. E. Swanson, S. A. Hoedl, S. K. L. Sjue and A. L. Sallaska, Second Joint Meeting of the APS/JPS, Maui, Hawaii, September 2005, Bull. Am. Phys. Soc. **50**, 56 (2005), Session BH2.

"Polarized neutron β-decay: the Proton asymmetry and recoil-order currents," S. Sjue and A. García, Second Joint Meeting of the APS/JPS, Maui, Hawaii, September 2005, Bull. Am. Phys. Soc. **50**, 75 (2005), Session CH2.

"Solid state ultra-cold neutron detectors," S. Hoedl, A. García, D. Melconian, A. Sallaska, S. Sjue and UCN Collabortors, Second Joint Meeting of the APS/JPS, Maui, Hawaii, September 2005, Bull. Am. Phys. Soc. **50**, 102 (2005), Session DK5.

"Electron capture branch of ^{100}Tc and the efficiency of a proposed Mo neutrino detector," S. Sjue, A. García, S. Hoedl, S. Triambak and E. Swanson, Second Joint Meeting of the APS/JPS, Maui, Hawaii, September 2005, Bull. Am. Phys. Soc. **50**, 115 (2005), Session EF9.

"Determination of energy loss of 3 MeV alpha particles in Ni foil and ^{3}He gas using a Mg(α, γ) resonance," K. P. Michnicki, C. Bordeanu, J. D. Lowrey, K. A. Snover and D. W. Storm, Contributed talk, Second Joint Meeting of the APS/JPS, Maui, Hawaii, September 2005, Bull. Am. Phys. Soc. **50**, 140 (2006) Session FR78.

"Muon-induced production of ^{16}N," N. Oblath, Second Joint Meeting of the APS/JPS, Maui, Hawaii, September 2005, Bull. Am. Phys. Soc. **50**, 157 (2006) Session JG7.

"Submillimeter tests of the gravitational inverse square law," E. G. Adelberger, Physics colloquium, University of California, Davis, CA, October 2005.

"The quantum handshake: An overview of the transactional interpretation of quantum mechanics," J. G. Cramer, Invited lecture, presented at the *Colloque International 'Charles Ehresmann : 100 ans'"*, Amiens, France, October 2005.

"Fluctuations and Correlations," T. A. Trainor, *1st International Workshop of the Virtual Institute 'Physics of Strongly Interacting Matter at High Densities' of the Helmholtz Society*, Monbach, Germany, October 2005.

"University of Washington lab report to SNEAP," J. F. Amsbaugh, G. C. Harper, A. W. Myers, D. W. Storm, T. D. VanWechel and D. I. Will, *Symposium for Northeastern Accelerator Personnel*, Upton, NY, October 2005.

"Radioactive ion beams at the University of Washington FN tandem facility," G. C. Harper, M. Bacrania, D. W. Storm and R. G. H. Robertson, *Symposium for Northeastern Accelerator Personnel*, Upton, NY, October 2005.

"The β decay of laser-cooled $^{37,38\mathrm{m}}$K as a probe of new physics," D. Melconian, Invited seminar, P-25 Division Los Alamos National Laboratory, Los Alamos, NM, October 2005.

"A torsion pendulum axion search," S. A. Hoedl, Visions for Discovery Symposium, Young Scholars Competition Finalist, University of California, Berkeley, CA, October 2005.

"The Majorana neutrinoless double-beta decay experiment," J. F. Wilkerson, Invited Talk, *PANIC 05 Satellite Meeting: Neutrino Planning Workshop*, October 2005.

"Tests of Newton's inverse square law at the dark energy length scale," E. G. Adelberger, Fermilab colloquium, Batavia, IL, November (2005).

"Sensitivity and discovery potential for neutrinoless double beta decay," J. F. Wilkerson, Invited Talk, *Neutrino Nuclear Responses 2005*, Osaka, Japan, December 2005.

"Weighing neutrinos - Future experiments," J. F. Wilkerson, Invited ICRR Seminar, Kamiokande Laboratory, Japan, December 2005.

"Test of Newton's inverse-square law and Einstein's Equivalence Principle," E. G. Adelberger, Physics colloquium, University of Illinois, Urbana Champaign, IL, December 2005.

"Relativity violations in matter and gravity," E. G. Adelberger, *AAAS symposium, Refining Einstein: the search for relativity violations*, St. Louis, MO, February 2006.

"Underground science facilities and the Majorana neutrinoless double-beta decay experiment," J. F. Wilkerson, Invited talk, Homestake Lab Workshop, Lead, SD, February 2006.

"The Majorana neutrinoless double-beta decay experiment," J. F. Wilkerson, presentation to the Homestake Scientfic Program Committee, Lead, SD, February 2006.

"Nu opportunities - explorations beyond the 'Standard Model'," J. F. Wilkerson, Invited Experimental Particle Physics Seminar, Yale University, February 2006.

"High energy physics with a torsion pendulum," S. A. Hoedl, University of California, UCLA High Energy Seminar, Los Angeles, CA, February 2006.

"The blind men and the quantum," J. G. Cramer, Keynote Talk, *NIAC*, Atlanta, GA, March 2006.

"Testing gravity at small and large length scales," E. G. Adelberger, *Confronting Gravity Symposium*, St. Thomas, Virgin Islands, March 2006.

"Tests of Newton's inverse square law at the dark energy length scale," E. G. Adelberger, Physics colloquium, Princeton University, NJ, April 2006.

"Tests of the gravitational inverse-square law at the dark energy length scale," E. G. Adelberger, American Physical Society, Dallas, Texas, April 2006, Bull. Am. Phys. Soc. **51**, 71 (2006), Session E61.

"Second-forbidden beta dacay of ^{8}B," M. Bacrania, D. Storm and R. G. H. Robertson, American Physical Society, Dallas, Texas, April 2006, Bull. Am. Phys. Soc. **51**, 90 (2006), Session H91.

"New CP-violation and preferred-frame tests with polarized electrons," C. Cramer, B. Heckel, T. Cook and E. G. Adelberger, American Physical Society, Dallas, Texas, April 2006, Bull. Am. Phys. Soc. **51**, 96 (2006), Session H14.

"An update on the Majorana-Gerda simulation package (MaGe)," M. Marino, American Physical Society, Dallas, Texas, April 2006, Bull. Am. Phys. Soc. **51**, 119 (2006), Session J95.

"A verification of the Majorana-Gerda simulation package (MaGe)," A. G. Schubert, American Physical Society, Dallas, Texas, April 2006, Bull. Am. Phys. Soc. **51**, 119 (2006), Session J96.

Conference presentation by collaborators of CENPA personnel:

"Precision measurements of the neutron's beta asymmetry using ultra-cold neutrons," M. F. Makela and the UCNA Collaboration, *Proceedings of the Particles and Nuclei International Conference 2005*, Santa Fe, NM, September 2005, to be published by the American Institute of Physics.

*UW collaborators for the various CENPA research groups are listed below (April 1, 2005 - March 31, 2006).

NA49: J. G. Cramer, T. A. Trainor

SAGE: J. F. Wilkerson

STAR: H. Bichsel, J. G. Cramer, D. T. Kettler, R. J. Porter, D. J. Prindle and T. A. Trainor

SNO: G. A. Cox, J. A. Detwiler, P. J. Doe, C. A. Duba, S. R. McGee, N. S. Oblath, K. Rielage, R. G. H. Robertson, L. C. Stonehill, B. L. Wall and J. F. Wilkerson

11.3 Degrees Granted, Academic Year, 2005-2006

Search for the second-forbidden beta decay of Boron-8, Minesh Bacrania (2006).

A New Equivalence Principle Test Using a Rotating Torsion Balance, Ki-Young Choi (2006).

A Short-Range Test of Newton's Gravitational Inverse-Square Law, Daniel Kapner (2005).

A Search for Matter Enhanced Neutrino Oscillations through Measurements of Day and Night Solar Neutrino Fluxes at the Sudbury Neutrino Observatory, Kathryn Miknaitis (2005).

Deployment and Background Characterization of the Sudbury Neutrino Observatory Neutral Current Detectors, Laura Stonehill (2005).